For reviewer #1

Changes in the manuscript:

Considering the specific comments, all the detailed changes as the reviewer requested have been made in the track version of the manuscript, please see the related file.

Responses to the specific comments

1. Abstract lines 25-26. Rewrite as "GNOS bending angles and short-range ECMWF forecast bending angles: : :.."

Author's response: Done

2. Page 2 line 2-radio occultation not capitalized.

Author's response: Done

3. Page 3 line 11-suggest deleting "kinds of".

Author's response: Done

4. Page 3 line 23-poor data were filtered out…(data plural)

Author's response: Done

5. Page 4 line 5-suggest deleting "in this work"

Author's response: Done

6. Page 4 line 7- are now assimilated...

Author's response: Done

7. Page 4 line 24-affected not effected.

Author's response: Done

8. Page 5 line 1-suggest deleting "the" before complicated Line 6-…not as good as that of L1 Line 7-Fig. 2 is difficult to read. Labels are too small and bars are too large, making figure out of proportion. Also, the abscissa and ordinate need labels. Line 10-can you provide references to say what is reasonable and what is not? Figs. 3 and 4-labels and legends need to be made larger.

Author's response: Done. The figures have been replotted.

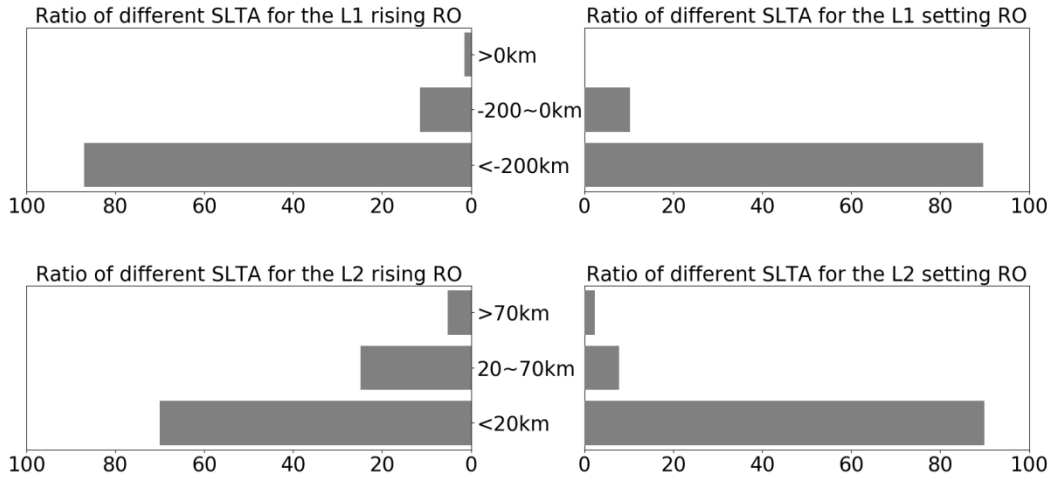

Figure 2. Ratio of different SLTA of the L1 C/A and L2 P for the rising and setting occultations, statistics result is from 28th Jan to 2nd Feb. 2017.

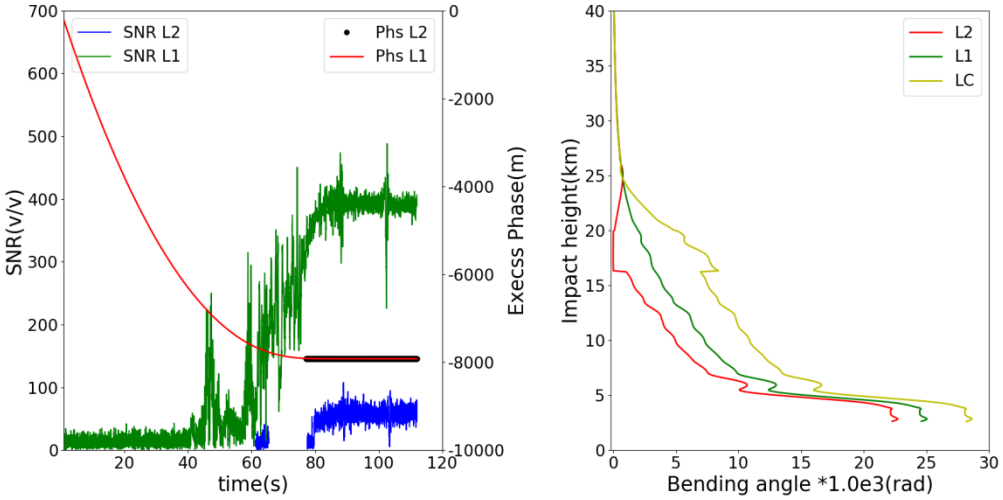

Figure 3.

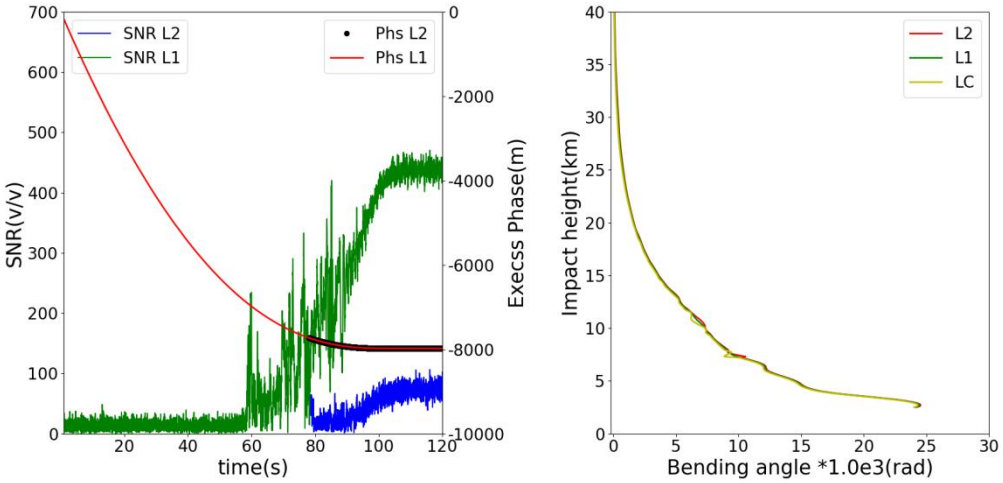

Figure 4.

9. Page 6 line 7-Is Culverwell and Healy really unpublished if it is a ROM SAF report? I suggest deleting (unpublished).

Author's response: This work is based on the work of Culverwell and Healy, which is an important source. Although it hasn't been published, we'd like to refer it as an informal report.

10. Figures 5 and 6-I know it is arbitrary, but it might be better to put the "before" panel on the left and the "after"panel on the right side of the figures. Also the labels and legends should be larger.

Author's response: Done.

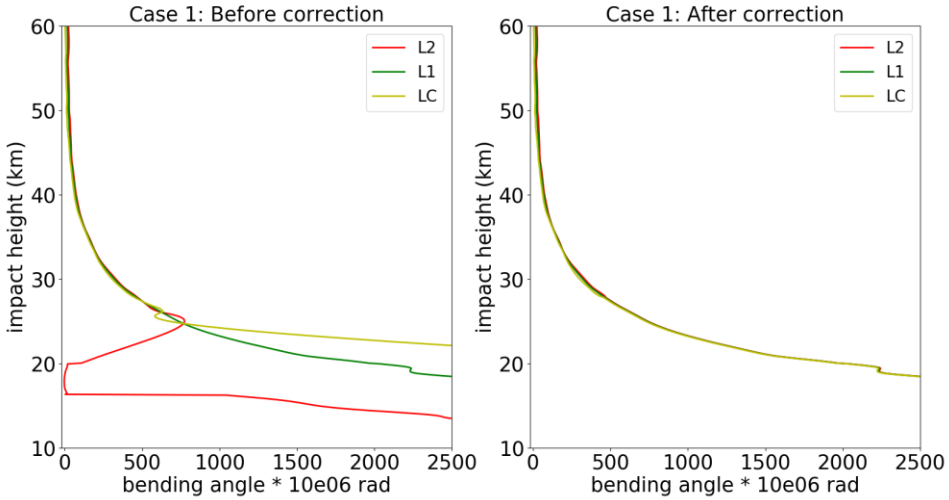

Figure 5. Case1: the bending angle of L2 (red), L1 (green) and LC (yellow) before (right) and after (left) correction.

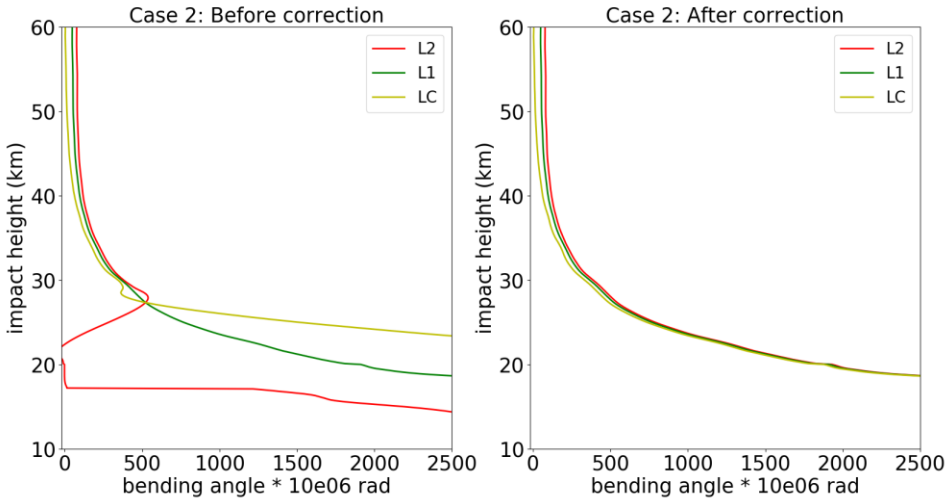

Figure 6. The same as Figure 5 but for Case 2.

11. Page 6 line 13: no period after Zeng.

Author's response: Done.

12. Page 7 line 14-reword to "L2 bending angles are very different from the L1 bending angles before correction." Line 16-reword to "..both the L1 and LC bending angles."

Author's response: Done.

13. The labels in Figs. 7 and 8 are a good size. Use this size in all the figures.

Author's response: Done.

14. Fig. 9-labels should be larger.

Author's response: Done.

15. Page 9 line 4-"noise_estimate" is sort of a 'clunky' name. Can you come up with a symbol or shorter name? Also, the left side of (4.1) is not quite the same as the name in the text. Line 26-additional rather than extra.

Author's response: Done. We will replace the "noise_estimate" as θ_α.

16. Page 10 lines 22-27-this discussion is confusing. It sounds like the %of "bad" profiles increases from 9.7% to 11.1% after QC. Please clarify and rewrite this paragraph.

Author's response: Combining other reviewers' comments, this part is not necessary and confusing; we decide to delete this part.

Changes in the manuscript: Reconsider the content of the file, we decide to keep this part. We carried out the statistics using more samples (three months of data) and reworded this part. Please see the track version from p10 to p11.

17. Page 12 line 9-when the L2 signal… Line 13-see comment #9 above Line 26-…by comparing with the background bending angles computed form the operational ECMWF forecasts.

Author's response: Done.

18. Page 13 line 10-reword to "We express our appreciation to…"

Author's response: Done.

Processing and quality control of FY-3C/GNOS data used in numerical weather prediction applications

Mi Liao[1], **Sean Healy[2]**, Peng Zhang[1]

[1] National Satellite Meteorological Center, Beijing, China

[2] European Centre for Medium-Range Weather Forecasts, Reading, UK

Correspondence to:

Sean Healy (sean.healy@ecmwf.int), Peng Zhang (zhangp@cma.gov.cn)

Abstract

The Chinese radio occultation sounder GNOS (Global Navigation Occultation Sounder) is on the FY-3C satellite, which was launched on September 23, 2013. Currently, GNOS data is transmitted via the Global Telecommunications System (GTS) providing 450 – 500 profiles per day for numerical weather prediction applications. This paper describes the processing for the GNOS profiles with large biases, related to L2 signal degradation. A new extrapolation procedure in bending angle space corrects the L2 bending angles, using a thin ionosphere model, and the fitting relationship between L1 and L2. We apply the approach to improve the L2 extrapolation of GNOS. The new method can effectively eliminate about 90% of the large departures. In addition to the procedure for the L2 degradation, this paper also describes our quality control (QC) for FY-3C/GNOS. A noise estimate for the new L2 extrapolation can be used as a QC parameter to evaluate the performance of the extrapolation. Mean phase delays of L1 and L2 in the tangent height interval of 60 to 80 km are analysed and applied in the QC as well. A statistical comparison between GNOS bending angles and short-range ECMWF (European Centre for Medium-Range Weather Forecasts) forecast ~~data~~ bending angles demonstrates that GNOS performs almost as well as GRAS, especially in the core region from around 10 to 35 km. The GNOS data with the new L2 extrapolation is suitable for assimilation into numerical weather prediction systems.

1 Introduction

GNOS is the first ~~Radio~~ radio ~~Occultation~~ occultation ~~(RO)~~ sounder on the Fengyun series of Chinese polar orbiting meteorological satellites. It is also the first multi-GNSS (Global Navigation Satellite System) RO receiver in orbit that can perform RO measurements from both GPS (Global Positioning System) and Chinese BDS (BeiDou Positioning System) signals. GNOS is manufactured by National Space Science Center (NSSC) of Chinese Academy Science (CAS), and is operated by the National Satellite Meteorological Center (NSMC) of the China Meteorological Administration (CMA). GNOS is also mounted on FY-3D (which was launched on November 2017) and it will be on all the subsequent Chinese Fengyun satellites. The FY-3 series is expected to provide GNOS RO measurements continuously at least until 2030 (Yang et al., 2012), so this is a potentially important source of data for numerical weather prediction (NWP) and climate reanalysis applications.

As a multi-GNSS receiver, GNOS has the ability of tracking up to eight GPS satellites and four BDS satellites for precise orbit determination (POD). In addition, it has velocity and anti-velocity antennas for simultaneously tracking at most six and four occultations from GPS and BDS, respectively. Because of the presence of two antennas in opposite directions, both the rising and setting occultations can be retrieved. More instrumental details are given in the Table 1, and in Bai et al. (2014). Currently, FY-3C GNOS GPS measurements can produce about 500 GPS-RO profiles per day for operational use in NWP systems, while GNOS from BDS signals are not yet operational, and produce only about 200 profiles because of fewer reference satellites.

As with the pre-existing GPS-RO sounders, such as the GPS/Met (Global Positioning System/Meteorology) experiment (Ware et al., 1996), the COSMIC (Constellation Observing System for Meteorology, Ionosphere, and Climate; Anthes et al., 2008), and the European Metop/GRAS (GNSS Receiver for Atmospheric Sounding) mission (Von Engeln et al., 2009), the raw observations from GNOS

consist of phase and signal to noise ratio (SNR) measurements. In addition, auxiliary information provided by the International GNSS Service (IGS), such as the GPS precise orbits, clock files, Earth orientation parameters, and the coordinates and measurements of the ground stations, are also needed. The IGS ultra rapid orbit products, with an approximate accuracy of 10 cm in orbit, are chosen for near-real-time operational use. The Low Earth Orbit (LEO) precise orbit determination (POD) can be estimated by integrating the equations of celestial motion (Beutler, 2005) using the Bernese software Version 5.0 (Dach et al., 2007). The single difference technique is applied to obtain the excess phase as a function of time in an Earth-centred inertial reference frame. The Radio Occultation Processing Package (ROPP) software (Version 6.0), developed by the EUMETSAT ROM SAF (Radio Occultation Meteorology Satellite Application Facility), is used to determine different ~~kinds of~~ atmospheric parameters (Culverwell et al., 2015). One-dimensional variational (1-D-Var) analysis, using background information from a T639L60 global forecast model, is used to retrieve temperature and humidity profiles. The T639L60 is a global medium-range weather forecast system of China, which became operational at CMA in 2009. However, since early 2017, some changes have been implemented in the operational stream. We obtain the auxiliary files through an ftp server in near real time provided by EUMETSAT GSN service, improving the timeliness to within three hours. In addition, the POD software was replaced by the PANDA (Positioning And Navigation Data Analyst), which is developed originally by the Wuhan university of China (Shi et al., 2008).

In the original operational stream, GPS-RO refractivity departure statistics were used in a preliminary check of data quality. Poor ~~quality~~ data ~~was~~ were filtered out with Quality Control (QC) based on the following rules. A profile is rejected if a fractional refractivity greater than 0.1 occurs at more than 20 % levels in the profile. In addition, the outliers on a specific level are then excluded if they exceed the three sigma from a statistical point of view. This QC excluded nearly 15% GNOS profiles. We found that most of the rejected profiles had large biases of up to 200%, in the vertical interval

between 5-30 km, peaking at around 20km, when compared to model data (Figure 1). These biases are not seen with other RO missions. It is known that GPS signal SNR falls with decreasing altitudes, and especially for the L2 frequency. Therefore, in some cases the linear combination (LC) of L1 and L2 bending angles can produce erroneous results. We found that the degradation of the GNOS L2 had a large impact on the retrieval quality when the measurements were processed with ROPP. Therefore, ~~in this work~~ we developed and tested a new L2 bending angle extrapolation method for GNOS data, and implemented it in ROPP. As a result of this work, the GNOS data ~~is~~ are now assimilated in operational NWP systems at, for example, the European Centre for Medium-Range Weather Forecasts (ECMWF), Deutscher Wetterdienst (DWD) and the Met Office.

In this paper, we will describe the new processing of GNOS data that reduces the large stratospheric biases in bending angle and refractivity, and present a quality control scheme for FY3C/GNOS. These results will be useful for understanding the statistical error characteristics and quality control of the GNOS data, and more generally the extrapolation approach may useful for other missions where one signal is lost early.

2 Large biases in the original GNOS processing

The ROPP software (Culverwell et al., 2015) is used to retrieve atmospheric parameters, such as bending angle, refractivity, dry temperature, temperature and humidity, from GNOS excess phase measurements. In the preliminary assessments for the FY-3C/GNOS GPS RO against NWP with the original processing system, it was found that the most obvious and prominent quality issue was the large departure biases, in the vertical range of 5-30 km, peaking at around 20km (Figure 1). The percentage of profiles ~~effected~~ affected was about 13~15%. This bias problem is not seen with other RO missions, and it was found to be related to GPS L2 signal tracking problems and the subsequent extrapolation of L2.

It was found that most of the bad cases are rising occultations, which is easy to

understand. To improve the tracking in the lower troposphere and the quality of rising occultations, open loop tracking is implemented for GNOS GPS L1 signal, but not for L2 (Ao et al., 2009). In general, ~~the~~ SNR falls under the complicated atmospheric conditions in troposphere because of atmospheric defocusing. The GPS L2 signal is modulated by a pseudo-random precision ranging code (P code) for the purpose of anti-spoofing. Although GPS L2 can be demodulated using the semi-codeless method, it will be at the expense of SNR and precision (Kursinski et al., 1997). Therefore, the performance of L2 signal tracking is not as good as that of L1, especially for the rising occultations. Figure 2 shows the lowest Straight Line Tangent Altitude (SLTA) percentages of L1 and L2 signals, for both the rising and the setting occultations. It shows that the lowest tracking height of L1 C/A of both the rising or setting measurements are reasonable (~~need to add references~~Sokolovskiy et al.,2001), with more than 98.5% profiles with a below zero SLTA. However, for the L2P, only 70% of the rising measurements reach below 20km. There are 24.8% of rising profiles stopping in the range of 20 ~70km, and 5.2% stopping above 70km, meaning effectively they contain no valid measurements. In contrast, 89.9% of setting occultations can get below 20km, which is better than the rising, but about 10% stop above that height. Those profiles that have bad L2 signal observations significantly affect the retrievals when using ROPP software to process the GNOS data. Figure 3 shows an example of GNOS performance in terms of excess phase, SNR, and bending angle for two bad cases where the L2 stops early. In these two cases, there are no valid L2 excess phase observations below 25km or 30km SLTA, respectively. However, there are L2 bending angles, extending to the near surface because of extrapolation within ROPP (ROM SAF, 2016). Although this ROPP extrapolation approach may be reasonable for other missions where L2 penetrates deeper, it does not appear to be valid for GNOS.

Figure 4 is the same as Figure 3 but for two good cases where the L2 measurements get to 20km SLTA. Compared with the bad cases, the good cases show deeper penetration for L2. Thus, the retrieved bending angles of L1, L2 and LC are overlapping, and show good consistency even at the lower part of the profiles.

带格式的：突出显示

带格式的：突出显示

带格式的：突出显示

3 New L2 extrapolation

As mentioned in the Section 2, some sort of extrapolation of the observed L2 signal is required before it can be combined with the L1 signal, in order to remove the ionospheric contribution to the bending. However, the current L2 extrapolation implemented in ROPP leads to obvious errors when processing GNOS RO data. Therefore, an alternative L2 extrapolation method has been implemented in the ROPP to solve the GNOS problem. The new approach is based on (unpublished) work by Culverwell and Healy (2015), who modelled the bending angles produced by a Chapman layer model ionosphere and other profiles, and established some basic theory for the relationship between fitting L1 and L2. The method adopted here is based on a "thin" ionospheric shell model, where the ionosphere approaches a Delta function, at a specified height (See section 3.1, Culverwell and Healy, 2015). Alternative approaches are described by Zeng. et al.~~, (2016)~~.

For a vertically localized region of refractivity, sited well above tangent points of interest, the ionospheric contribution to the bending angle, α, at frequency f can be simply expressed by (Eq. 2.6, Culverwell and Healy, 2015):

$$\alpha(a) = 2a\frac{k_4}{f^2}\int_a^\infty \frac{x n_e(x)}{(x^2-a^2)^{\frac{3}{2}}}dx \qquad (3.1)$$

where $x = nr$, is product of the refractive index, n, and radius value r, a is the impact parameter, $k_4 = \frac{e^2}{8\pi^2 m_e \varepsilon_0} = 40.3 m^3 s^{-2}$, and n_e is the electron number density. Commonly, the electron number density can be expressed in terms of the vertically integrated total electron content, TEC, which is defined as $TEC = \int n_e dr$. The equation above can be simplified by assuming a very narrow ionospheric shell and written as (Eq. 3.2, Culverwell and Healy, 2015):

$$\alpha(a) = 2a\frac{k_4}{f^2} TEC \frac{r_0}{(r_0{}^2-a^2)^{\frac{3}{2}}} \qquad (for\ a < r_0) \qquad (3.2)$$

r_0 is height of the peak electron density, which is assumed to be 300 km above the surface in this work.

The GPS L1 and L2 frequency bending angle difference is expressed as:

$$\alpha_2(a) - \alpha_1(a) = 2ak_4TEC\left(\frac{1}{f_2^2} - \frac{1}{f_1^2}\right)\frac{r_0}{(r_0{}^2 - a^2)^{\frac{3}{2}}} \qquad (3.3)$$

If we define $x_{so} = 2ak_4TEC\left(\frac{1}{f_2^2} - \frac{1}{f_1^2}\right)$, then,

$$\alpha_2(a) = \alpha_1(a) + x_{so}\frac{r_0}{(r_0{}^2 - a^2)^{\frac{3}{2}}} \qquad (3.4)$$

In this work we estimate x_{so} from a least-square fit based on observed L1 and L2 bending angle differences produced with geometrical optics, over a 20 km vertical above the lowest valid L2 bending angle value. The maximum height of the vertical interval is limited to be 70 km.

Two bad profiles, where the L2 signal stops above 20 km SLTA, have been chosen for demonstrating the extrapolation method. Their detailed information is listed in Table 2. Because the ionospheric effect becomes smaller in relative terms with the decreasing height, the magnitude of the relative L2-L1 bending angle differences gets smaller with height. Seen from the direct comparisons between the new and the old extrapolation results of case 1 (Figure 5 and 6), L2 bending angles are very different from the L1 bending angles before correction~~is very different to L1 before correction~~. After applying the new extrapolation approach, the L2 bending angles below 20 km are consistent with both L1 and LC bending angles. It is concluded that a more reliable LC bending angle can be obtained by using the new L2 extrapolation approach than the original L2 extrapolation method implemented in ROPP.

带格式的：突出显示

Clearly, using the new simple ionospheric model for the L2 extrapolation performs very well for the bad profiles with large biases. It is also useful to demonstrate the new extrapolation method for normal cases. Here the normal profiles are defined as the lowest SLTA reaching below 20 km, and the mean standard deviation to the reanalysis data is within 2% from surface to 35 km. Therefore, two good profiles (Table 3) are selected to test the new extrapolation.

Generally, the new extrapolation method does not degrade the good profiles. In fact, the new method smooths some occultation points, and improves the consistency of L1 and L2, as shown in Figure 7 and 8, for example.

An alternative way to demonstrate the accuracy of the different extrapolation methods is to compare their refractivity retrievals with the forecast model data. One day of data is used to test the new L2 extrapolation method. Figure 9 shows that the new method can effectively eliminate ~90 % of the problematic "branches" with the large percentage refractivity errors often are exceeding 100 %. In this plot, eight profiles still have a large bias after the new extrapolation, because the L2 SLTA stops above 70 km, which is out of the processing range used in the extrapolation (below 70 km). These cases can be removed by including some simple additional QC steps.

带格式的：突出显示

4 Quality control methods

Although the new L2 extrapolation method removes more than 90% poor quality profiles, there are still some profiles with obvious errors. Therefore, additional QC methods need to be implemented. Based on the GPS RO error sources and characteristics, many internal QC methods have proposed in the literature. For example, the COSMIC Data Analysis and Archive Center (CDAAC) define an altitude, *Z*, below which a low quality of L2 signal has been detected. The maximum difference of Ll and L2 bending angle above Z, and the ionospheric scintillation index analyzed from the amplitude of L1 signal at high altitudes are used in the QC (Kuo et al., 2004). Gorbunov (2002) proposed a QC procedure in terms of the analysis of the amplitude of the RO data transformed by the Canonical Transform (CT) or the Full Spectrum Inversion (FSI) method (Gorbunov and Lauritsen, 2004), which is useful to catch the corrupted data because of phase lock loop failures. Beyerle et al. (2004) also suggested a QC approach to reject the RO observations degraded by ionospheric disturbances based on the phase delay of L1 and L2 signals.

In light of the characteristics of GNOS RO data, we developed and tested some new internal QC methods to detect the poor quality profiles.

4.1 Noise estimate of the L1 and L2 fit

As noted earlier, as a result to L2 signal tracking problems, around 15% profiles are degraded with the old processing. After applying the new L2 extrapolation method, most of them can be effectively corrected. As seen from the Eq. 3.4, the key to the correction is how well the retrieved parameter, x_{so}, fits the difference of L1 and L2 bending angles in the 20km fitting interval. Currently, 25 km or the minimum L2 SLTA is the lower limit of the fitting interval.

We have introduced a new parameter, ~~NEF~~θ_α~~ means noise Noise_estimate Estimate of the Fit~~, to test the quality of the least-square fit in the 20 km interval. It can be expressed as:

带格式的：字体：倾斜

带格式的：字体：倾斜

$$\theta_\alpha \sim\sim noise\_estimate \sim\sim NEF = \frac{\sqrt{\sum\left(x_{so} * \frac{r_0}{\left(r_0^2 - a^2\right)^{\frac{3}{2}}} - \Delta\alpha(a)\right)^2}}{n} * 10^6 \quad (4.1)$$

Where $\Delta\alpha$ is the difference of L1 and L2 bending angles, and the sum is over the 20 km fitting interval. The physical meaning of θ_α~~NEF noise_estimate~~ is easy to understand. It is the standard deviation of the difference between the fit and observations. If the θ_α~~NEFnoise_estimate~~ is small, x_{so}, is fitted well, then the L2 extrapolation using the x_{so} is probably adequate.

A histogram of the θ_α~~NEFnoise_estimate~~ values has been obtained by accumulating statistics over a seven day period (Figure 10), and we use this to determine a QC threshold value. In the operational GNOS processing, if the value of the θ_α~~NEFnoise_estimate~~ is greater than 20 micro-radians, the profiles will be rejected. We have used one day of data to test the performance of the θ_α~~NEF noise_estimate~~ as a QC parameter, for detecting the large bias cases. The θ_α~~NEF noise_estimate~~ of the good profiles are highly focused on the values are below 20; while the θ_α~~NEF noise_estimate~~ of the bad profiles, with large biases, have the largest θ_α~~NEF noise_estimate~~ values. It demonstrates that setting the θ_α~~NEF noise_estimate~~ parameter threshold at 20 microradians can distinguish between many of the good and the bad GNOS cases. This parameter can be used as one factor, but other parameters are still needed to complete the QC.

4.2 Mean phase delays of L1 and L2

The θ_α ~~*noise_estimate NEF*~~ QC parameter does not detect all the poor quality profiles, and we need ~~extra~~ additional quality control methods to identify them. We find that it is also necessary to monitor the performance of GNOS mean L1 and L2 phase delays in the height interval of 60 to 80 km, because this can also indicate the observational quality of GPS RO data. However, the L1 and L2 SNR values, ~~that~~ which are commonly used as a QC indicator, are not found to be useful for identifying the large bias cases of GNOS data. For the rising profiles, the absolute accumulated phase delay should increase with height. Despite reasonable SNR above the height of 60km , in some cases the mean phase delays have small values, leading to problems in the inversions.

Figure 11 and Figure 12 show the histograms of the L1 and L2 mean delay phase in rising occultations. They show that there is a clear separation of the mean phase delays. To clarify the quality of the two groups of samples, we identify them as "GOOD" or "BAD" profiles. The criterion for good or bad is that the mean bias relative to the background data is smaller than or greater than 5% at the height interval of 10 to 40km, respectively. Figure 13 and 14 demonstrate the distribution of L1 and L2 mean phase delay. Different colour represents different overlap density, the dark blue is the lowest density and the dark red is the highest one. The colours between them represent increasing density. The "GOOD" samples gather around -8000 meters, while the "BAD" samples accumulate around -100 meters. Therefore, we can identify most of the bad rising occultations, when both L1 and L2 absolute mean phase values are smaller than –150 m. This threshold value is empirical considering the amount of the samples. Unavoidably, a small number of good profiles could be wrongly detected as well and few bad ones could be missed. Generally, the statistical performance is reasonable, as will be demonstrated in Section 4.3.~~relationship between the poor profiles and the mean phase delay of L1 and L2.~~

带格式的：缩进：首行缩进： 0 字符

~~Therefore, we can identify most of the bad rising occultations, when both L1 and L2 mean phase values are greater than - 150 m. Unavoidably, a few of the good profiles could be wrongly detected as well and few bad ones could be missed. However, the statistical performance is reasonable, as will be demonstrated in Section 4.3.~~

4.3 The statistical performance of the applied QC methods

After checking a number of QC parameters, we use the following three QC tests:

(1) If the occultation is rising, and the absolute~~both~~ mean phase delays of L1 and L2 are both smaller~~greater~~ than -150m, the profile will be identified as "bad";

(2) If the value of θ_α ~~*NEF noise estimate*~~ is greater than 20 microradians, the profile will be identified as "bad";

(3) If the lowest SLTA of L2 is greater than 50 km, the profile will be identified as "bad".

These have been tested with three months of data, as to whether they can identify the "good" or "bad" large bias cases. The criterion for good or bad is similar to those mentioned above that the mean bias relative to the background data is smaller than or greater than 2% at the height interval of 10 to 40km, respectively .

41,928 samples are collected from April 1 to June 30, 2018. There are 38,752 good profiles and 3,176 bad profiles evaluated by background data (e.g. The ECMWF reanalysis). The QC scheme applied in this paper identifies 37,627 good profiles and 4,301 bad ones. According to statistics, the number of profiles that can be accurately identified is 36,957, the accuracy rate is 95.4%, the number of missed is 1,795, the missed rate is 4.6%, 670 are misjudged, and the false positive rate is 1.8%. See Table 4 for clarification. Unavoidably, a small number of good profiles could be wrongly detected as well and few bad ones could be missed. In general, the performance of this kind of QC method can effectively identify most of the bad profiles.~~For example, t~~These have been tested with one day of data, as to whether they can identify the "bad" large bias cases. The percentage of the true bad profiles for one day is 9.7% of the data. After applying the QC method, the ratio of the profiles identified as "bad" is

~~11.1%. Unavoidably, a small number of good profiles could be wrongly detected as well and few bad ones could be missed. 8.0% of the bad profiles can be correctly identified, It can be correctly identified 8.0% of the bad profiles, which means 3.1% profiles are mistakenly identified and 1.7% of the profiles are still missing (Table 4). In general, the performance of this kind of QC method can effectively identify most of the bad profiles.~~

5 Comparison with ECMWF forecast data

This section demonstrates the performances of the comparison between the observational GNOS bending angles and the simulated ones using ECMWF short-range forecast data. GNOS bending angle profiles are those which are carried out using the new L2 extrapolation and quality controls mentioned in section 3 and section 4, respectively. The period is from 6th July to 2nd Aug. 2018. The ECMWF data used as the background is the state-of-the-art short-range forecast data with 137 vertical levels extending from surface to 0.01 hPa. Using the 2D bending angle forward operator, ECMWF forecast data can be projected into the bending angle space at the GNOS locations.

GNOS observations are provided BUFR format for NWP applications, with the bending angles given on 247 vertical levels from the surface to 60 km. To provide a context for the comparisons, Metop-A GRAS profiles from the same period are also selected as a benchmark. Figure 13 displays the mean bias for the GNOS and GRAS bending angle profiles both separated into rising and setting occultations, showing that GNOS and GRAS are very consistent with each other above 10 km. Figure 14 shows the standard deviation of the bending angle departures for the GNOS and GRAS. Their standard deviations are about 1% between 10 – 35 km, increasing to about 12% at 50 km and more than 15% below 5 km impact height. It is clear that the GNOS standard deviations are comparable to GRAS in the 10 - 40km interval. The difference in the 20 to 25 km interval is related to the transition from wave optics to geometric optics for the GNOS. The GRAS standard deviations are worse in the

troposphere but this is probably due to sampling; essentially GRAS is able to measure more difficult cases. Generally, the two datasets have similar error characteristics in terms of both the mean bias and standard deviation over most of the height interval, but especially in the GPS-RO core range between 10-35 km.

6 Conclusions

This study has focused on three main areas. Firstly, we have developed and tested a new L2 extrapolation for GNOS GPS-RO profiles. Secondly, we have investigated QC methods for GNOS after applying the new L2 extrapolation. Thirdly, we have estimated the bending angle departure statistics by comparing GNOS and ECMWF short-range forecast data. The main results are summarized below.

We have identified and investigated the GNOS GPS-RO cases that fail quality control with large bending angle departures, after the processing with the ROPP software. These large departures can be attributed to the GPS L2 signal tracking problems for signals that stop above 20 km in terms of SLTA, and the related L2 extrapolation. The percentage of the profiles with large departure is about 13~15%. Therefore, we focused on a better L2 extrapolation for GNOS when the L2 signal stops early. A new L2 extrapolation approach has been implemented in ROPP to mitigate the problem. (These modifications will be available in ROPP 9.1; see http://www.romsaf.org/ropp/) The main procedure is in bending angle space, and it is based on the (unpublished) study of Culverwell and Healy (2015). The new method can effectively remove about 90% of the large departures. The remaining poor cases are mostly due to the L2 being completely missing.

We have studied and established the quality control methods suitable for GNOS GPS-RO profiles after correcting the large departures. The new L2 extrapolation *NEF* ~~*noise_estimate*~~ value can be taken as a QC parameter to evaluate the performance of the extrapolation. It is the standard deviation of the difference between the fit and observations above the extrapolated height. The mean phase delays of L1 and L2 in the tangent height interval of 60 to 80 km are analysed and applied in the QC as well. The lowest SLTA of L2 is also set as a threshold to identify the bad profiles. Using

the parameters mentioned above, the QC method can correctly identify 95.4% of the profiles.~~identify 82.5% of the bad profiles with a mean bias is greater than 5%.~~

Finally, we have assessed the quality of the GNOS bending angles by comparing with the background bending angles computed from the operational ECMWF ~~short range~~ forecasts. GRAS profiles from the same period are selected as a benchmark. The departure statistics for the GNOS and GRAS bending angle profiles in terms of the mean bias and standard deviations are similar at most of the heights, especially in the GPS-RO core region between 10-35 km.

The GNOS measurements processed with methods outlined in this study have been assimilated into operational NWP systems since March 6, 2018.

Acknowledgments

This work was undertaken as part of a visiting scientist study funded by the Radio Occultation Meteorology Satellite Application Facility (ROM SAF), which is a decentralised processing centre under the European Organisation for the Exploitation of Meteorological Satellites (EUMETSAT).

We ~~have to~~ express ~~my~~ our appreciation to Christian Marquardt for his valuable suggestions with respect to the RO processing and QC methods. In addition, we want to thank Ian Culverwell and Chris Burrow for their discussions. Finally, we would like to thank the fund support of National Key R&D Program of China (No.*2018YFB0504900*) and Special Fund for Meteorology Research in the Public Interest (No.*201506074)*.

References

Anthes, R. A., Ector, D., Hunt, D. C., Kuo, Y.-H., Rocken, C., Schreiner, W. S., Sokolovskiy, S. V., Syndergaard, S., Wee, T.- K., Zeng, Z., Bernhardt, P. A., Dymond, K. F., Chen, Y., Liu, H., Manning, K., Randel, W. J., Trenberth, K. E., Cucurull, L., Healy, S. B., Ho, S.-P., McCormick, C., Meehan, T. K., Thompson, D.

C., and Yen, N. L.: The cosmic/formosat-3 mission: Early results, B. Am. Meteorol. Soc., 89, 313–333, 2008.

Ao, C. O., Hajj, G. A., Meehan, T. K., Dong, D., Iijima, B. A., Mannucci, J. A., and Kursinski, E. R.: Rising and setting GPS occultations by use of open-loop tracking, J. Geophys. Res., 114, D04101, doi:10.1029/2008JD010483, 2009.

Bai, W. H., Sun, Y. Q., Du, Q. F., Yang, G. L., Yang, Z. D., Zhang, P., Bi, Y. M., Wang, X. Y., Cheng, C., and Han, Y.: An introduction to the FY3 GNOS instrument and mountain-top tests, Atmos. Meas. Tech., 7, 1817–1823, doi:10.5194/amt-7-1817-2014, 2014.

Beutler, G.: Methods of Celestial Mechanics, Springer-Verlag, Berlin, Heidelberg, New York, Germany, USA, ISBN 3-211- 82364-6, 2005.

Beyerle, G., 1. Wickert., T Schmidt, and C. Reigber., Atmospheric sounding by GNSS radio occultation: An analysis of the negative refractivity bias using CHAMP observations, J Geophys.Res., 109, D01106, doi:10.102912003JD003922,2004.

Culverwell, I. D. and S. B. Healy: Simulation of L1 and L2 bending angles with a model ionosphere, ROM SAF Report 17, 2015. Available at http://www.romsaf.org/general-documents/rsr/rsr_17.pdf, 2015.

Culverwell, I. D., Lewis, H. W., Offiler, D., Marquardt, C., and Burrows, C. P.: The Radio Occultation Processing Package, ROPP, Atmos. Meas. Tech., 8, 1887-1899, https://doi.org/10.5194/amt-8-1887-2015, 2015.

Dach, R., Hugentobler, U., Fridez, P., and Meindl, M.: Bernese GPS Software Version 5.0. Astronomical Institute, University of Bern, Switzerland, 2007.

Gorbunov, M. E.: Ionospheric correction and statistical optimization of radio occultation data, Radio Sci., 37, 17-1–17-9, doi:10.1029/2000RS002370, 2002.

Gorbunov, M. E. and Lauritsen, K. B.: Analysis of wave fields by Fourier Integral Operators and their application for radio occultations, Radio Sci., 39, RS4010, doi:10.1029/2003RS002971, 2004.

Kuo, Y.-H., Wee, T.-K., Sokolovskiy, S., Rocken, C., Schreiner, W., Hunt, D., and Anthes, R. A.: Inversion and error estimation of GPS radio occultation data, J.

Meteor. Soc. Japan, 82, 507–531,2004.

Kursinski, E. R., Hajj, G. A., Hardy, K. R., Schofield, J. T., and Lin- field, R.: Observing Earth's atmosphere with radio occultation measurements, J. Geophys. Res., 102, 23429–23465, 1997.

ROM SAF http://www.romsaf.org/product_documents/romsaf_atbd_ba.pdf, 2016.

Shi C, Zhao Q, Lou Y. Recent development of PANDA software in GNSS data processing[J]. Proc. SPIE, 7285:231-249, 2008.

Sokolovskiy, S. V., Tracking tropospheric radio occultation signals from low Earth orbit, Radio Sci., 36(3), 483– 498, 2001.

Von Engeln, A., Healy, S., Marquardt, C., Andres, Y., and Sancho, F.: Validation of operational GRAS radio occultation data, Geo- phys. Res. Lett., 36, L17809, doi:10.1029/2009GL039968, 2009.

Ware, R., Rocken, C., Solheim, F., Exner, M., Schreiner, W., An- thes, R., Feng, D., Herman, B., Gorbunov, M., Sokolovskiy, S., Hardy, K., Kuo, Y., Zou, X., Trenberth, K., Meehan, T., Melbourne, W., and Businger, S.: GPS sounding of the atmosphere from lower Earth orbit: preliminary results, B. Am. Meteorol. Soc., 77, 19–40, 1996.

Yang, J., Zhang, P., Lu, N.-M., Yang, Z.-D., Shi, J.-M., and Dong, C.-H.: Improvements on global meteorological observations from the current Fengyun 3 satellites and beyond, Int. J. Digital Earth, 5, 251–265, 2012.

Zeng.Z., Sokolovskiy,S., Schreiner,W., Hunt,D., Lin,J., and Kuo,Y.-H.: Ionospheric correction of GPS radio occultation data in the troposphere, Atmos. Meas. Tech., 9, 335–346, 2016.

Table 1 Main instrumental parameters for FY-3C/GNOS

Parameters	FY-3C/GNOS
Orbit Height	~836 km
Orbit Type	sun synchronous
Spacecraft mass	~750kg
Instrument mass	7.5kg
Constellation	GPS L1 C/A, L2 P
	BDS B1I,B2I
Channels	GPS：14 BDS：8
Sampling	POD 1Hz
	ATM.occ. (closed loop)50Hz
	ATM.occ.(open loop) 100 Hz
	ION occ. 1Hz
Open loop	GPS L1 C/A
Clock stability	1×10－12（1secAllan）
Pseudo-range precision	≤30cm
Carrier phase precision	≤2mm
Beam width of atmosphere occultation antenna	≥±30°(azimuth)

Table 2. Details of the selected bad occultations

No.	Occ. time (yymmdd.hhmm)	Longitude (deg.)	Latitude (deg.)	Occ. direction	SLTA_L2 (km)
1	170128.0332	-99.154	25.070	rising	21.917
2	170128.0740	24.705	-4.222	rising	25.793

Table 3. Details of the good profiles

No.	Occ. time (yymmdd.hhmm)	Longitude (degree)	Latitude (degree)	Occ. direction	SLTA_L2 (km)
1	20170128.0103	149.508	-38.445	rising	4.011
2	20170128.0251	70.857	-51.463	rising	12.928

~~Table 4. The 2×2 table values~~

		~~Bad case (True)~~	
		~~YES~~	~~NO~~
~~Bad case (Identified by QC parameters)~~	~~YES~~	~~8.0% (hits)~~	~~3.1%(false identified)~~
	~~NO~~	~~1.7%(misses)~~	~~87.2%(correct negatives)~~

Table 4. The 2×2 table values

		Evaluated by background data	
		GOOD (38752 profiles)	BAD (3176 profiles)
Identified by QC parameters	GOOD (37627 profiles)	36957 (hits)	670(misses)
	BAD (4301 profiles)	1795(false identified)	2506(correct negatives)

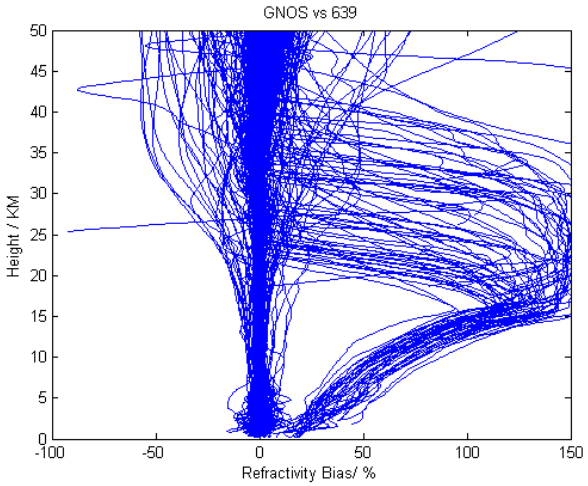

Figure 1. FY-3C/ GNOS GPS refractivity bias compared to T639 (the Chinese forecast model data), on 28th Jan.2017 with 489 samples.

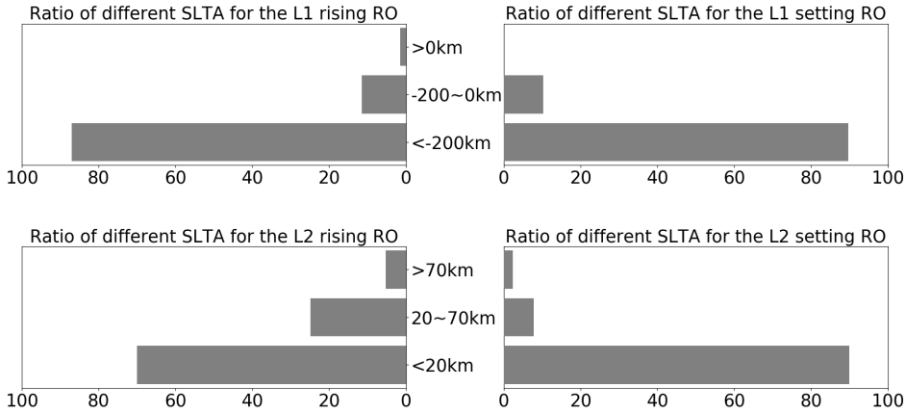

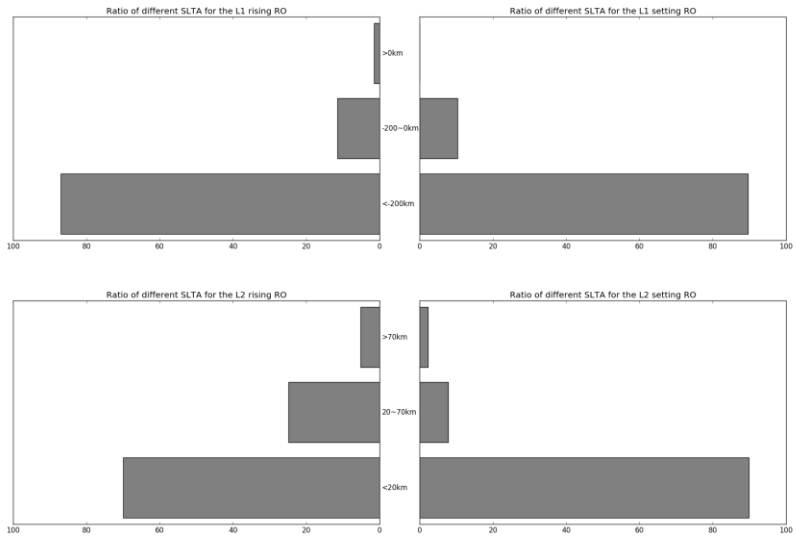

Figure 2. Ratio of different SLTA of the L1 C/A and L2 P for the rising and setting occultations, statistics result is from 28th Jan to 2nd Feb. 2017.

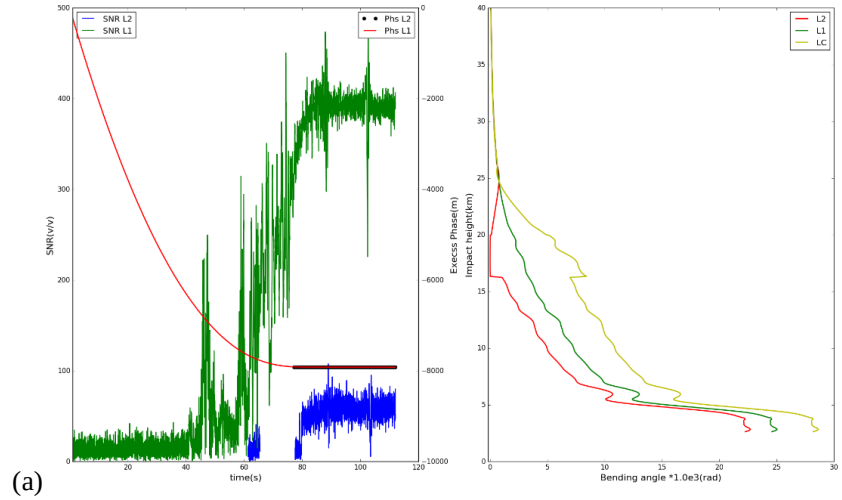
SNR L2
SNR L1
Phs L2
Phs L1
SNR(v/v)
Execss Phase(m)
time(s)
L2
L1
LC
Impact height(km)
Bending angle *1.0e3(rad)

(a)

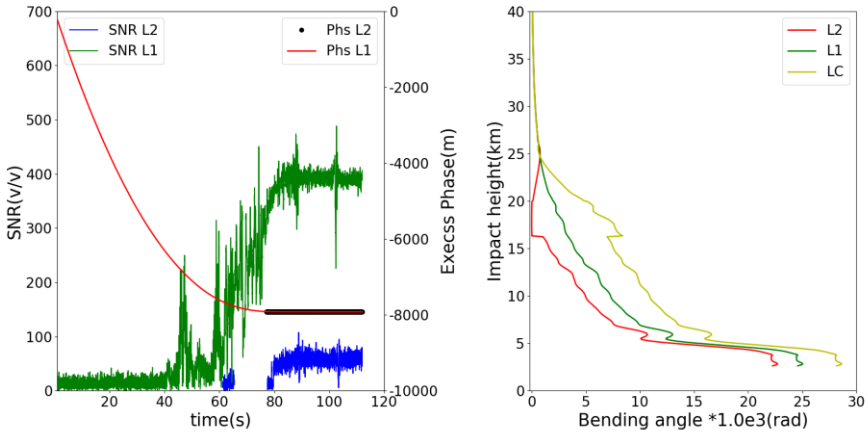
SNR L2
SNR L1
Phs L2
Phs L1
SNR(v/v)
Execss Phase(m)
time(s)
L2
L1
LC
Impact height(km)
Bending angle *1.0e3(rad)

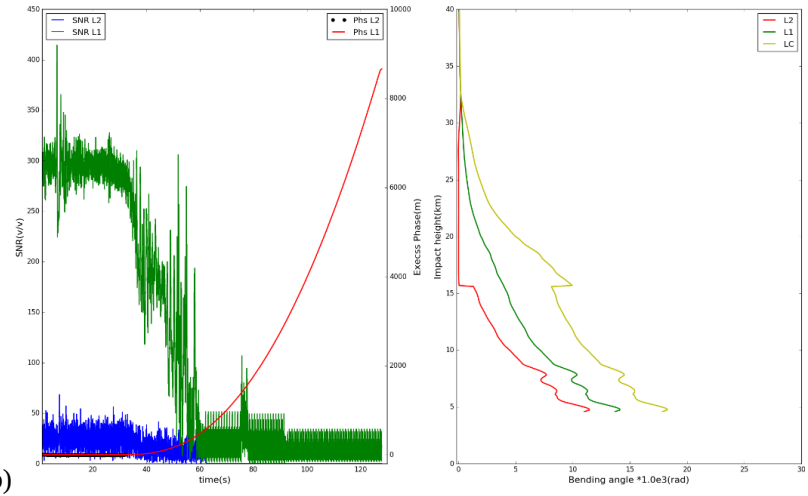
SNR L2
SNR L1
Phs L2
Phs L1
SNR(v/v)
Execss Phase(m)
time(s)
L2
L1
LC
Impact height(km)
Bending angle *1.0e3(rad)

(b)

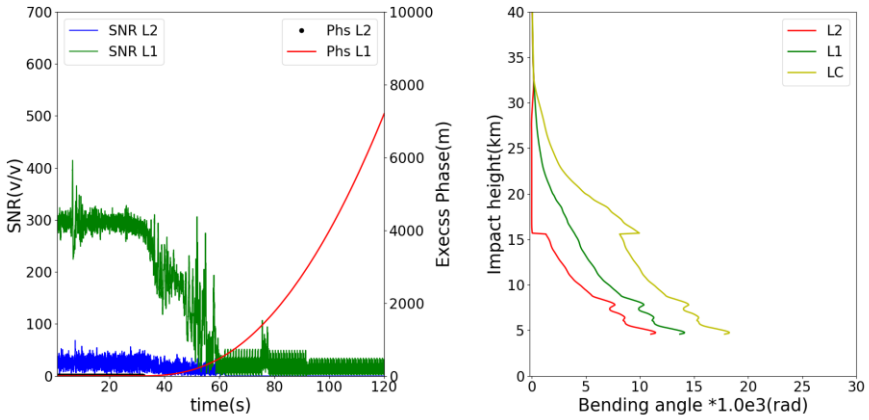

Figure 3. Two bad cases (a) A rising profile (FY3C_GNOSX_GBAL_L1_20170128_0332_AEG15_MS.NC), (b) a setting profile (FY3C_GNOSX_GBAL_L1_20170128_0850_AEG18_MS.NC). Example L1 (red) and L2 (black) SNR and excess phase measured data. The resulting L1 bending angle (green), L2 bending angle (red), and LC bending angle (yellow) profiles as a function of impact parameter computed using ropp_pp routines.

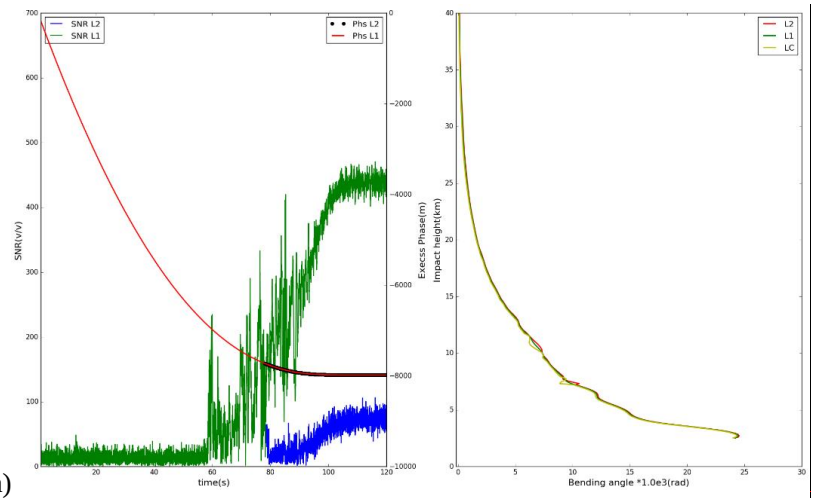

(a)

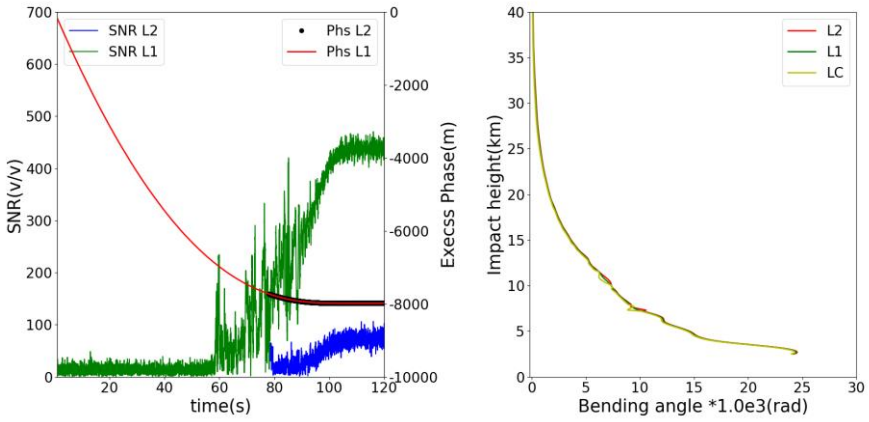

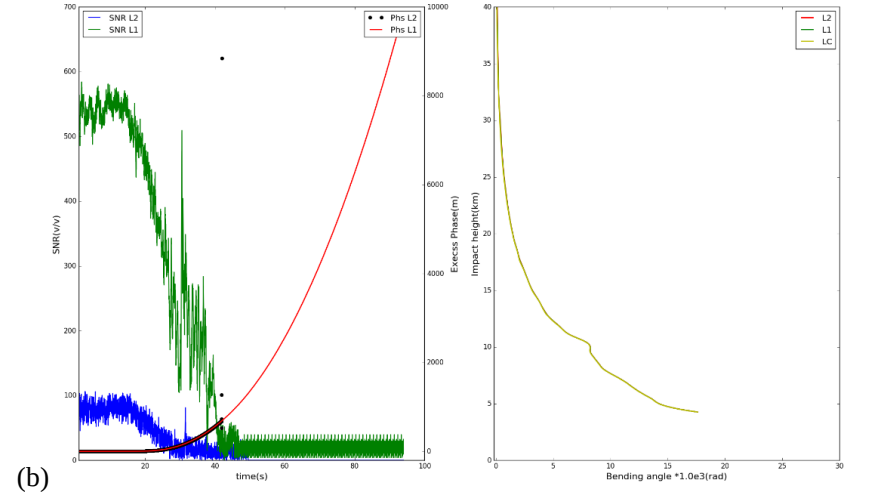

(b)

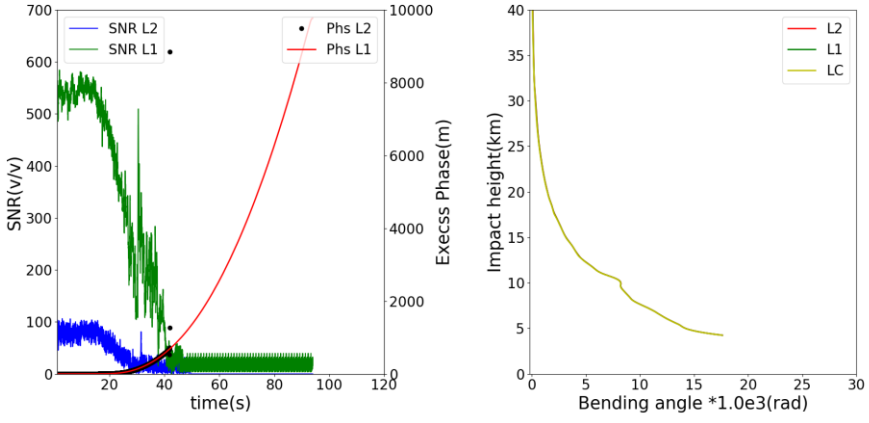

Figure 4. Two good cases (a) A rising profile (FY3C_GNOSX_GBAL_L1_20170128_1138_AEG27_MS.NC), (b) a setting profile

(FY3C_GNOSX_GBAL_L1_20170128_1648_AEG31_MS.NC). Example L1 (red) and L2 (black) SNR and excess phase measured data. The resulting L1 bending angle (green), L2 bending angle (red), and LC bending angle (yellow) profiles as a function of impact parameter computed using ROPP routines.

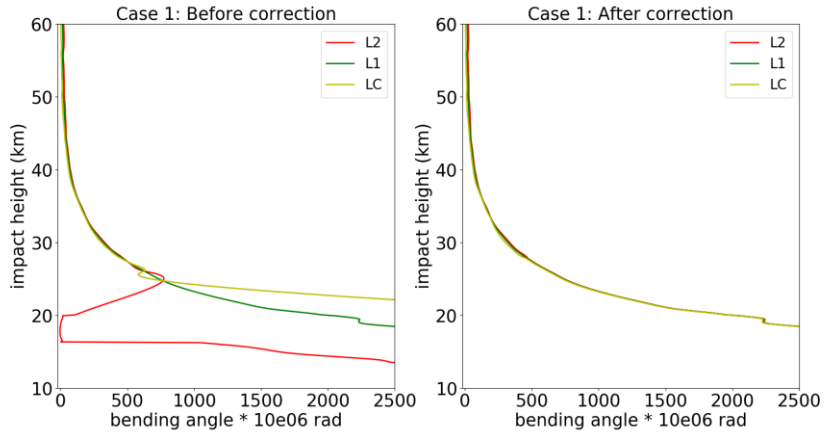

Figure 5. Case1: the bending angle of L2 (red), L1 (green) and LC (yellow) before (right) and after (left) correction.(FY3C_GNOSX_GBAL_L1_20170128_0332_AEG15_MS.NC)

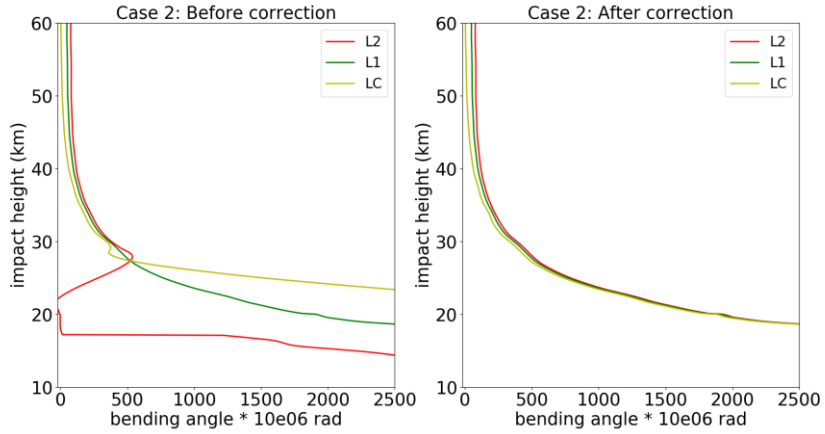

Figure 6. The same as Figure 5 but for Case 2.
(FY3C_GNOSX_GBAL_L1_20170128_0850_AEG18_MS.NC)

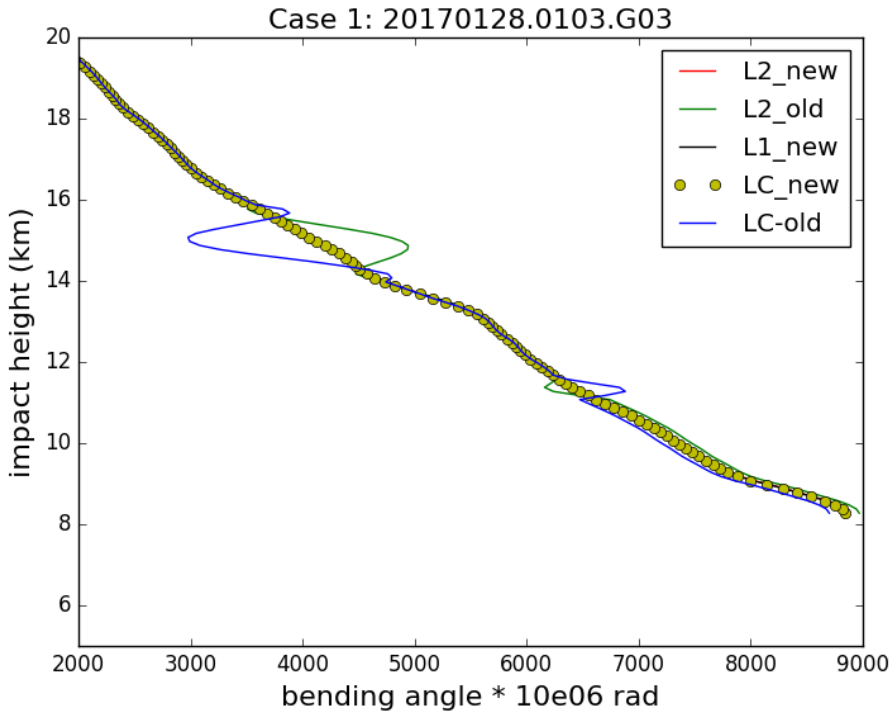

Figure 7. Good Case 1: the bending angle of L2, L1 and LC before and after correction.

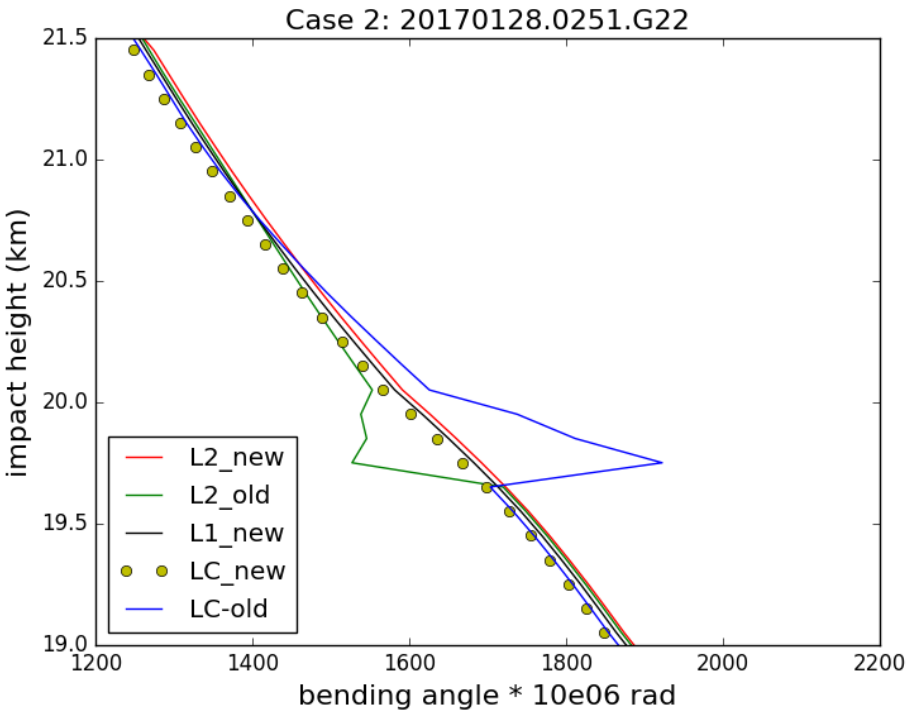

Figure 8. Good Case2: the bending angle of L2, L1 and LC before and after correction.

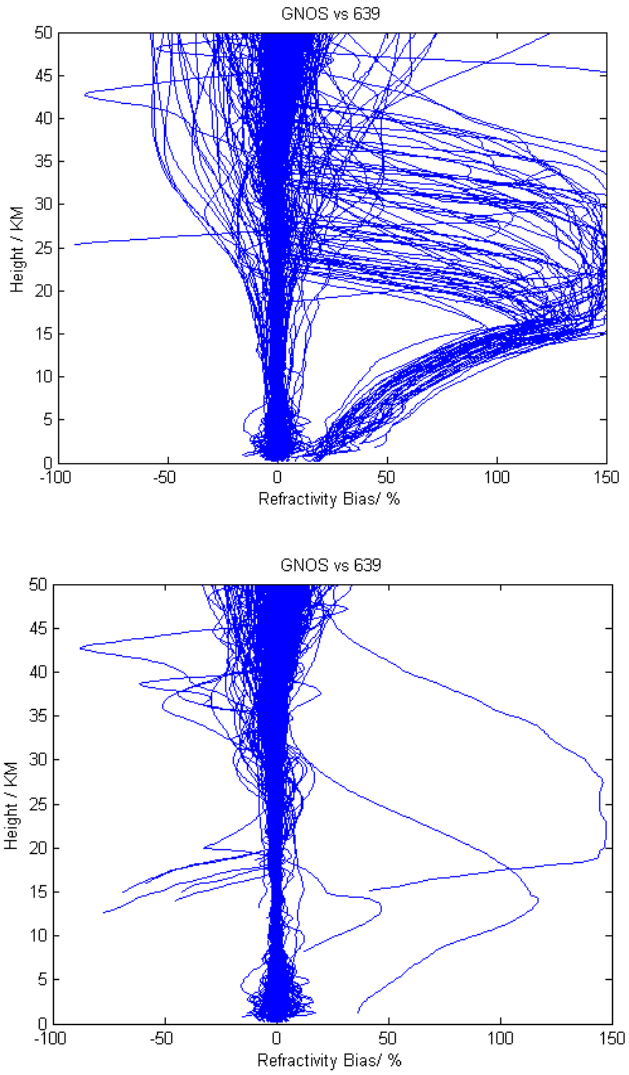

Figure 9. FY-3C/ GNOS GPS refractivity bias compared to T639 (the Chinese forecast model data), on 28th Jan.2017 with 489 samples. The upper plot reproduces Figure 1 and is the result of the original GNOS GPS data, and the lower plot isafter implementing the new L2 extrapolation approach.

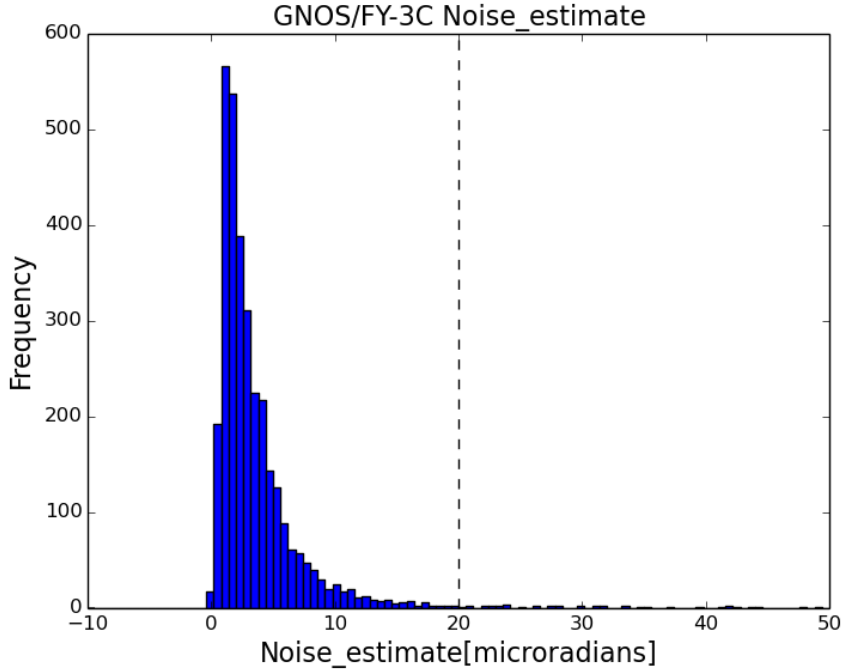

Figure 10. The histogram of the *noise_estimate* parameter using seven days of data from 16th Feb. to 22nd Feb 2017

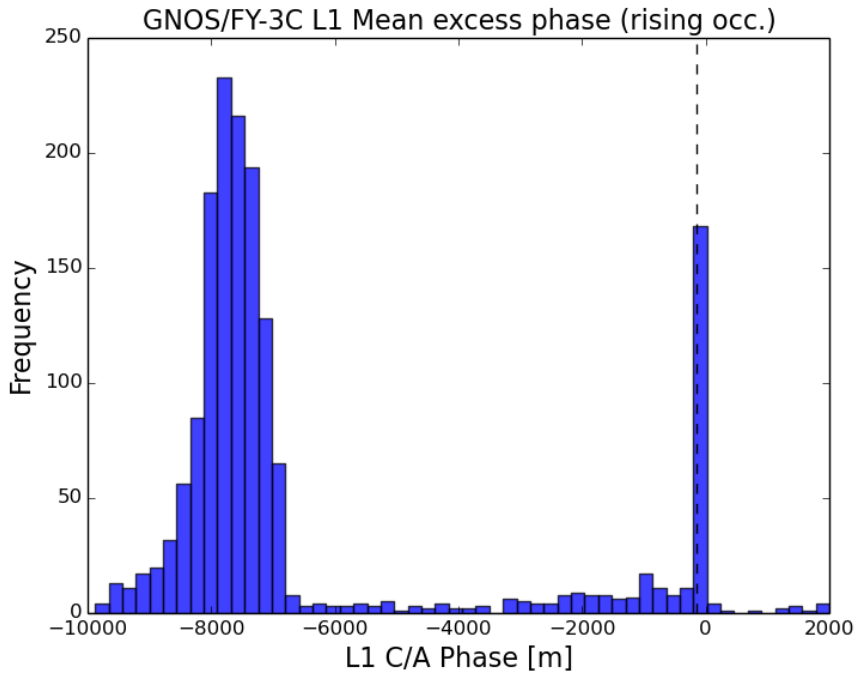

Figure 11. The histograms of L1 mean excess phase for the rising occultation at the height of 60 – 80 km SLTA using seven days of data from 16th Feb. to 22nd Feb.2017.

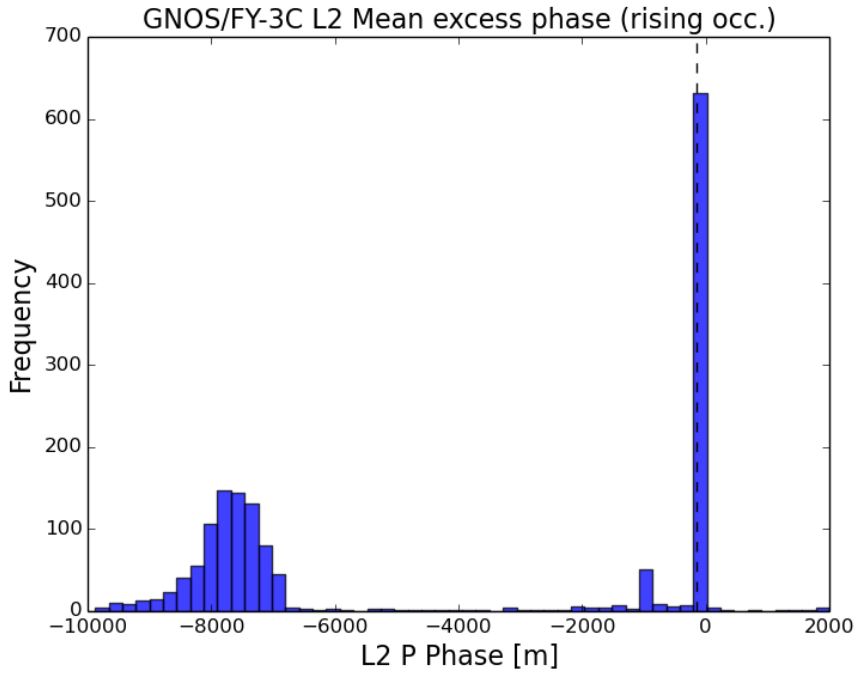

Figure 12. The histograms of L2 mean excess phase for the rising occultation at the height of 60 – 80 km SLTA using seven days of data from 16th Feb. to 22nd Feb.2017.

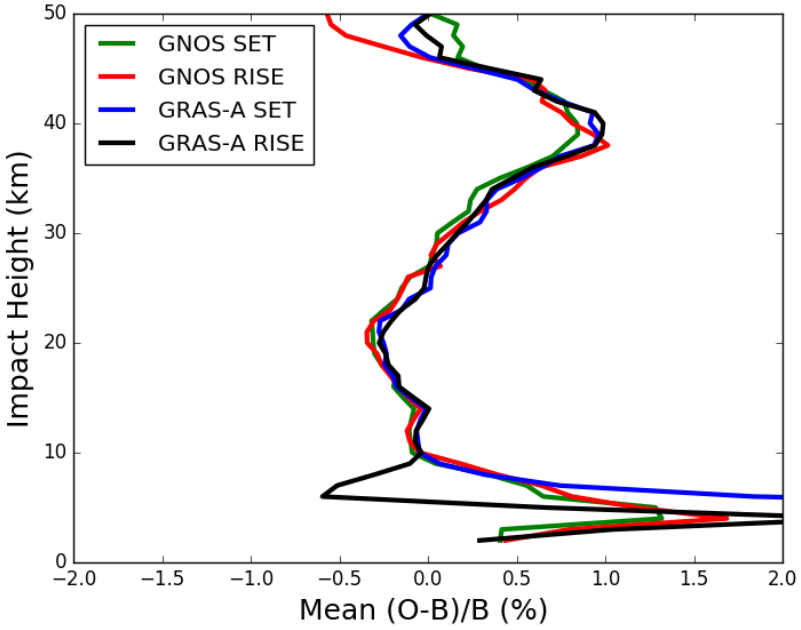

Figure 13. Global bending angle departure results, as a function of impact height, for the mean bias. The green, red, blue and black lines are representative of setting occultation for GNOS, rising occultation for GNOS, setting occultation for GRAS and rising occultation for GRAS.

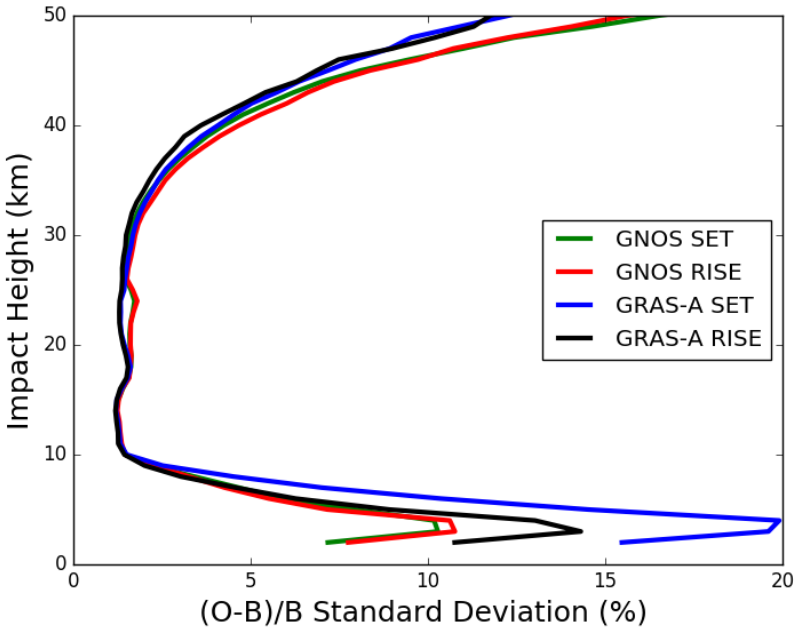

Figure 14. Global bending angle departure results, as a function of impact height, for the standard deviation. The green, red, blue and black lines are representative of setting occultation for GNOS, rising occultation for GNOS, setting occultation for GRAS and rising occultation for GRAS.

For reviewer #2

1.

Reviewer's comment: Page 2 (lines 24-30), page 3 (lines 1–2): As with the pre-existing GPS-RO sounders…, the raw observations from GNOS consist of phase and signal to noise ratio (SNR) measurements. In addition, auxiliary information provided by the International GNSS Service (IGS), such as the GPS precise orbits, clock files, Earth orientation parameters, and the coordinates and measurements of the 1 ground stations, are also needed.

What about the navigation bits? Does Beidou have navigation bits, similar to GPS/GLONASS ones? If so, are they also provided for the precise demodulation?

Author's response: The navigation bits contain information concerning the satellite clock, the satellite orbit, the satellite health status, and various other data. Beidou have navigation bits too. IGS provides the Beidou navigation bits, but not in near real time. The timeliness can be about 7 days.

Changes in the manuscript: This is not shown in the revised manuscript. Because we believe it's not much related to the paper.

2.

Reviewer's comment: Page 3 (line 26): if they exceed the three sigma from a statistical point of view.

… if they exceed 3 times the standard deviation. How is the standard deviation defined?

Author's response: GNOS data is compared to background data, e.g. ECMWF reanalysis. The standard deviation is defined as $\mathrm{std} = \frac{\sqrt{\sum(x_i - \bar{x})^2}}{n}$, n is number, $x_i = \left(\frac{O-B}{B}\right) * 100\%$, $\bar{x}$ is the average of x_i.

Changes in the manuscript: This part is overlapped with the first part of the section 2. For better elaboration, we decide to delete this part in the revised manuscript. The correction is at p3 line 22-30 in the track changes version.

3.

Reviewer's comment: Page 4 (lines 4–6): Therefore in this work we developed and tested a new L2 bending angle extrapolation method for GNOS data, and implemented it in ROPP.

Once speaking about a "new" method of the L2 extrapolation, one must cite the papers describing the "old" extrapolation technique.

There may also be some other publications on this topic. These papers cited, the differences between the old and new approaches must be discussed. Is it the "old" extrapolation method that the authors call the "ROPP extrapolation"? Or does ROPP use a different method? What is the reason of the failure of the old extrapolation technique for the GNOS data?

Author's response: We agree that the "standard" ROPP should be described in more detail in the revised manuscript.

In the context of the difficulties processing GNOS data, ROPP includes a pre-processing step in order to correct degraded L2 data. The approach is based on Gorbunov et al (2005,2006), and it is used routinely for other GPS-RO missions. Briefly, smoothed L1 and L2 bending angle and impact parameters are computed. An impact height, PC, above which the L2 data is considered reliable, is estimated using an empirical "badness score". The empirical badness score at time t, is

defined as,

$$Q(t) = \left(\frac{\mathrm{abs}(\overline{p_1(t)} - \overline{p_2(t)})}{\Delta p_a} + \frac{\delta p_2(t)}{\Delta p_b}\right)^2$$

where δp_2 is a measure of the width of the L2 spectrum, $\overline{p_1(t)}$ and $\overline{p_2(t)}$ are the L1 and L2 impact parameters, respectively, computed from smoothed timeseries, Δp_a=200 m and Δp_b=150 m (See also, Eq. 11 Gorbunov et al, 2006 for a slightly modified form). The largest $Q(t)$ value in the impact height interval between 15 km to 50 km is stored as the badness score for the occultation, potentially for quality control purposes.

The mean L1 and L2 bending angle and impact parameters are then computed in a 2 km impact parameter interval directly above PC. Simulated L2 bending angles and impact parameters are computed by adding the mean (L2-L1) differences to both the L1 bending angle and impact parameter values, using the data in the 2 km interval. Simulated L2 and L1 phase values are then computed from these bending angles. Corrected L2 excess phase values are computed by merging the observed L2 phase above PC, with the simulated values below PC, using a smooth transition over 2 km, centred on PC. The corrected L2 phase values are subsequently used in the wave optics processing of the L2 signals.

A difficulty with the GNOS processing is related to determining the impact height PC, used for both the computation of the mean L1 and L2 differences, and defining the transition between observed and modelled L2 phase values. Although the "badness score" is used to determine PC, PC also has a maximum value (20 km). This is defined as the wave optics processing height (25 km) minus a 5 km "safety border". Therefore, the mean bending angles and impact parameters used in the L2-L1 correction can only be computed in a 2 km interval up to a maximum impact height of 22 km. Unfortunately, this is not high enough for GNOS L2 signals, with the result that the mean L2-L1 bending angle and impact parameters computed in the 2 km interval above PC are corrupted.

M. E. Gorbunov, K. B. Lauritsen, A. Rodin, M. Tomassini, and L. Kornblueh (2005), Analysis of the CHAMP Experimental Data on Radio-Occultation Sounding of the Earth's Atmosphere, Izvestiya, Atmospheric and Oceanic Physics, 41, No. 6, 726–740.

Gorbunov, M. E., K. B. Lauritsen, A. Rhodin, M. Tomassini, and L. Kornblueh (2006), Radio holographic filtering, error estimation, and quality control of radio occultation data, J. Geophys. Res., 111, D10105, doi:10.1029/2005JD006427.

Changes in the manuscript: We add the description for the failure of ROPP software processing GNOS observations in the section 1 and 2, at p4 line 1 to 20, p6 to p7 in the track changes version. 4.

Reviewer's comment: The paper by Zou and Zeng is in the reference list, but is not discussed nor referenced in the text. Please provide a comparative analysis of the old and new QC methods with the explanation of why the old QC methods are not sufficient for your data analysis. In particular, will the "badness score" introduced by Gorbunov et al. and successfully applied for CHAMP, COSMIC, METOP and other observations, be also useful for the FY3C/GNOS data analysis? If not, why?

Author's response: Thanks for the comments. More references will be cited and discussed in the revised manuscript. Originally, we'd like to find out a method to identify the quality of GNOS

profiles based on physical meaning and without using background data, just as the "badness score". When we look at the performance of "badness score", it is not suitable for GNOS (see fig1). The values of L2 badness score range from 15 to 1000 plus. The reason might be related to some empirical parameters. The explanation can be partly found in the previous answer. Other missions work well using "badness score" since the lowest straight line tangent altitude of L2 is low enough. When discussed with scientists from EUMETSAT, GRAS can get down to 15km for more than 90%. But it is not the case for GNOS. Only 70% of L2 signal can be reached below 20km. So the noise_estimate parameter as the quantity evaluation of the new L2 extrapolation method is used as a quality indicator, which could show the performance of L2 extrapolation and identify the bad profiles.

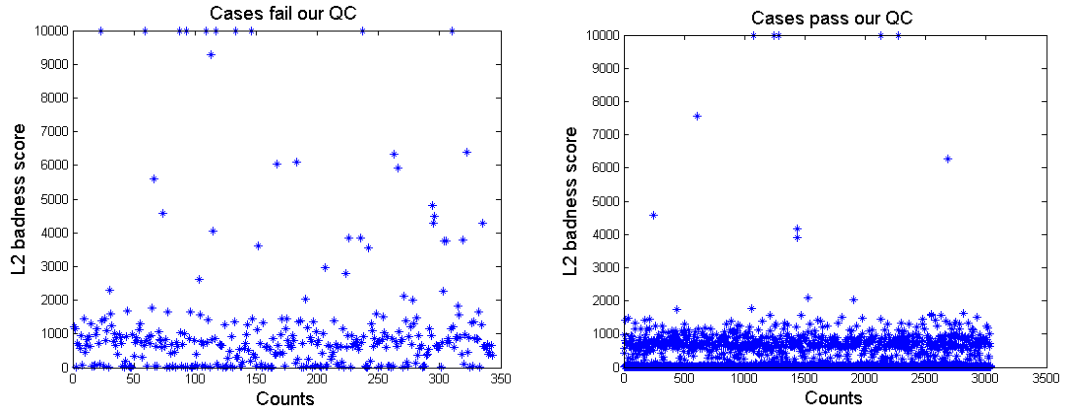

Fig 1. The cases of L2 badness score fail our QC and pass our QC

Changes in the manuscript: please see the p10, from Line 15 to 28 in the track changes version.

5.

Reviewer's comment: Page 9 (lines 3–7): The physical meaning of noise_estimate is easy to understand.

What is easy to understand is the fact that $\Delta\alpha$ is restricted to be close enough to its estimate obtained from a simple ionospheric model. Nevertheless, it is a good idea for the authors to explicitly mention this rather than appeal that something is "easy to understand". Still, some questions remain. Does n in formula (4.1) stay for refractivity of number of data? Number of data is definitely missing somewhere, because the sum in this formula needs to be normalized by the number of data. If n is refractivity, at what height is it taken? Provide explanations or definition regarding n.

Author's response: Thanks for the suggestion. n in formula 4.1 is the number of data. This will be fixed in the revised manuscript.

Changes in the manuscript: please see the p11, line 11 to 22 in the track changes version.

6.

Reviewer's comment: Page 11 (lines 21–22): The GRAS standard deviations are worse in the troposphere might due to sampling; essentially GRAS is able to measure more difficult cases. This statement needs more explanation. What are "more difficult cases"? Do they mostly occur in tropics? Can the authors provide any examples? Is it possible to evaluate a regionalized statistics (tropics, mid-, and polar latitudes)?

Author's response: The comparison between GRAS and GNOS is not the most important part of

the manuscript, thus a general remark is made. Regionalized statistics results can be seen in SC5 by Sean Healy. For more details of different kinds of statistics can be found on ROM SAF web pages. GNOS occultations are routinely available from the ROM SAF web pages. See, http://www.romsaf.org/monitoring/matched.php

Changes in the manuscript: Please see the p14 from line 9 to 22 in the track changes version.

Processing and quality control of FY-3C/GNOS data used in numerical weather prediction applications

Mi Liao[1], **Sean Healy[2]**, Peng Zhang[1]

[1] National Satellite Meteorological Center, Beijing, China

[2] European Centre for Medium-Range Weather Forecasts, Reading, UK

Correspondence to:

Sean Healy (sean.healy@ecmwf.int), Peng Zhang (zhangp@cma.gov.cn)

Abstract

The Chinese radio occultation sounder GNOS (Global Navigation Occultation Sounder) is on the FY-3C satellite, which was launched on September 23, 2013. Currently, GNOS data is transmitted via the Global Telecommunications System (GTS) providing 450 – 500 profiles per day for numerical weather prediction applications. This paper describes the processing for the GNOS profiles with large biases, related to L2 signal degradation. A new extrapolation procedure in bending angle space corrects the L2 bending angles, using a thin ionosphere model, and the fitting relationship between L1 and L2. We apply the approach to improve the L2 extrapolation of GNOS. The new method can effectively eliminate about 90% of the large departures. In addition to the procedure for the L2 degradation, this paper also describes our quality control (QC) for FY-3C/GNOS. A noise estimate for the new L2 extrapolation can be used as a QC parameter to evaluate the performance of the extrapolation. Mean phase delays of L1 and L2 in the tangent height interval of 60 to 80 km are analysed and applied in the QC as well. A statistical comparison between GNOS and ECMWF (European Centre for Medium-Range Weather Forecasts) forecast data demonstrates that GNOS performs almost as well as GRAS, especially in the core region from around 10 to 35 km. The GNOS data with the new L2 extrapolation is suitable for assimilation into numerical weather prediction systems.

1 Introduction

GNOS is the first Radio Occultation (RO) sounder on the Fengyun series of Chinese polar orbiting meteorological satellites. It is also the first multi-GNSS (Global Navigation Satellite System) RO receiver in orbit that can perform RO measurements from both GPS (Global Positioning System) and Chinese BDS (BeiDou Positioning System) signals. GNOS is manufactured by National Space Science Center (NSSC) of Chinese Academy Science (CAS), and is operated by the National Satellite Meteorological Center (NSMC) of the China Meteorological Administration (CMA). GNOS is also mounted on FY-3D (which was launched on November 2017) and it will be on all the subsequent Chinese Fengyun satellites. The FY-3 series is expected to provide GNOS RO measurements continuously at least until 2030 (Yang et al., 2012), so this is a potentially important source of data for numerical weather prediction (NWP) and climate reanalysis applications.

As a multi-GNSS receiver, GNOS has the ability of tracking up to eight GPS satellites and four BDS satellites for precise orbit determination (POD). In addition, it has velocity and anti-velocity antennas for simultaneously tracking at most six and four occultations from GPS and BDS, respectively. Because of the presence of two antennas in opposite directions, both the rising and setting occultations can be retrieved. More instrumental details are given in the Table 1, and in Bai et al. (2014). Currently, FY-3C GNOS GPS measurements can produce about 500 GPS-RO profiles per day for operational use in NWP systems, while GNOS from BDS signals are not yet operational, and produce only about 200 profiles because of fewer reference satellites.

As with the pre-existing GPS-RO sounders, such as the GPS/Met (Global Positioning System/Meteorology) experiment (Ware et al., 1996), the COSMIC (Constellation Observing System for Meteorology, Ionosphere, and Climate; Anthes et al., 2008), and the European Metop/GRAS (GNSS Receiver for Atmospheric Sounding) mission (Von Engeln et al., 2009), the raw observations from GNOS consist of phase and signal to noise ratio (SNR) measurements. In addition, auxiliary information provided by the International GNSS Service (IGS), such as the GPS

precise orbits, clock files, Earth orientation parameters, and the coordinates and measurements of the ground stations, are also needed. The IGS ultra rapid orbit products, with an approximate accuracy of 10 cm in orbit, are chosen for near-real-time operational use. The Low Earth Orbit (LEO) precise orbit determination (POD) can be estimated by integrating the equations of celestial motion (Beutler, 2005) using the Bernese software Version 5.0 (Dach et al., 2007). The single difference technique is applied to obtain the excess phase as a function of time in an Earth-centred inertial reference frame. The Radio Occultation Processing Package (ROPP) software (Version 6.0), developed by the EUMETSAT ROM SAF (Radio Occultation Meteorology Satellite Application Facility), is used to determine different kinds of atmospheric parameters (Culverwell et al., 2015). One-dimensional variational (1-D-Var) analysis, using background information from a T639L60 global forecast model, is used to retrieve temperature and humidity profiles. The T639L60 is a global medium-range weather forecast system of China, which became operational at CMA in 2009. However, since early 2017, some changes have been implemented in the operational stream. We obtain the auxiliary files through an ftp server in near real time provided by EUMETSAT GSN service, improving the timeliness to within three hours. In addition, the POD software was replaced by the PANDA (Positioning And Navigation Data Analyst), which is developed originally by the Wuhan university of China (Shi et al., 2008).

~~In the original operational stream, GPS-RO refractivity departure statistics were used in a preliminary check of data quality. Poor quality data was filtered out with Quality Control (QC) based on the following rules. A profile is rejected if a fractional refractivity greater than 0.1 occurs at more than 20 % levels in the profile. In addition, the outliers on a specific level are then excluded if they exceed the three sigma from a statistical point of view. This QC excluded nearly 15% GNOS profiles. We found that most of the rejected profiles had large biases of up to 200%, in the vertical interval between 5-30 km, peaking at around 20km, when compared to model data (Figure 1). These biases are not seen with other RO missions.~~ It is known that GPS signal SNR

falls with decreasing altitudes, and especially for the L2 frequency. Montenbruck (2003) and Bergeton (2005) tried to use high quality single frequency to process atmospheric radio occultations without the degraded L2 signal, but have limitations in the condition of high ionspheric oscillations. Dual-frequency for atmosphere radio occultation is still essential. Gorbonov developed an indicator (2005) to estimate the quality of L2 signal in the low atmosphere, and use it to judge where needs to linearly extrapolate the difference of L1 and L2 signal. Z.Zeng (2016) investigates the optimal height for the extrapolation of L1-L2 by modelling the ionospheric bending angle using an approximate expression. These methods are successfully applied for CHAMP,COSMIC, Metop and other missions. ~~Therefore, in some cases the linear combination (LC) of L1 and L2 bending angles can produce erroneous results. We found that~~However, the degradation of the GNOS L2 had a large impact on the retrieval quality when the measurements were processed with ROPP. ROPP includes a pre-processing step in order to correct degraded L2 data. The approach is based on Gorbunov et al (2005, 2006). The old approach in ROPP requires the L2 penetrating down into 20km at least. It is hard for GNOS to get the entire L2 signal down into 20km. The reason for GNOS losing L2 signal tracking is that GNOS has a lower SNR compared to other missions. Additionally, the GNOS antenna is smaller and not well located on the satellite. Consequently, we have to use additional cables, which results in a larger decrease of SNR than expected. Therefore, in this work we developed and tested a new L2 bending angle extrapolation method for GNOS data, and implemented it in ROPP. As a result of this work, the GNOS data is now assimilated in operational NWP systems at, for example, the European Centre for Medium-Range Weather Forecasts (ECMWF), Deutscher Wetterdienst (DWD) and the Met Office.

In this paper, we will describe the new processing of GNOS data that reduces the large stratospheric biases in bending angle and refractivity, and present a quality control scheme for FY3C/GNOS. These results will be useful for understanding the statistical error characteristics and quality control of the GNOS data, and more generally the extrapolation approach may useful for other missions where one signal is lost early.

2 Large biases in the original GNOS processing

The ROPP software (Culverwell et al., 2015) is used to retrieve atmospheric parameters, such as bending angle, refractivity, dry temperature, temperature and humidity, from GNOS excess phase measurements. In the preliminary assessments for the FY-3C/GNOS GPS RO against NWP with the original processing system, it was found that the most obvious and prominent quality issue was the large departure biases, in the vertical range of 5-30 km, peaking at around 20km (Figure 1). The percentage of profiles effected was about 13~15%. This bias problem is not seen with other RO missions, and it was found to be related to GPS L2 signal tracking problems and the subsequent extrapolation of L2.

It was found that most of the bad cases are rising occultations, which is easy to understand. To improve the tracking in the lower troposphere and the quality of rising occultations, open loop tracking is implemented for GNOS GPS L1 signal, but not for L2 (Ao et al., 2009). In general, the SNR falls under the complicated atmospheric conditions in troposphere because of atmospheric defocusing. The GPS L2 signal is modulated by a pseudo-random precision ranging code (P code) for the purpose of anti-spoofing. Although GPS L2 can be demodulated using the semi-codeless method, it will be at the expense of SNR and precision (Kursinski et al., 1997). Therefore, the performance of L2 signal tracking is not as good as L1, especially for the rising occultations. Figure 2 shows the lowest Straight Line Tangent Altitude (SLTA) percentages of L1 and L2 signals, for both the rising and the setting occultations. It shows that the lowest tracking height of L1 C/A of both the rising or setting measurements are reasonable, with more than 98.5% profiles with a below zero SLTA. However, for the L2P, only 70% of the rising measurements reach below 20km. There are 24.8% of rising profiles stopping in the range of 20 ~70km, and 5.2% stopping above 70km, meaning effectively they contain no valid measurements. In contrast, 89.9% of setting occultations can get below 20km, which is better than the rising, but about 10% stop above that height. Those profiles that have bad L2 signal observations

significantly affect the retrievals when using ROPP software to process the GNOS data.Figure 3 shows an example of GNOS performance in terms of excess phase, SNR, and bending angle for two bad cases where the L2 stops early. In these two cases, there are no valid L2 excess phase observations below 25km or 30km SLTA, respectively. However, there are L2 bending angles, extending to the near surface because of extrapolation within ROPP (ROM SAF, 2016). Although this ROPP extrapolation approach may be reasonable for other missions where L2 penetrates deeper, it does not appear to be valid for GNOS.

Figure 4 is the same as Figure 3 but for two good cases where the L2 measurements get to 20km SLTA. Compared with the bad cases, the good cases show deeper penetration for L2. Thus, the retrieved bending angles of L1, L2 and LC are overlapping, and show good consistency even at the lower part of the profiles.

ROPP includes a pre-processing step designed to correct degraded L2 data. The approach is based on Gorbunov et al (2005, 2006), and it is used successfully for other GPS-RO missions. Briefly, smoothed L1 and L2 bending angle and impact parameters are computed. An impact height, "PC", above which the L2 data is considered reliable, is estimated using an empirical "badness score". The empirical badness score at time t, is defined as,

$$Q(t) = \left(\frac{abs(\overline{p_1(t)} - \overline{p_2(t)})}{\Delta p_a} + \frac{\delta p_2(t)}{\Delta p_b}\right)^2 \quad (2.1)$$

where δp_2 is a measure of the width of the L2 spectrum, $\overline{p_1(t)}$ and $\overline{p_2(t)}$ are the L1 and L2 impact parameters, respectively, computed from smoothed timeseries, Δp_a=200 m and Δp_b=150 m (See also, Eq. 11 Gorbunov et al, 2006 for a slightly modified form). The largest $Q(t)$ value in the impact height interval between 15 km to 50 km is stored as the badness score for the occultation, potentially for quality control purposes.

The mean L1 and L2 bending angle and impact parameters are then computed in a 2 km impact parameter interval directly above PC. Simulated L2 bending angles and impact parameters are computed by adding the mean (L2-L1) differences to both the L1 bending angle and impact parameter values, using the data in the 2 km interval. Simulated L2 and L1 phase values are then computed from these bending angles. Corrected L2 excess phase values are computed by merging the observed L2 phase above PC, with the simulated values below PC, using a smooth transition over 2 km, centered on PC. The corrected L2 phase values are subsequently used in the wave optics processing of the L2 signals.

A specific difficulty with the GNOS processing is related to determining the impact height PC, used for both the computation of the mean L1 and L2 differences, and defining the transition between observed and modelled L2 phase values. Although the "badness score" is used to determine PC, PC also has a maximum value (20 km). This is defined as the wave optics processing height (25 km) minus a 5 km "safety border". Therefore, the mean bending angles and impact parameters used in the L2-L1 correction can only be computed in a 2 km interval up to a maximum impact height of 22 km. Unfortunately, this is not high enough for GNOS L2 signals, with the result that the mean L2-L1 bending angle and impact parameters computed in the 2 km interval above PC are corrupted, prior to the extrapolation.

3 New L2 extrapolation

As mentioned in the Section 2, some sort of extrapolation of the observed L2 signal is required before it can be combined with the L1 signal, in order to remove the ionospheric contribution to the bending. However, the current L2 extrapolation implemented in ROPP leads to obvious errors when processing GNOS RO data. Therefore, an alternative L2 extrapolation method has been implemented in the ROPP to solve the GNOS problem. The new approach is based on (unpublished) work by Culverwell and Healy (2015), who modelled the bending angles produced by a

Chapman layer model ionosphere and other profiles, and established some basic theory for the relationship between fitting L1 and L2. The method adopted here is based on a "thin" ionospheric shell model, where the ionosphere approaches a Delta function, at a specified height (See section 3.1, Culverwell and Healy, 2015). Alternative approaches are described by Zeng. et al., (2016).

For a vertically localized region of refractivity, sited well above tangent points of interest, the ionospheric contribution to the bending angle, α, at frequency f can be simply expressed by (Eq. 2.6, Culverwell and Healy, 2015):

$$\alpha(a) = 2a\frac{k_4}{f^2}\int_a^\infty \frac{xn_e(x)}{(x^2-a^2)^{\frac{3}{2}}}dx \qquad (3.1)$$

where $x = nr$, is product of the refractive index, n, and radius value r, a is the impact parameter, $k_4 = \frac{e^2}{8\pi^2 m_e \varepsilon_0} = 40.3m^3s^{-2}$, and n_e is the electron number density. Commonly, the electron number density can be expressed in terms of the vertically integrated total electron content, TEC, which is defined as $TEC = \int n_e dr$. The equation above can be simplified by assuming a very narrow ionospheric shell and written as (Eq. 3.2, Culverwell and Healy, 2015):

$$\alpha(a) = 2a\frac{k_4}{f^2}TEC\frac{r_0}{(r_0{}^2-a^2)^{\frac{3}{2}}} \qquad (for\ a < r_0) \qquad (3.2)$$

r_0 is height of the peak electron density, which is assumed to be 300 km above the surface in this work.

The GPS L1 and L2 frequency bending angle difference is expressed as:

$$\alpha_2(a) - \alpha_1(a) = 2ak_4TEC(\frac{1}{f_2^2} - \frac{1}{f_1^2})\frac{r_0}{(r_0{}^2-a^2)^{\frac{3}{2}}} \qquad (3.3)$$

If we define $x_{so} = 2ak_4TEC(\frac{1}{f_2^2} - \frac{1}{f_1^2})$, then,

$$\alpha_2(a) = \alpha_1(a) + x_{so}\frac{r_0}{(r_0{}^2-a^2)^{\frac{3}{2}}} \qquad (3.4)$$

In this work we estimate x_{so} from a least-square fit based on observed L1 and L2 bending angle differences produced with geometrical optics, over a 20 km vertical above the lowest valid L2 bending angle value. The maximum height of the vertical

interval is limited to be 70 km.

Two bad profiles, where the L2 signal stops above 20 km SLTA, have been chosen for demonstrating the extrapolation method. Their detailed information is listed in Table 2. Because the ionospheric effect becomes smaller in relative terms with the decreasing height, the magnitude of the relative L2-L1 bending angle differences gets smaller with height. Seen from the direct comparisons between the new and the old extrapolation results of case 1 (Figure 5 and 6), L2 is very different to L1 before correction. After applying the new extrapolation approach, the L2 bending angles below 20 km are consistent with both L1 and LC. It is concluded that a more reliable LC bending angle can be obtained by using the new L2 extrapolation approach than the original L2 extrapolation method implemented in ROPP.

Clearly, using the new simple ionospheric model for the L2 extrapolation performs very well for the bad profiles with large biases. It is also useful to demonstrate the new extrapolation method for normal cases. Here the normal profiles are defined as the lowest SLTA reaching below 20 km, and the mean standard deviation to the reanalysis data is within 2% from surface to 35 km. Therefore, two good profiles (Table 3) are selected to test the new extrapolation.

Generally, the new extrapolation method does not degrade the good profiles. In fact, the new method smooths some occultation points, and improves the consistency of L1 and L2, as shown in Figure 7 and 8, for example.

An alternative way to demonstrate the accuracy of the different extrapolation methods is to compare their refractivity retrievals with the forecast model data. One day of data is used to test the new L2 extrapolation method. Figure 9 shows that the new method can effectively eliminate ~90 % of the problematic “branches” with the large percentage refractivity errors often are exceeding 100 %. In this plot, eight profiles still have a large bias after the new extrapolation, because the L2 SLTA stops above 70 km, which is out of the processing range used in the extrapolation (below 70 km). These cases can be removed by including some simple additional QC steps.

4 Quality control methods

Although the new L2 extrapolation method removes more than 90% poor quality profiles, there are still some profiles with obvious errors. Therefore, additional QC methods need to be implemented. Based on the GPS RO error sources and characteristics, many internal QC methods have proposed in the literature. For example, the COSMIC Data Analysis and Archive Center (CDAAC) define an altitude, *Z*, below which a low quality of L2 signal has been detected. The maximum difference of Ll and L2 bending angle above Z, and the ionospheric scintillation index analyzed from the amplitude of L1 signal at high altitudes are used in the QC (Kuo et al., 2004). Gorbunov (2002) proposed a QC procedure in terms of the analysis of the amplitude of the RO data transformed by the Canonical Transform (CT) or the Full Spectrum Inversion (FSI) method (Gorbunov and Lauritsen, 2004), which is useful to catch the corrupted data because of phase lock loop failures. Beyerle et al. (2004) also suggested a QC approach to reject the RO observations degraded by ionospheric disturbances based on the phase delay of L1 and L2 signals. Zou et al (2006) use the bi-weight check, removing large departure data from the statistical point of view. More recently, Liu et al (2018) introduced a local spectral width based quality control, which improves the application in lower troposphere. The quality indicator "badness score" in ROPP is successfully applied for CHAMP, COSMIC, METOP and other observations. However, just like the failure of processing GNOS data, the badness score is not adequate for identifying the GNOS data. The reason might be related to the empirical parameters (see formula 2.1). These parameters are formed based on the performances of CHAMP, COSMIC and METOP missions, whose L2 signals are not degraded too much as GNOS. Considering the new L2 extrapolation method and the characteristics of GNOS data, we introduce a new indicator to detect the poor quality profiles based on the noise estimate of the L1 and L2 fit.

~~In light of the characteristics of GNOS RO data, we developed and tested some new internal QC methods to detect the poor quality profiles.~~

4.1 Noise estimate of the L1 and L2 fit

As noted earlier, as a result to L2 signal tracking problems, around 15% profiles are degraded with the old processing. After applying the new L2 extrapolation method, most of them can be effectively corrected. As seen from the Eq. 3.4, the key to the correction is how well the retrieved parameter, x_{so}, fits the difference of L1 and L2 bending angles in the 20km fitting interval. Currently, 25 km or the minimum L2 SLTA is the lower limit of the fitting interval.

We have introduced a new parameter, *noise_estimate*, to test the quality of the least-square fit in the 20 km interval. It can be expressed as:

$$noise_{\_estimate} = \frac{\sqrt{\sum(x_{so} * \frac{r_0}{(r_0{}^2 - a^2)^{\frac{3}{2}}} - \Delta\alpha(a))^2}}{n} * 10^6 \quad (4.1)$$

wWhere $\Delta\alpha$ is the difference of L1 and L2 bending angles, and the sum is over the n (L2-L1) values in the 20 km fitting interval. The parameter $noise_{\_estimate}$ is the root-mean-square of the difference between the fitting model and (L2-L1) values. Clearly, it provides information about how well we are able to fit the L2-L1 bending angle differences with the model, in a fitting interval where we trust the data. We assume that if the fitting model can reproduce the L2-L1 bending angle differences accurately in the fitting interval, we can then use the retrieved parameter x_{so} to extrapolate the L2-L1 differences below 25 km, to produce reasonable ionospheric corrected bending angles used for NWP applications. ~~20 km fitting interval. The physical meaning of *noise_estimate* is easy to understand. It is the standard deviation of the difference between the fit and observations. If the *noise_estimate* is small, x_{so}, is fitted well, then the L2 extrapolation using the x_{so} is probably adequate.~~

A histogram of the *noise_estimate* values has been obtained by accumulating statistics over a seven day period (Figure 10), and we use this to determine a QC threshold value. In the operational GNOS processing, if the value of the *noise_estimate* is greater than 20 micro-radians, the profiles will be rejected. We have used one day of data to test the performance of the *noise_estimate* as a QC parameter, for detecting the large bias cases. The *noise_estimate* of the good profiles are highly

focused on the values are below 20; while the *noise_estimate* of the bad profiles, with large biases, have the largest *noise_estimate* values. It demonstrates that setting the *noise_estimate* parameter threshold at 20 microradians can distinguish between many of the good and the bad GNOS cases. This parameter can be used as one factor, but other parameters are still needed to complete the QC.

4.2 Mean phase delays of L1 and L2

The *noise_estimate* QC parameter does not detect all the poor quality profiles, and we need extra quality control methods to identify them. We find that it is also necessary to monitor the performance of GNOS mean L1 and L2 phase delays in the height interval of 60 to 80 km, because this can also indicate the observational quality of GPS RO data. However, the L1 and L2 SNR values, that are commonly used as a QC indicator, are not found to be useful for identifying the large bias cases of GNOS data.

Figure 11 and Figure 12 show the histograms of the L1 and L2 mean delay phase in rising occultations. They show that there is a clear relationship between the poor profiles and the mean phase delay of L1 and L2. Therefore, we can identify most of the bad rising occultations, when both L1 and L2 mean phase values are greater than -150 m. Unavoidably, a few of the good profiles could be wrongly detected as well and few bad ones could be missed. However, the statistical performance is reasonable, as will be demonstrated in Section 4.3.

4.3 The statistical performance of the applied QC methods

After checking a number of QC parameters, we use the following three QC tests:

(1) If the occultation is rising, and the both mean phase delays of L1 and L2 are greater than -150m, the profile will be identified as “bad”;

(2) If the value of *noise_estimate* is greater than 20 microradians, the profile will

be identified as “bad”;

(3) If the lowest SLTA of L2 is greater than 50 km, the profile will be identified as “bad”.

For example, these have been tested with one day of data, as to whether they can identify the “bad” large bias cases. The percentage of the bad profiles for one day is 9.7% of the data. After applying the QC method, the ratio of the profiles identified as “bad” is 11.1%. It can be correctly identified 8.0% of the bad profiles, which means 3.1% profiles are mistakenly identified and 1.7% of the profiles are still missing (Table 4). In general, the performance of this kind of QC method can effectively identify most of the bad profiles.

5 Comparison with ECMWF forecast data

This section demonstrates the performances of the comparison between the observational GNOS bending angles and the simulated ones using ECMWF short-range forecast data. GNOS bending angle profiles are those which are carried out using the new L2 extrapolation and quality controls mentioned in section 3 and section 4, respectively. The period is from 6th July to 2nd Aug. 2018. The ECMWF data used as the background is the state-of-the-art short-range forecast data with 137 vertical levels extending from surface to 0.01 hPa. Using the 2D bending angle forward operator, ECMWF forecast data can be projected into the bending angle space at the GNOS locations.

GNOS observations are provided BUFR format for NWP applications, with the bending angles given on 247 vertical levels from the surface to 60 km. To provide a context for the comparisons, Metop-A GRAS profiles from the same period are also selected as a benchmark. Figure 13 displays the mean bias for the GNOS and GRAS bending angle profiles both separated into rising and setting occultations, showing that GNOS and GRAS are very consistent with each other above 10 km. Figure 14 shows the standard deviation of the bending angle departures for the GNOS and

GRAS. Their standard deviations are about 1% between 10 – 35 km, increasing to about 12% at 50 km and more than 15% below 5 km impact height. It is clear that the GNOS standard deviations are comparable to GRAS in the 10 - 40km interval. The difference in the 20 to 25 km interval is related to the transition from wave optics to geometric optics for the GNOS. The GRAS standard deviations are worse in the troposphere but this is probably due to sampling; essentially GRAS is able to measure more difficult cases. Generally, the two datasets have similar error characteristics in terms of both the mean bias and standard deviation over most of the height interval, but especially in the GPS-RO core range between 10-35 km. The standard deviations of the GNOS departures below 10 km are smaller than the GRAS statistics. However, we do not believe that this indicates that GNOS data is superior to GRAS below 10 km. In general, GRAS measurements tend to penetrate more deeply in the troposphere, and this will affect the statistical comparison with GNOS. Furthermore, the difference between the setting and rising GRAS statistics is known but not fully understood, and it is an area of current investigation. Nevertheless, we believe that Figures 15-16 provide evidence that the GNOS and GRAS measurements have similar performance in the "core region" as a result the processing and QC methods introduced here.

Note that further GNOS occultation departure statistics, including comparisons with other GPS-RO measurements in bending angle space, are now routinely available from the ROM SAF web pages.
See,http://www.romsaf.org/monitoring/matched.php

6 Conclusions

This study has focused on three main areas. Firstly, we have developed and tested a new L2 extrapolation for GNOS GPS-RO profiles. Secondly, we have investigated QC methods for GNOS after applying the new L2 extrapolation. Thirdly, we have estimated the bending angle departure statistics by comparing GNOS and ECMWF short-range forecast data. The main results are summarized below.

We have identified and investigated the GNOS GPS-RO cases that fail quality

control with large bending angle departures, after the processing with the ROPP software. These large departures can be attributed to the GPS L2 signal tracking problems for signals that stop above 20 km in terms of SLTA, and the related L2 extrapolation. The percentage of the profiles with large departure is about 13~15%. Therefore, we focused on a better L2 extrapolation for GNOS when L2 signal stops early. A new L2 extrapolation approach has been implemented in ROPP to mitigate the problem. (These modifications will be available in ROPP 9.1; see http://www.romsaf.org/ropp/) The main procedure is in bending angle space, and it is based on the (unpublished) study of Culverwell and Healy (2015). The new method can effectively remove about 90% of the large departures. The remaining poor cases are mostly due to the L2 being completely missing.

We have studied and established the quality control methods suitable for GNOS GPS-RO profiles after correcting the large departures. The new L2 extrapolation *noise_estimate* value can be taken as a QC parameter to evaluate the performance of the extrapolation. It is the standard deviation of the difference between the fit and observations above the extrapolated height. The mean phase delays of L1 and L2 in the tangent height interval of 60 to 80 km are analysed and applied in the QC as well. The lowest SLTA of L2 is also set as a threshold to identify the bad profiles. Using the parameters mentioned above, the QC method can identify 82.5% of the bad profiles with a mean bias is greater than 5%.

Finally, we have assessed the quality of the GNOS bending angles by comparing with operational ECMWF short-range forecasts. GRAS profiles from the same period are selected as a benchmark. The departure statistics for the GNOS and GRAS bending angle profiles in terms of the mean bias and standard deviations are similar at most of the heights, especially in the GPS-RO core region between 10-35 km.

The GNOS measurements processed with methods outlined in this study have been assimilated into operational NWP systems since March 6, 2018.

Acknowledgments

This work was undertaken as part of a visiting scientist study funded by the Radio Occultation Meteorology Satellite Application Facility (ROM SAF), which is a decentralised processing centre under the European Organisation for the Exploitation of Meteorological Satellites (EUMETSAT).

We have to express my appreciation to Christian Marquardt for his valuable suggestions with respect to the RO processing and QC methods. In addition, we want to thank Ian Culverwell and Chris Burrow for their discussions. Finally, we would like to thank the fund support of National Key R&D Program of China (No.*2018YFB0504900*) and Special Fund for Meteorology Research in the Public Interest (No.*201506074)*.

References

Anthes, R. A., Ector, D., Hunt, D. C., Kuo, Y.-H., Rocken, C., Schreiner, W. S., Sokolovskiy, S. V., Syndergaard, S., Wee, T.- K., Zeng, Z., Bernhardt, P. A., Dymond, K. F., Chen, Y., Liu, H., Manning, K., Randel, W. J., Trenberth, K. E., Cucurull, L., Healy, S. B., Ho, S.-P., McCormick, C., Meehan, T. K., Thompson, D. C., and Yen, N. L.: The cosmic/formosat-3 mission: Early results, B. Am. Meteorol. Soc., 89, 313–333, 2008.

Ao, C. O., Hajj, G. A., Meehan, T. K., Dong, D., Iijima, B. A., Mannucci, J. A., and Kursinski, E. R.: Rising and setting GPS occultations by use of open-loop tracking, J. Geophys. Res., 114, D04101, doi:10.1029/2008JD010483, 2009.

Bai, W. H., Sun, Y. Q., Du, Q. F., Yang, G. L., Yang, Z. D., Zhang, P., Bi, Y. M., Wang, X. Y., Cheng, C., and Han, Y.: An introduction to the FY3 GNOS instrument and mountain-top tests, Atmos. Meas. Tech., 7, 1817–1823, doi:10.5194/amt-7-1817-2014, 2014.

Beutler, G.: Methods of Celestial Mechanics, Springer-Verlag, Berlin, Heidelberg, New York, Germany, USA, ISBN 3-211- 82364-6, 2005.

Beyerle, G., 1. Wickert., T Schmidt, and C. Reigber., Atmospheric sounding by

GNSS radio occultation: An analysis of the negative refractivity bias using CHAMP observations, J Geophys.Res., 109, D01106, doi:10.102912003JD003922,2004.

Culverwell, I. D. and S. B. Healy: Simulation of L1 and L2 bending angles with a model ionosphere, ROM SAF Report 17, 2015. Available at http://www.romsaf.org/general-documents/rsr/rsr_17.pdf, 2015.

Culverwell, I. D., Lewis, H. W., Offiler, D., Marquardt, C., and Burrows, C. P.: The Radio Occultation Processing Package, ROPP, Atmos. Meas. Tech., 8, 1887-1899, https://doi.org/10.5194/amt-8-1887-2015, 2015.

Dach, R., Hugentobler, U., Fridez, P., and Meindl, M.: Bernese GPS Software Version 5.0. Astronomical Institute, University of Bern, Switzerland, 2007.

Gorbunov, M. E.: Ionospheric correction and statistical optimization of radio occultation data, Radio Sci., 37, 17-1–17-9, doi:10.1029/2000RS002370, 2002.

Gorbunov, M. E. and Lauritsen, K. B.: Analysis of wave fields by Fourier Integral Operators and their application for radio occultations, Radio Sci., 39, RS4010, doi:10.1029/2003RS002971, 2004.

Kuo, Y.-H., Wee, T.-K., Sokolovskiy, S., Rocken, C., Schreiner, W., Hunt, D., and Anthes, R. A.: Inversion and error estimation of GPS radio occultation data, J. Meteor. Soc. Japan, 82, 507–531,2004.

Kursinski, E. R., Hajj, G. A., Hardy, K. R., Schofield, J. T., and Lin- field, R.: Observing Earth's atmosphere with radio occultation measurements, J. Geophys. Res., 102, 23429–23465, 1997.

ROM SAF http://www.romsaf.org/product_documents/romsaf_atbd_ba.pdf, 2016.

Shi C, Zhao Q, Lou Y. Recent development of PANDA software in GNSS data processing[J]. Proc. SPIE, 7285:231-249, 2008.

Von Engeln, A., Healy, S., Marquardt, C., Andres, Y., and Sancho, F.: Validation of operational GRAS radio occultation data, Geo- phys. Res. Lett., 36, L17809, doi:10.1029/2009GL039968, 2009.

Ware, R., Rocken, C., Solheim, F., Exner, M., Schreiner, W., An- thes, R., Feng, D., Herman, B., Gorbunov, M., Sokolovskiy, S., Hardy, K., Kuo, Y., Zou, X.,

Trenberth, K., Meehan, T., Melbourne, W., and Businger, S.: GPS sounding of the atmosphere from lower Earth orbit: preliminary results, B. Am. Meteorol. Soc., 77, 19–40, 1996.

Yang, J., Zhang, P., Lu, N.-M., Yang, Z.-D., Shi, J.-M., and Dong, C.-H.: Improvements on global meteorological observations from the current Fengyun 3 satellites and beyond, Int. J. Digital Earth, 5, 251–265, 2012.

Zeng.Z., Sokolovskiy,S., Schreiner,W., Hunt,D., Lin,J., and Kuo,Y.-H.: Ionospheric correction of GPS radio occultation data in the troposphere, Atmos. Meas. Tech., 9, 335–346, 2016.

Table 1 Main instrumental parameters for FY-3C/GNOS

Parameters	FY-3C/GNOS
Orbit Height	~836 km
Orbit Type	sun synchronous
Spacecraft mass	~750kg
Instrument mass	7.5kg
Constellation	GPS L1 C/A, L2 P
	BDS B1I,B2I
Channels	GPS：14 BDS：8
Sampling	POD 1Hz
	ATM.occ. (closed loop)50Hz
	ATM.occ.(open loop) 100 Hz
	ION occ. 1Hz
Open loop	GPS L1 C/A
Clock stability	1×10－12（1secAllan）
Pseudo-range precision	≤30cm
Carrier phase precision	≤2mm
Beam width of atmosphere occultation antenna	≥±30°(azimuth)

Table 2. Details of the selected bad occultations

No.	Occ. time (yymmdd.hhmm)	Longitude (deg.)	Latitude (deg.)	Occ. direction	SLTA_L2 (km)
1	170128.0332	-99.154	25.070	rising	21.917
2	170128.0740	24.705	-4.222	rising	25.793

Table 3. Details of the good profiles

No.	Occ. time (yymmdd.hhmm)	Longitude (degree)	Latitude (degree)	Occ. direction	SLTA_L2 (km)
1	20170128.0103	149.508	-38.445	rising	4.011
2	20170128.0251	70.857	-51.463	rising	12.928

Table 4. The 2×2 table values

		Bad case (True)	
		YES	NO
Bad case (Identified by QC parameters)	YES	8.0% (hits)	3.1%(false identified)
	NO	1.7%(misses)	87.2%(correct negatives)

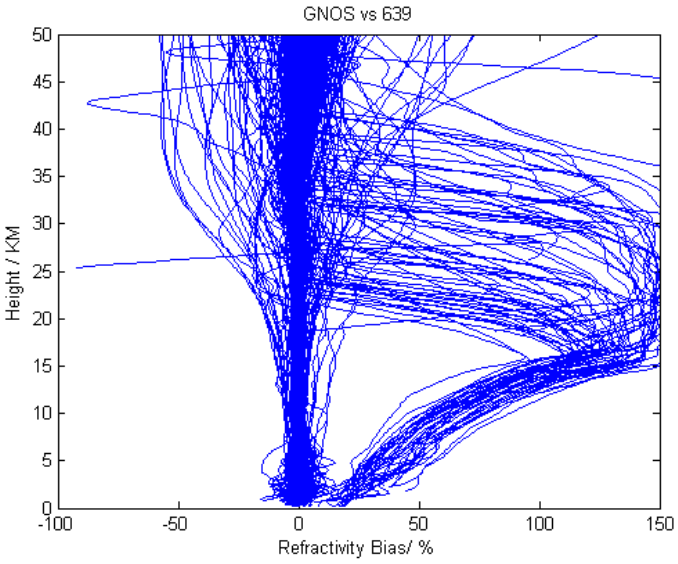

Figure 1. FY-3C/ GNOS GPS refractivity bias compared to T639 (the Chinese forecast model data), on 28th Jan.2017 with 489 samples.

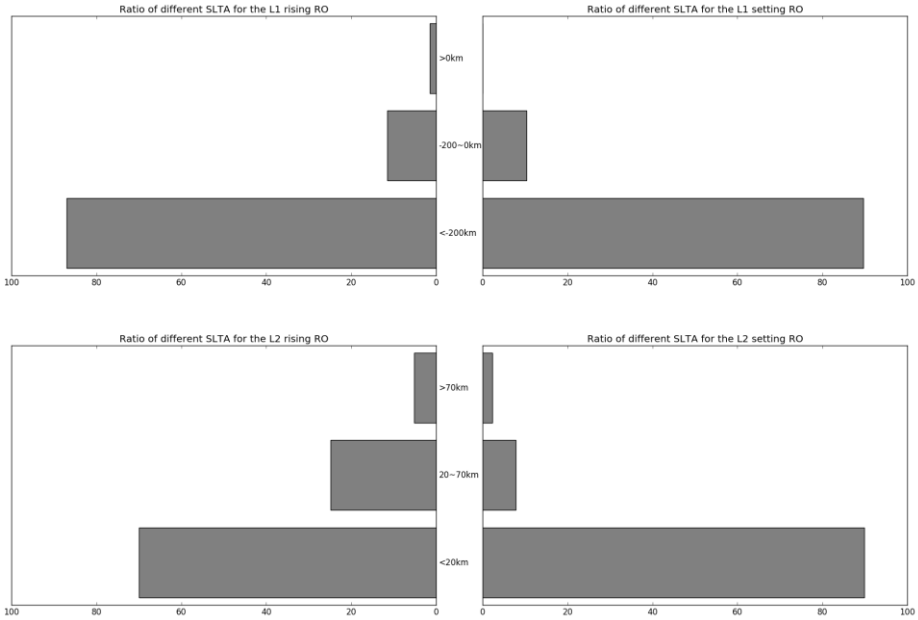

Figure 2. Ratio of different SLTA of the L1 C/A and L2 P for the rising and setting occultations, statistics result is from 28th Jan to 2nd Feb. 2017.

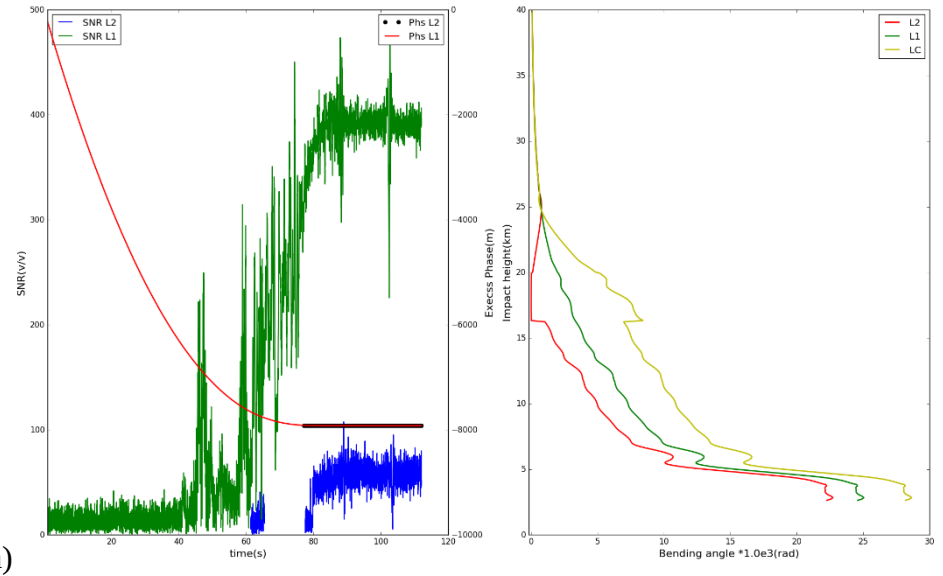

(a)

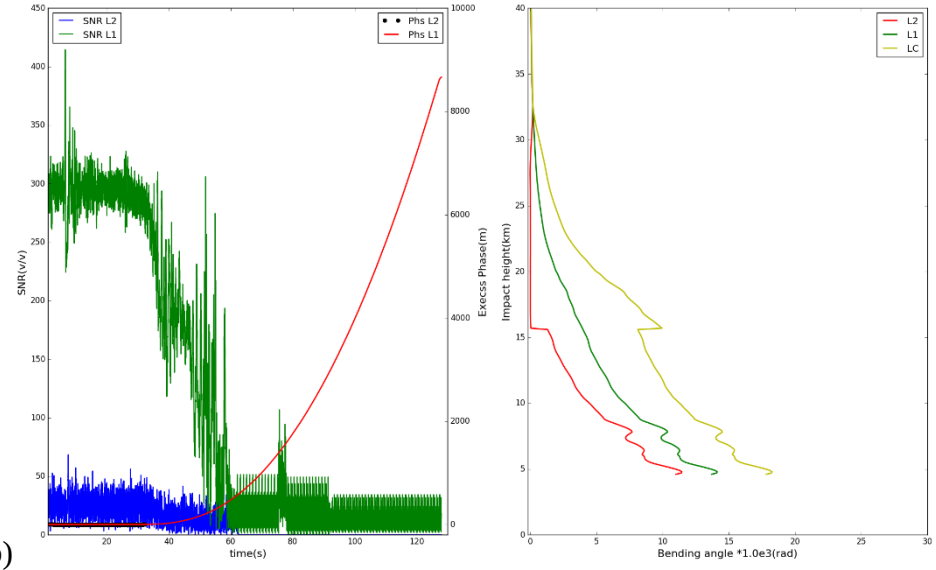

(b)

Figure 3. Two bad cases (a) A rising profile (FY3C_GNOSX_GBAL_L1_20170128_0332_AEG15_MS.NC), (b) a setting profile (FY3C_GNOSX_GBAL_L1_20170128_0850_AEG18_MS.NC). Example L1 (red) and L2 (black) SNR and excess phase measured data. The resulting L1 bending angle (green), L2 bending angle (red), and LC bending angle (yellow) profiles as a function of impact parameter computed using ropp_pp routines.

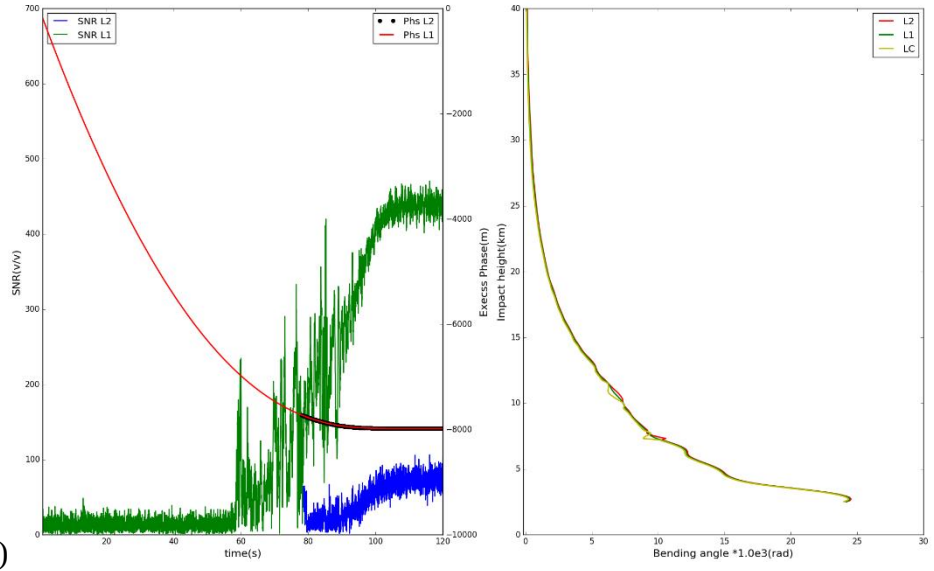

(a)

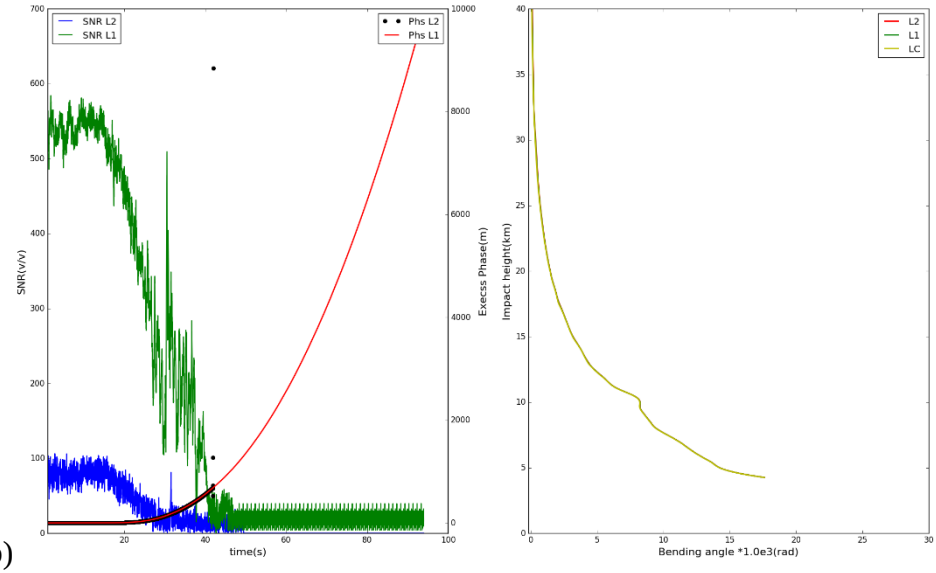

(b)

Figure 4. Two good cases (a) A rising profile (FY3C_GNOSX_GBAL_L1_20170128_1138_AEG27_MS.NC), (b) a setting profile (FY3C_GNOSX_GBAL_L1_20170128_1648_AEG31_MS.NC). Example L1 (red) and L2 (black) SNR and excess phase measured data. The resulting L1 bending angle (green), L2 bending angle (red), and LC bending angle (yellow) profiles as a function of impact parameter computed using ROPP routines.

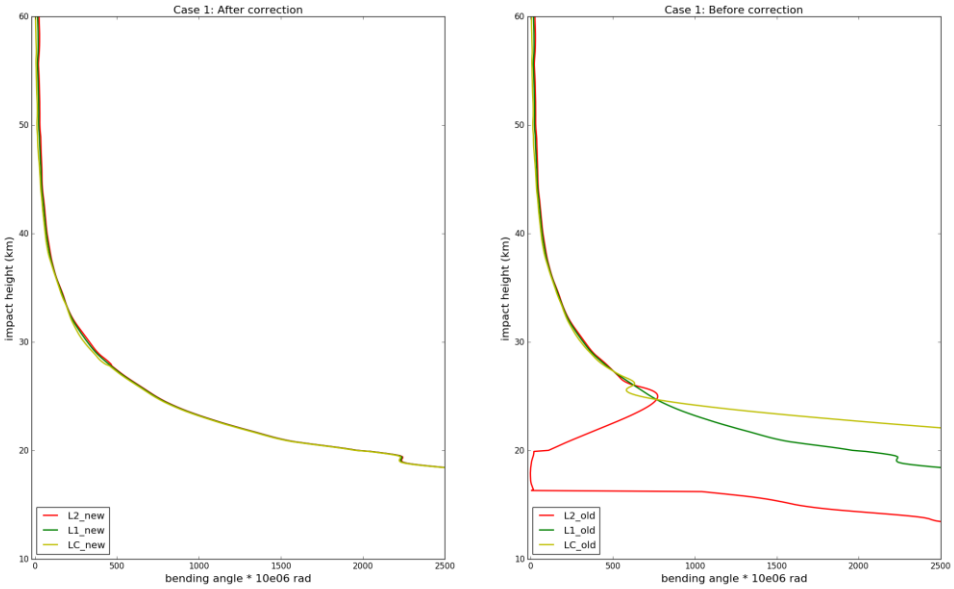

Figure 5. Case1: the bending angle of L2 (red), L1 (green) and LC (yellow) before (right) and after (left) correction.

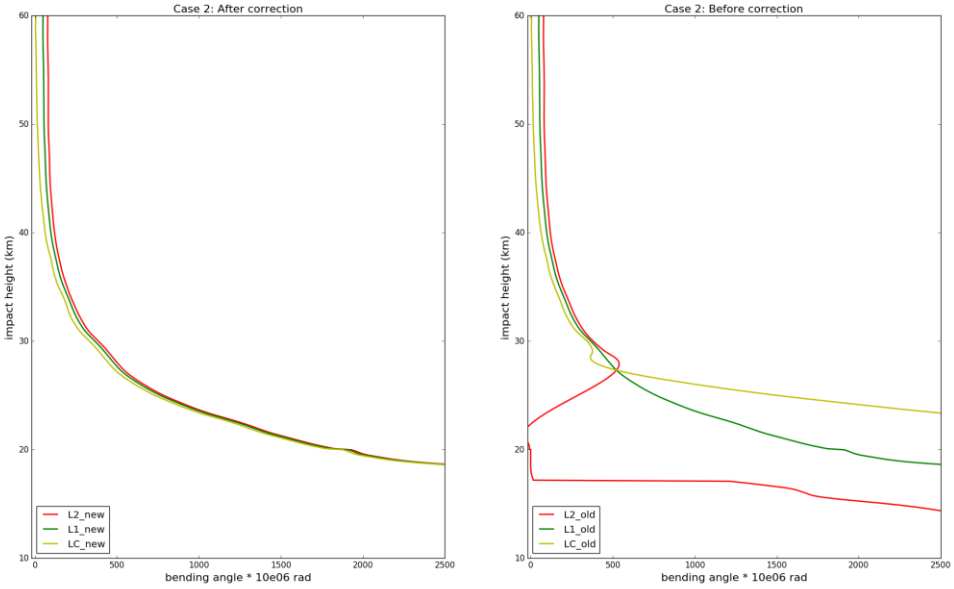

Figure 6. The same as Figure 5 but for Case 2.

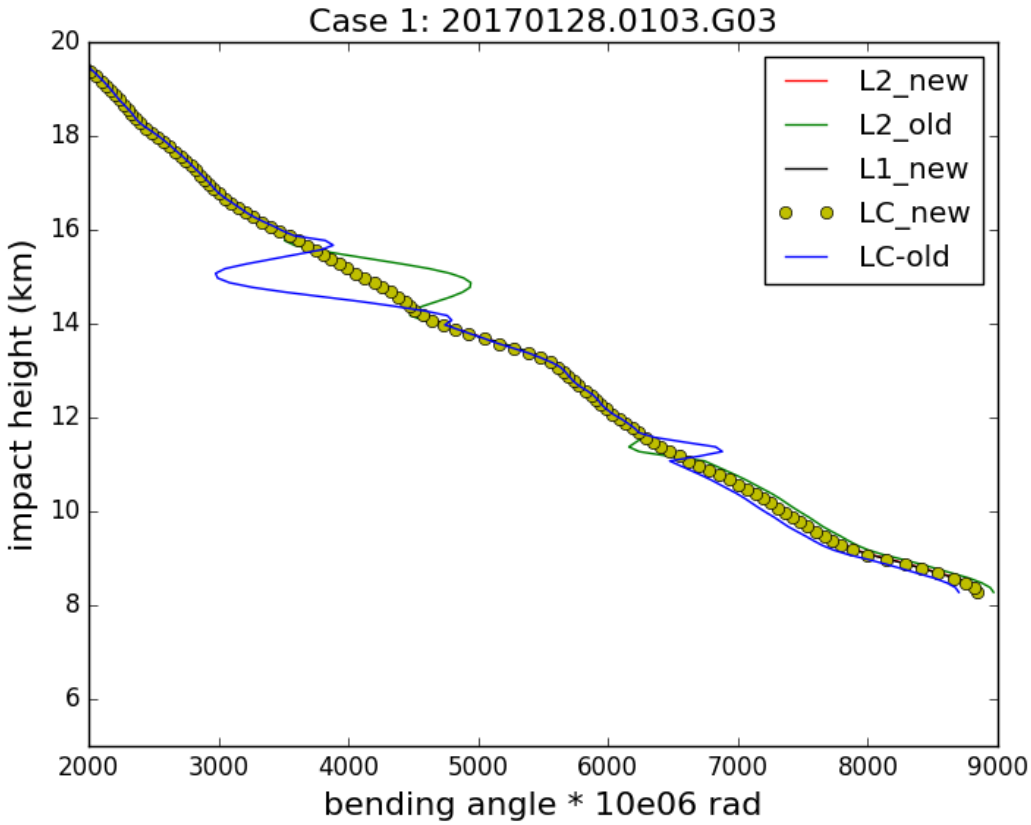

Figure 7. Good Case 1: the bending angle of L2, L1 and LC before and after correction.

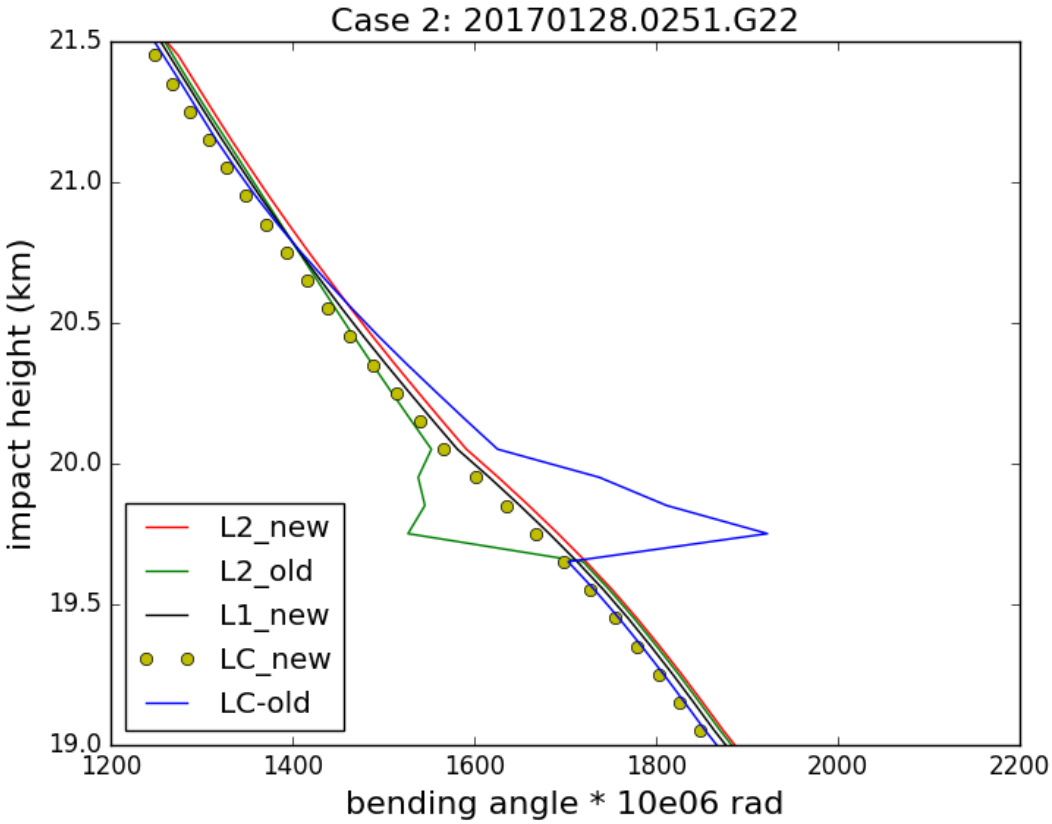

Figure 8. Good Case2: the bending angle of L2, L1 and LC before and after correction.

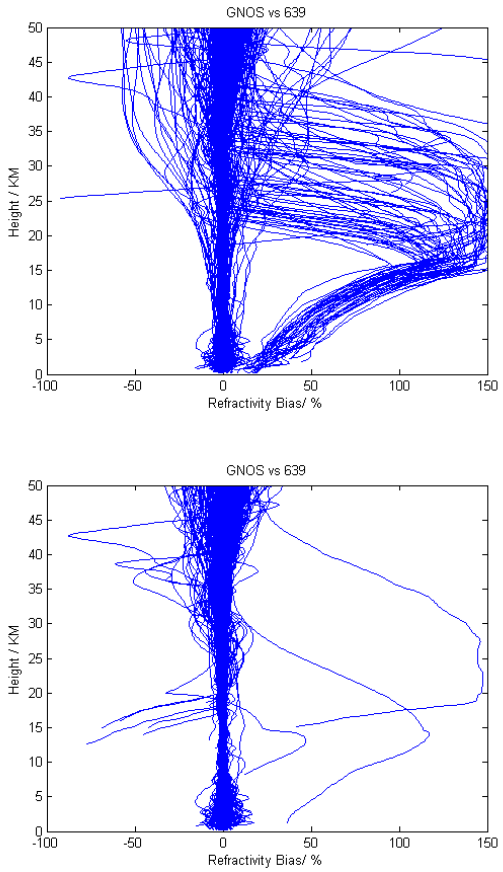

Figure 9. FY-3C/ GNOS GPS refractivity bias compared to T639 (the Chinese forecast model data), on 28th Jan.2017 with 489 samples. The upper plot reproduces Figure 1 and is the result of the original GNOS GPS data, and the lower plot isafter implementing the new L2 extrapolation approach.

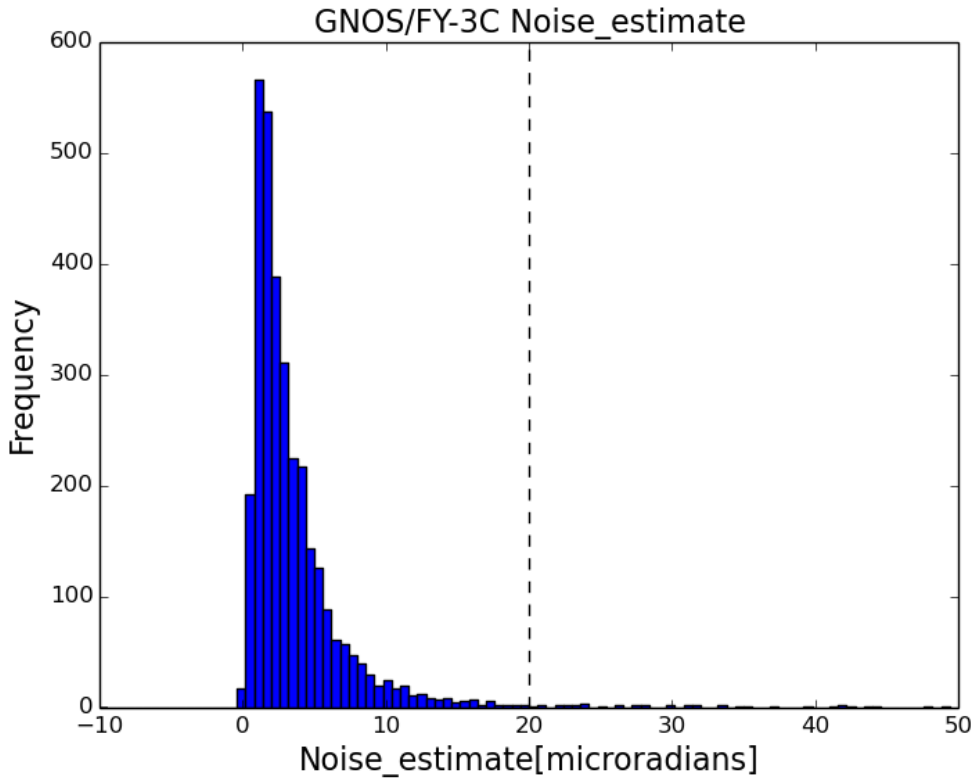

Figure 10. The histogram of the *noise_estimate* parameter using seven days of data from 16th Feb. to 22nd Feb 2017

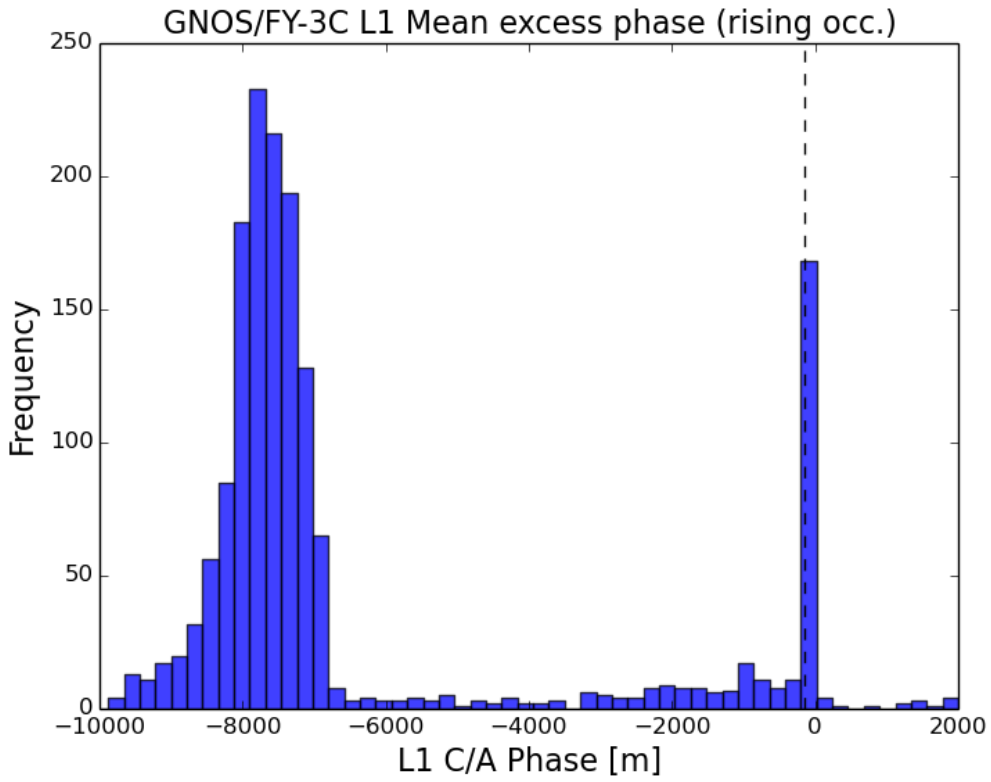

Figure 11. The histograms of L1 mean excess phase for the rising occultation at the height of 60 – 80 km SLTA using seven days of data from 16th Feb. to 22nd Feb.2017.

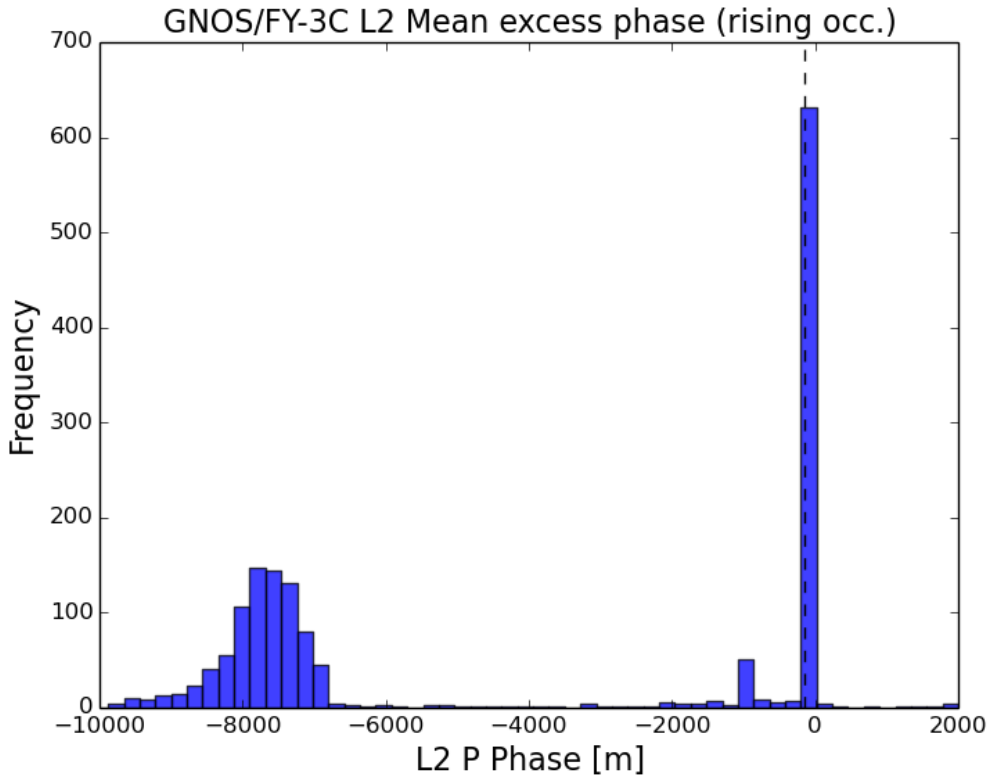

Figure 12. The histograms of L2 mean excess phase for the rising occultation at the height of 60 – 80 km SLTA using seven days of data from 16th Feb. to 22nd Feb.2017.

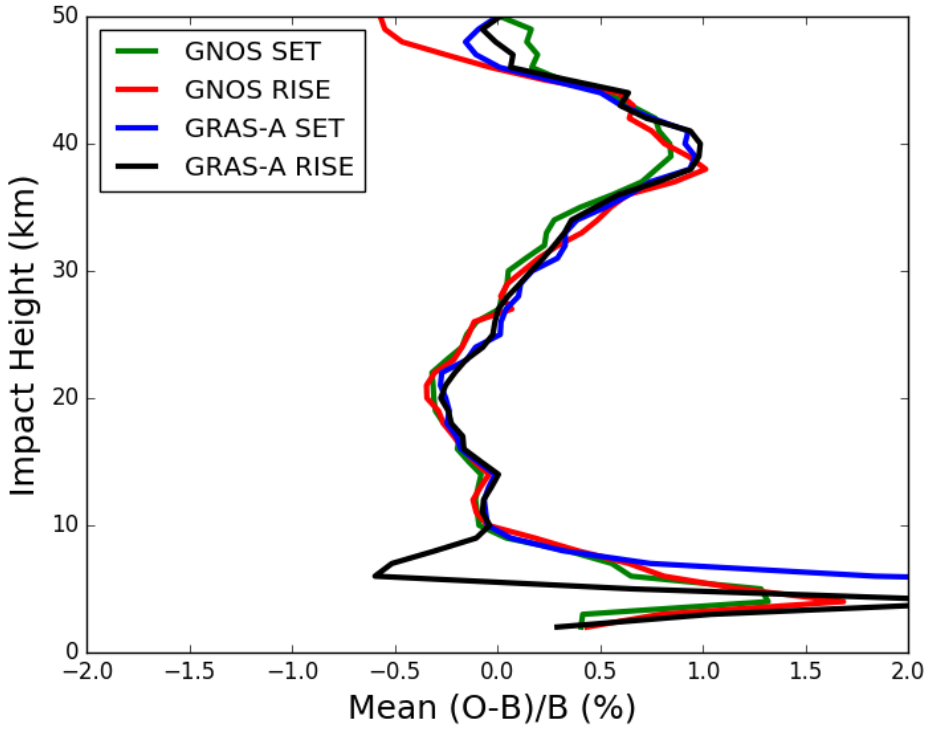

Figure 13. Global bending angle departure results, as a function of impact height, for the mean bias. The green, red, blue and black lines are representative of setting occultation for GNOS, rising occultation for GNOS, setting occultation for GRAS and rising occultation for GRAS.

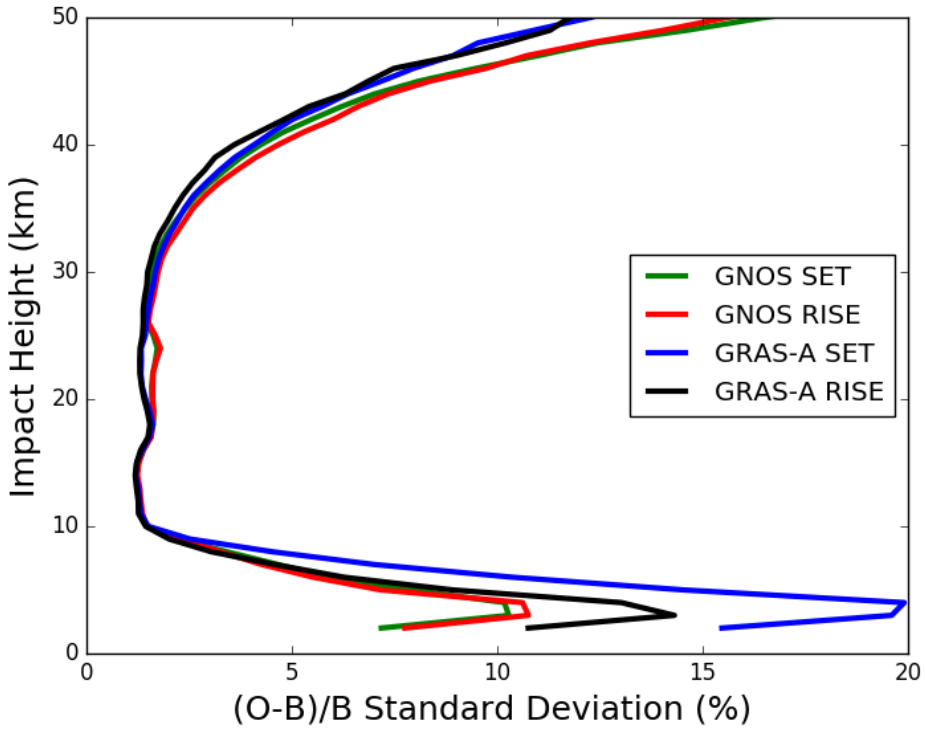

Figure 14. Global bending angle departure results, as a function of impact height, for the standard deviation. The green, red, blue and black lines are representative of setting occultation for GNOS, rising occultation for GNOS, setting occultation for GRAS and rising occultation for GRAS.

For reviewer #3

Responses to the specific comments

1.

Reviewer's comment: Introduction. The manuscript lacks motivation. Since the authors present a new methodology to correct the L2 signal bending, the "old" ROPP L2 signal correction approach should be described. Additionally, the differences between the "old" and the "new" approaches should be emphasized and discussed in detail. Currently, the reader cannot understand why the current ROPP approach does not work for the GNOS retrievals and all relevant references are missing.

Author's response: Thank you for pointing out the problem. We will add the relevant references and additional discussion about the old and approaches to clarify the GNOS retrievals in the revised manuscript. In the response to the reviewer #2, we explain why the current ROPP approach does not work for the GNOS. Generally, the old approach requires the L2 penetrating down into 20km at least.

Changes in the manuscript: In the track version manuscript for review #3, the introduction is reworded in P4 from line 2 to 17. The reason for the failure of ROPP processing for GNOS is described in detail in section 2, that's from P5 to P7.

2.

Reviewer's comment: Introduction: P. 3; Line 30. "These biases are not seen with other RO missions." Yes, the L2 signal is weaker than the L1 signal. However, other RO missions do not lose L2 signal tracking that much high up in the neutral atmosphere. The authors should explain why GNOS loses L2 signal tracking in the stratosphere at ~ 20 km, unlike all other RO missions. The authors state that the most prominent quality issue was the large departures biases, in the vertical range of 5 – 30 km. This altitude covers the middle troposphere up to the middle stratosphere. Then, within this context, if GNOS loses 30% of the profiles below 20 km (see P. 5; Line 11), then the authors should explain how does GNOS contribute to Numerical Weather Prediction (NWP) and specify the most effective altitude range of the GNOS RO profiles.

Author's response: The reason for GNOS losing L2 signal tracking is that GNOS has a lower SNR compared to other missions. Additionally, the GNOS antenna is smaller and not well located on the satellite. Consequently, we have to use additional cables, which results in a larger decrease of SNR than expected. Scientists from EUMETSAT confirmed that GRAS can get down to 15 km for more than 90% of the cases, but it is not the case for GNOS. Only 70% of L2 can reach below 20km. However, note that GNOS on FY3C is just the first Chinese GPS-RO mission. For the second satellite, FY3D, GNOS has more antenna units and in turn, has higher SNR than FY3C. Thus, the L2 signal tracking gets better. The proportion of the large departures biases in FY3D is smaller than in FY3C as well.

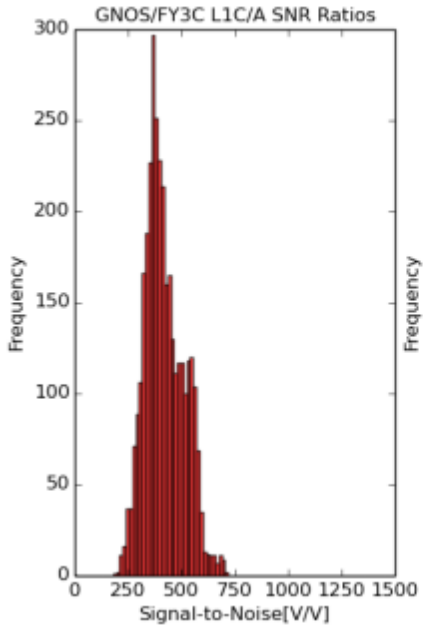
GNOS/FY3C L1C/A SNR Ratios
Frequency
Signal-to-Noise[V/V]
0
50
100
150
200
250
300
0 250 500 750 1000 1250 1500

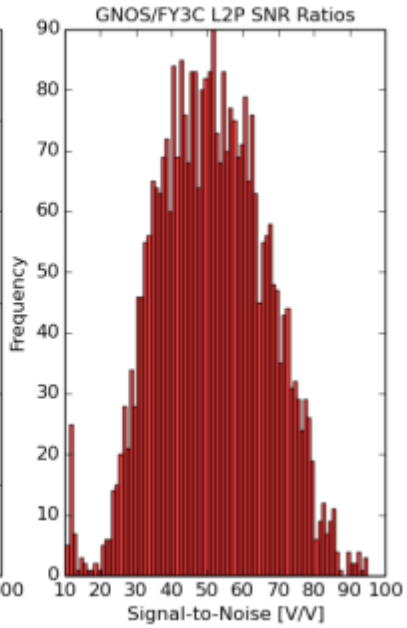
GNOS/FY3C L2P SNR Ratios
Frequency
Signal-to-Noise [V/V]
0
10
20
30
40
50
60
70
80
90
10 20 30 40 50 60 70 80 90 100

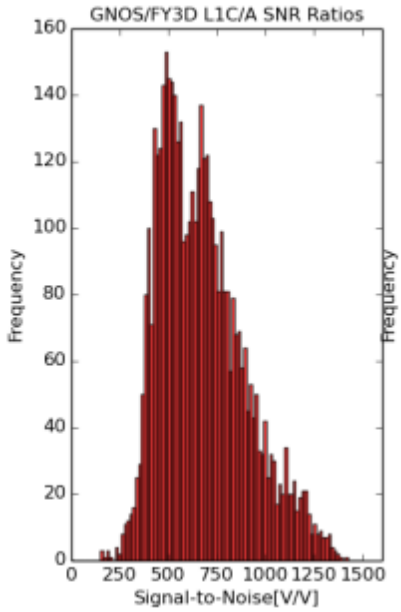
GNOS/FY3D L1C/A SNR Ratios
Frequency
Signal-to-Noise[V/V]
0
20
40
60
80
100
120
140
160
0 250 500 750 1000 1250 1500

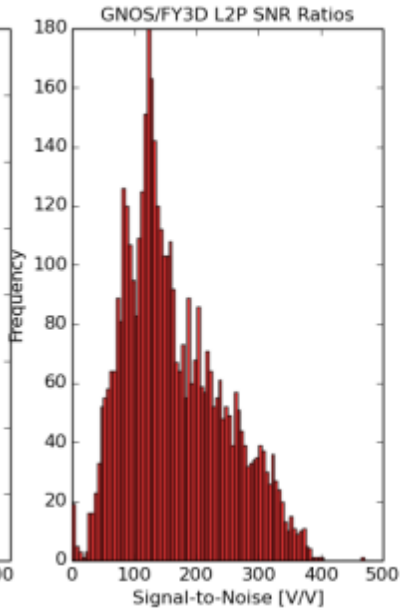
GNOS/FY3D L2P SNR Ratios
Frequency
Signal-to-Noise [V/V]
0
20
40
60
80
100
120
140
160
180
0 100 200 300 400 500

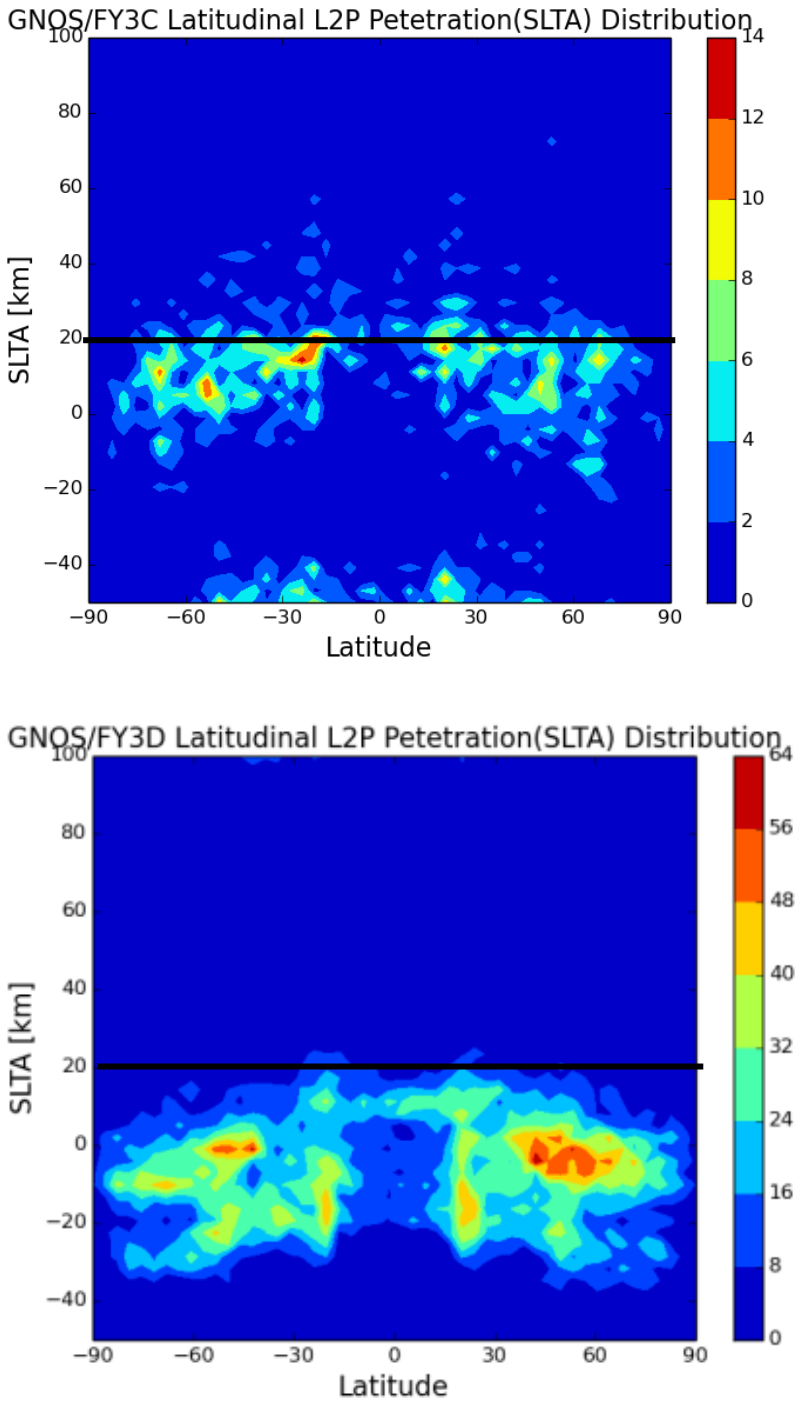

Figure 1

It is true that GNOS initially lost 30% of the profiles below 20 km, but that was before applying the new L2 extrapolation method outlined in the paper. After adopting the new method, we can process more GNOS profiles successfully. .

Regarding the impact on numerical weather prediction, GNOS was tested in the ECMWF assimilation system for the period November 23, 2017 to March 5,2018, prior to operational assimilation in the ECMWF system in March 2018. GNOS is assimilated operationally in the impact height interval from 8 km to 50 km in the extra-tropics, and from 10 km to 50 km in the

tropics. Although the medium-range forecast scores were generally neutral, in the short-range, the assimilation of GNOS data clearly improved the fit to other GPS-RO data, such as Metop GRAS A,B GRAS, COSMIC-6 etc. Figure 2 shows the improvement in the GPS-RO departure statistics for short-range forecasts when GNOS data is assimilated. This Figure could be added the final manuscript, but the main focus of the paper is how the current operational FY3C GNOS data is processed, rather than the impact in NWP systems.

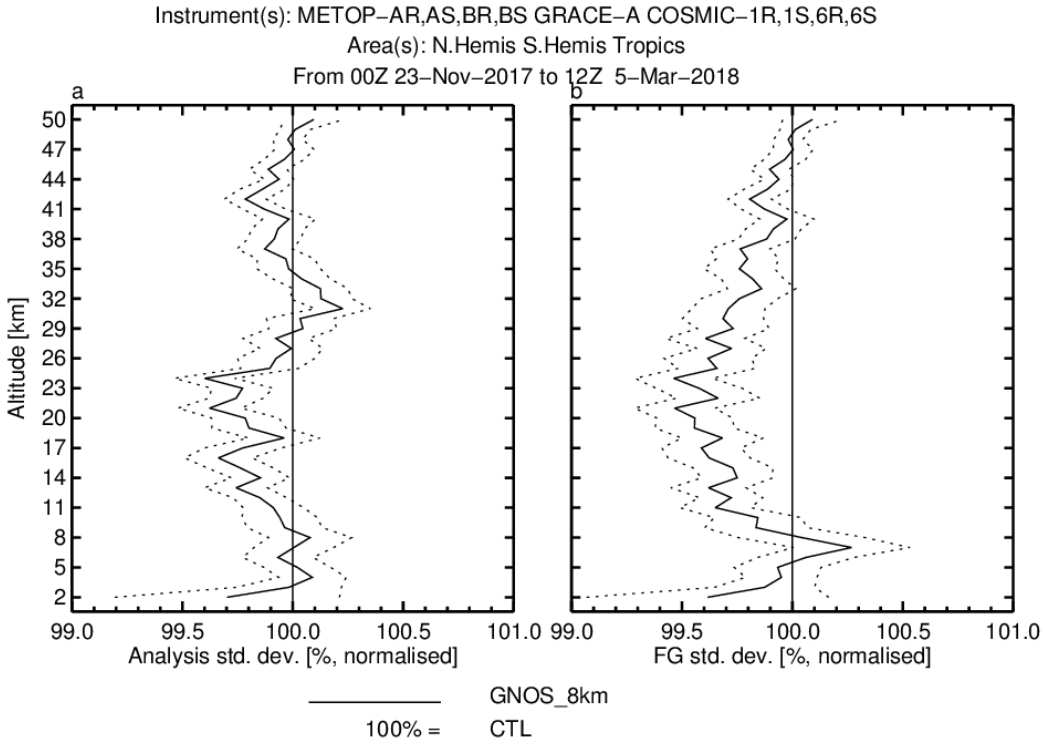

Figure 2: The percentage change in the GPS-RO departure statistics as a result of assimilating the GNOS measurements. The change in the standard deviation of the background (o-b) departures are on the right, and the analysis (o-a) departures are on the left. The statistics are globally averaged, and the dotted lines indicated 95 % statistical significance. Values less than 100 % on the left hand side indicate that the short-range forecasts fit the other GPS-RO data more closely as a result of assimilating GNOS.

Changes in the manuscript: we add the followings in the p4, line3. “The reason for GNOS losing L2 signal tracking is that GNOS has a lower SNR compared to other missions. Additionally, the GNOS antenna is smaller and not well located on the satellite. Consequently, we have to use additional cables, which results in a larger decrease of SNR than expected.”

To reduce misunderstanding, the sentence regarding the assimilation progress is removed to the last paragraph of the manuscript. P4, line 22 to 25.

3.

Reviewer’s comment: New L2 extrapolation: Equation (3.4) states that the bending angle in L2 frequency equals the bending angle in L1 frequency plus a correction factor, which is proportional to the ionospheric TEC. The problem in Equation (3.3) is that it is derived using Equation (3.2), which is valid only for ionospheric bending and not for neutral atmosphere bending, as specifically mentioned in Culverwell and Healy (2015). Within the neutral atmosphere the

ionospheric bending becomes negligible and the signal bending at tropospheric and stratospheric altitudes has an exponential dependency on the impact parameter – different than Equation (3.2). Therefore, how could the authors apply Equation (3.2) to correct for the L2 bending angle within the neutral atmosphere using bending angle approximations derived for ionospheric bending only – particularly when applying this method from the lowest altitude the L2 signal is lost and 20 km up with a maximum upper limit of 70 km that is around the bottom side of the ionospheric D layer?

Author's response: As to this comment, Sean Healy gave a detailed response in SC1.
Changes in the manuscript: This part is reworded in P8 to P9.

4.

Reviewer's comment: Equation (4.1): The Xso is estimated from the least squares fit between the observed L1 and L2 bending angles. Then again, the new noise_estimate the authors introduce defines a new statistical metric based on how close the Xso is to the observed L1 and L2 bending angle difference. But, the Xso was estimated in Equation (3.4) to fit the minimum bending angle difference in L1 and L2. This noise_estimate appears to be misleading, without physical underpinning and with an over-fitting nature that beats down the scatter. Additionally, P. 9; Line 8: "The physical meaning of noise_estimate is easy to understand." Is not easy to understand and the authors should explain the rationale of defining it, because the Xso has already been estimated well via Equation (3.4). Also, how do the authors decide on the 20 microradiances as the threshold value?

Author's response: The "noise_estimate" provides information about how well we are able to fit the L2-L1 bending angle differences in the in the fitting interval where we trust the data, using the retrieved value Xso. Hence, the noise estimate is the least squares solution cost function value, divided by the number of points in the 20 km fitting interval. The fitting model is physically based, albeit assuming a simple ionospheric model, as discussed below. If the fitting model can reproduce the L2-L1 bending angle differences accurately, we can use the Xso to extrapolate the L2-L1 differences below 25 km, to produce ionospheric corrected bending angles used for NWP applications. The 20 microradian threshold is empirical, but it is informed by the assumed bending angle error statistics used in the assimilation of GNSS-RO data. Typically, the assumed bending angle error is 1.25 % from around 10 km to ~32 km. For example, this translates into around 6 microradians at 25 km, increasing to 13 microradians at 20 km. The 20 microradian threshold is designed to screen out cases where the L2-L1 extrapolation could introduce significant additional errors. We agree that the "easy to understand" statement should be clarified and expanded upon. However, the "over-fitting" comment is not clear.
Changes in the manuscript: The changes can be found in P10, line 4 to 19.

5.

Reviewer's comment: Section 4.2: The authors do not explain why is it necessary to monitor the performance of GNOS mean L1 and L2 phase delays in the height interval of 60 to 80 km. Also, why the mean phase and not the phase variation with altitude within this height range? What GNOS product is assimilated in NWP models and how does monitoring the 60-80 km phase delays help us to QC the profile below?

Author's response: We take these phase delays as one of QC factors because empirically it was found to determine the performance of GNOS when compared with reanalysis data. When encountering the bad profiles, the rising L1 and L2 mean phase delays have small values. The result is only based on FY3C. Subsequently, when we look at FY3D, this phenomenon disappears. Thus this factor is not a general one. We are considering cutting this part of from the manuscript.
Changes in the manuscript: Although the mean phase delay is not suit for FY3D, it is still kept as it is applied in FY3C. The phase variation with altitude is also a good way to monitor the performances of the observations. Beyerle et al. (2004) also suggested a QC approach to reject the RO observations degraded by ionospheric disturbances based on the phase delay of L1 and L2 signals. GNOS bending angle profiles are assimilated in NWP. Excess phase is the input of bending angle inversion. It's better to monitor the near-raw observations before messing up with the following processing. The correction is made at P14 in the track changes version.

6.
Reviewer's comment: P. 10; Line 21: "...these have been tested with one day of data..." The statistical sampling used in the determination of the statistical performance of the QC methods is low and does not represent the statistical performance of the GNOS profiles around the globe and under different seasons.

Author's response: One day of data was used to initially estimate the various QC parameters and then these were tested over longer periods. Clearly, the new L2 extrapolation method is rather effective at eliminating the large errors for the longer period, globally (See Figure 13,14)The plot shown here is just an example.
Changes in the manuscript: We carried out a new statistics using three months of data April 1 to June 30, 2018. In the corresponding part, we reinterpret the performance of the QC. Please see the detailed changes in the track version in P15 line 14 to 26.
7.
Reviewer's comment: Section 5: The authors explanation of the 15% disagreement between the GNOS and GRAS profiles below 10 km is inadequate. Ideally, collocated profiles between GNOS and GRAS should be used to quantify the degree of agreement or disagreement. However, if there are not enough collocated profiles between July 6 and August 2, 2018, perhaps the authors could use the entire time period GNOS provides RO profiles and if there are still not enough collocated profiles the authors could bin their profiles either into latitude sectors or seasons and then compare with GRAS to create an ensemble study to greatly increase the statistical sampling. The results represent a limited statistical sampling to support the authors' claims.

Author's response: Statistics for matched occultations are routinely available from the ROM SAF web pages. See,
http://www.romsaf.org/monitoring/matched.php
An example for GNOS versus Metop-A GRAS is attached. The GNOS data presented on these pages is processed with the method outlined in the paper. However, we do not believe that the matched occultation statistics provide any additional information, relative to the bending angle departure statistics computed with an accurate short-range forecast.

Changes in the manuscript: We reword this part. Please see P17 from line 4 to 17.

Minor comments

a)

Reviewer's comment: P. 2; Line 16: "...velocity and anti-velocity antennas..." Do you mean fore and aft antennas?

Author's response: Yes

b)

Reviewer's comment: P. 2; Line 19: What is the GNOS inclination in Table 1?

Author's response: The inclination of FY3C/GNOS is 98.75 °

Changes in the manuscript: We add the inclination of GNOS in Table 1.

c)

Reviewer's comment:P. 2; Line 17: Is BDS global or region constellation. Mention geographic restrictions of RO.

Author's response: BDS both has global and region constellation. The distribution of BDS RO can be shown as follows, also it can be refered to Mi Liao et al.,2016

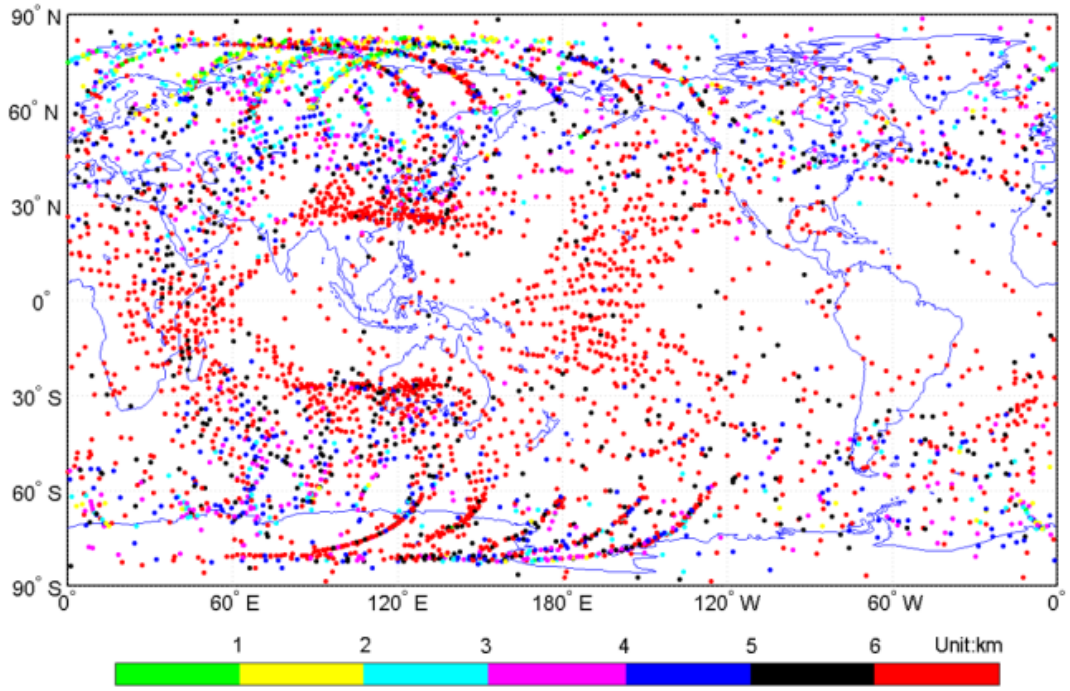

Figure 3. Map of the GNOS BDS occultation coverage from 1 November to 31 December 2013, with a total of 4648 samples. Different colours indicate different penetration depths.

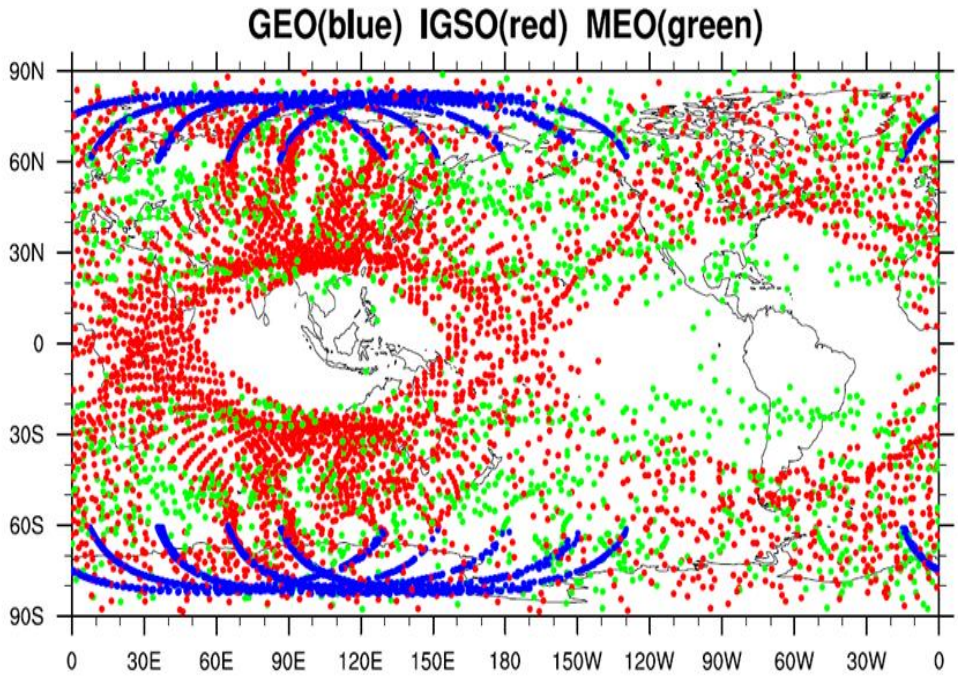

Figure 4. Map of the GNOS BDS occultation coverage

Different colours indicate different constellations. MEO have the same altitude as GPS.

d)

Reviewer's comment:P. 3; Line 22: "...departure statistics..." From what?

Author's response: From background data, such as forecast data.

Changes in the manuscript: This part is overlapped with the first part of the section 2. For better elaboration, we decide to delete this part in the revised manuscript. The correction is at p3 line 22-30 in the track changes version.

e)

Reviewer's comment: P. 3; Line 25: Why more than 20% levels of the profile? How was this threshold selected? Explain.

Author's response: Compared with background data, the bad profiles are defined as the mean biases greater than 10% (100*(O-B)/B) from 5km to 30 km. As we know that the bias of RO at that height is about 1% in normal case. If the threshold is set as 10%, the large departure profiles can be identified.

Changes in the manuscript: This part is overlapped with the first part of the section 2. For better elaboration, we decide to delete this part in the revised manuscript. The correction is at p3 line 22-30 in the track changes version.

f)

Reviewer's comment: P. 4; Line 10: What is the most effective altitude range that GNOS provides the best RO profiles and explain how this information is used in NWP and how does it improve NWP. Include references to support claims.

Author's response: Currently, there are no published papers talking about the GNOS in NWP. Only some technical reports from personal communications. However, see Figure 2 above.

Changes in the manuscript: The impact of NWP using GNOS is not the main focus of the paper.To reduce misunderstanding, the sentence regarding the assimilation progress is removed to the last paragraph of the manuscript just as a general remark. P4, line 22 to 25.

g)

Reviewer's comment: P. 4; Line 14: "...may..." replace with "...could be..."

Author's response: Fine.

Changes in the manuscript: Done.

h)

Reviewer's comment: P. 5; Line 11: Is this L2 signal loss at 20 km normal? Usually L2 signal is lost in the middle troposphere which is about 5 km. Explain.

Author's response: This can be seen from my reply to your second major comment.

Changes in the manuscript: We add the explanation in P4 line 14 to 17 of the track changes version.

i)

Reviewer's comment: P. 5; Line 27: "...consistency..." replace with "...agreement..."

Author's response: Fine.

Changes in the manuscript: Done.

j)

Reviewer's comment: P. 6; Line 5: Define "obvious errors".

Author's response: Fine.

Changes in the manuscript: Reword as "large bending angle and refractivity departures" in P.8 line12 of the track changes version.

k)

Reviewer's comment: P. 6; Line 9: Define "other profiles".

Author's response: Fine.

Changes in the manuscript: Delete the ambiguous words.

l)

Reviewer's comment:P. 6; Line 11: This definition of the ionosphere is crude, general, and unrealistic. Usually, the ionosphere is represented with multiple Chapman profiles with different scale heights. Mathematically, the Dirac function obtains a value of 0 at altitudes outside a very small neighborhood of the peak height.

Author's response: The ionospheric model is crude, and it would not be valid if we were attempting to retrieve ionospheric information. However, we are only interested in modelling the impact of the ionosphere on bending angles with a tangent height well below the ionosphere, typically in the 25-60 km vertical interval. The ionospheric bending in this interval varies slowly with height (impact parameter). For example, adding a sporadic E layer would not change the shape of the L2-L2 difference curve below 60 km significantly. Conversely, we cannot retrieve an E-Layer from the L2-L1 differences below 60 km. Some authors assume that the L2-L1 is a constant. We use the delta function model because it produces a more realistic, slow variation of L2-L1 with height.

Changes in the manuscript: Please see the changes made in the P8 line 27 to P9 line7, and P10 line 4 to 9.

m)

Reviewer's comment: P. 6; Line 27: Why the peak height is 300 km? What led to this selection? The rule of thumbs says that per 100 km different in ionospheric shell height leads to 1 TECU error in the ionospheric total electron content. How sensitive is the estimation of Xso to the ionospheric TEC?

Author's response: Xso should be proportional to the ionospheric TEC because the L2-L1 differences should be proportional to the TEC. However, we are not trying to retrieve the TEC here. We estimate Xso in order to extrapolate the L2-L1 differences below 25 km using a reasonable curve. We apply the Chapman layer ionospheric model. Statistically, the peak height is around 300km, see the Culverwell and Healy, 2015 (ROM SAF). Experiments for testing the sensitivity of the peak height from 250km to 350km, in 10km increments, show that the final corrected bending angle is not sensitive to the peak height. The largest difference is about 10^{-5} urad. The plot (not shown here) is hard to differentiate the different results. Thus we think the 300km is reasonable. This will be noted in the revised paper.
Changes in the manuscript: Please see the changes made in the P10 line 11 to 19.

n)
Reviewer's comment: P. 7; Equation (3.4): This equation describes the ionospheric bending angle and not the neutral atmosphere. How can the authors apply this equation to correct for the L2 bending in the neutral atmosphere?

Author's response: This can be found in the comment of SC1 by Sean Healy.
Changes in the manuscript: This can be found the explanation in the Part3 of the track changes version.

Processing and quality control of FY-3C/GNOS data used in numerical weather prediction applications

Mi Liao[1], **Sean Healy[2]**, Peng Zhang[1]

[1] National Satellite Meteorological Center, Beijing, China

[2] European Centre for Medium-Range Weather Forecasts, Reading, UK

Correspondence to:

Sean Healy (sean.healy@ecmwf.int), Peng Zhang (zhangp@cma.gov.cn)

Abstract

The Chinese radio occultation sounder GNOS (Global Navigation Occultation Sounder) is on the FY-3C satellite, which was launched on September 23, 2013. Currently, GNOS data is transmitted via the Global Telecommunications System (GTS) providing 450 – 500 profiles per day for numerical weather prediction applications. This paper describes the processing for the GNOS profiles with large biases, related to L2 signal degradation. A new extrapolation procedure in bending angle space corrects the L2 bending angles, using a thin ionosphere model, and the fitting relationship between L1 and L2. We apply the approach to improve the L2 extrapolation of GNOS. The new method can effectively eliminate about 90% of the large departures. In addition to the procedure for the L2 degradation, this paper also describes our quality control (QC) for FY-3C/GNOS. A noise estimate for the new L2 extrapolation can be used as a QC parameter to evaluate the performance of the extrapolation. Mean phase delays of L1 and L2 in the tangent height interval of 60 to 80 km are analysed and applied in the QC as well. A statistical comparison between GNOS and ECMWF (European Centre for Medium-Range Weather Forecasts) forecast data demonstrates that GNOS performs almost as well as GRAS, especially in the core region from around 10 to 35 km. The GNOS data with the new L2 extrapolation is suitable for assimilation into numerical weather prediction systems.

1 Introduction

GNOS is the first Radio Occultation (RO) sounder on the Fengyun series of Chinese polar orbiting meteorological satellites. It is also the first multi-GNSS (Global Navigation Satellite System) RO receiver in orbit that can perform RO measurements from both GPS (Global Positioning System) and Chinese BDS (BeiDou Positioning System) signals. GNOS is manufactured by National Space Science Center (NSSC) of Chinese Academy Science (CAS), and is operated by the National Satellite Meteorological Center (NSMC) of the China Meteorological Administration (CMA). GNOS is also mounted on FY-3D (which was launched on November 2017) and it will be on all the subsequent Chinese Fengyun satellites. The FY-3 series is expected to provide GNOS RO measurements continuously at least until 2030 (Yang et al., 2012), so this is a potentially important source of data for numerical weather prediction (NWP) and climate reanalysis applications.

As a multi-GNSS receiver, GNOS has the ability of tracking up to eight GPS satellites and four BDS satellites for precise orbit determination (POD). In addition, it has velocity and anti-velocity antennas for simultaneously tracking at most six and four occultations from GPS and BDS, respectively. Because of the presence of two antennas in opposite directions, both the rising and setting occultations can be retrieved. More instrumental details are given in the Table 1, and in Bai et al. (2014). Currently, FY-3C GNOS GPS measurements can produce about 500 GPS-RO profiles per day for operational use in NWP systems, while GNOS from BDS signals are not yet operational, and produce only about 200 profiles because of fewer reference satellites.

——As with the pre-existing GPS-RO sounders, such as the GPS/Met (Global Positioning System/Meteorology) experiment (Ware et al., 1996), the COSMIC (Constellation Observing System for Meteorology, Ionosphere, and Climate; Anthes et al., 2008), and the European Metop/GRAS (GNSS Receiver for Atmospheric Sounding) mission (Von Engeln et al., 2009), the raw observations from GNOS consist of phase and signal to noise ratio (SNR) measurements. In addition, auxiliary information provided by the International GNSS Service (IGS), such as the GPS

带格式的：缩进：首行缩进： 0 字符

precise orbits, clock files, Earth orientation parameters, and the coordinates and measurements of the ground stations, are also needed. The IGS ultra rapid orbit products, with an approximate accuracy of 10 cm in orbit, are chosen for near-real-time operational use. The Low Earth Orbit (LEO) precise orbit determination (POD) can be estimated by integrating the equations of celestial motion (Beutler, 2005) using the Bernese software Version 5.0 (Dach et al., 2007). The single difference technique is applied to obtain the excess phase as a function of time in an Earth-centred inertial reference frame. The Radio Occultation Processing Package (ROPP) software (Version 6.0), developed by the EUMETSAT ROM SAF (Radio Occultation Meteorology Satellite Application Facility), is used to determine different kinds of atmospheric parameters (Culverwell et al., 2015). One-dimensional variational (1-D-Var) analysis, using background information from a T639L60 global forecast model, is used to retrieve temperature and humidity profiles. The T639L60 is a global medium-range weather forecast system of China, which became operational at CMA in 2009. However, since early 2017, some changes have been implemented in the operational stream. We obtain the auxiliary files through an ftp server in near real time provided by EUMETSAT GSN service, improving the timeliness to within three hours. In addition, the POD software was replaced by the PANDA (Positioning And Navigation Data Analyst), which is developed originally by the Wuhan university of China (Shi et al., 2008).

~~In the original operational streamstatistics, GPS RO refractivity departure statistics were used in a preliminary check of data quality. Poor quality data was filtered out with Quality Control (QC) based on the following rules. A profile is rejected if a fractional refractivity greater than 0.1 occurs at more than 20 % levels in the profile. In addition, the outliers on a specific level are then excluded if they exceed the three sigma from a statistical point of view. This QC excluded nearly 15% GNOS profiles. We found that most of the rejected profiles had large biases of up to 200%, in the vertical interval between 5-30 km, peaking at around 20km, when compared to model data (Figure 1). These biases are not seen with other RO missions.~~ It is known that

GPS signal SNR falls with decreasing altitudes, and especially for the L2 frequency. Montenbruck (2003) and Bergeton (2005) tried to use high quality single frequency to process atmospheric radio occultations without the degraded L2 signal, but have limitations in the condition of high ionspheric oscillations. Dual-frequency for atmosphere radio occultation is still essential. Gorbonov developed an indicator (2005) to estimate the quality of L2 signal in the low atmosphere, and use it to judge where needs to linearly extrapolate the difference of L1 and L2 signal. Z.Zeng (2016) investigates the optimal height for the extrapolation of L1-L2 by modelling the ionospheric bending angle using an approximate expression. These methods are successfully applied for CHAMP,COSMIC, Metop and other missions. ~~Therefore, in some cases the linear combination (LC) of L1 and L2 bending angles can produce erroneous results. We found that~~However, the degradation of the GNOS L2 had a large impact on the retrieval quality when the measurements were processed with ROPP. ROPP includes a pre-processing step in order to correct degraded L2 data. The approach is based on Gorbunov et al (2005, 2006). The old approach in ROPP requires the L2 penetrating down into 20km at least. It is hard for GNOS to get the entire L2 signal down into 20km. The reason for GNOS losing L2 signal tracking is that GNOS has a lower SNR compared to other missions. Additionally, the GNOS antenna is smaller and not well located on the satellite. Consequently, we have to use additional cables, which results in a larger decrease of SNR than expected. Therefore, ~~in this work~~ we developed and tested a new L2 bending angle extrapolation method for GNOS data, and implemented it in ROPP. ~~As a result of this work, the GNOS data is now assimilated in operational NWP systems at, for example, the European Centre for Medium-Range Weather Forecasts (ECMWF), Deutscher Wetterdienst (DWD) and the Met Office.~~

In this paper, we will describe the new processing of GNOS data that reduces the large stratospheric biases in bending angle and refractivity, and present a quality control scheme for FY3C/GNOS. These results will be useful for understanding the statistical error characteristics and quality control of the GNOS data, and more generally the extrapolation approach may useful for other missions where one signal

带格式的：缩进：首行缩进： 0 字符

is lost early.

2 Large biases in the original GNOS processing

2

The ROPP software (Culverwell et al., 2015) is used to retrieve atmospheric parameters, such as bending angle, refractivity, dry temperature, temperature and humidity, from GNOS excess phase measurements. The~~A~~ g~~G~~eometrical optics approach (e.g., K~~u~~ursinski et al., 1997) is used to process the L1 and L2 phase delays to bending angle space above 25 km, and the Canonical Transform 2 (CT2) (Gorbunov and Lauritsen, 2004) technique is used for both L1 and L2 signals below 25 km. The combined statistical optimisation ionospheric correction method (Gorbunov 2002) produces "optimised" bending angles that are subsequently used in an Abel transform to produce refractivity profiles. We note that most NWP centres assimilate either bending angle or refractivity profiles.

In the preliminary assessments for the FY-3C/GNOS GPS RO refractivity retrievals against NWP with the original ROPP processing system, it was found that the most obvious and prominent quality issue was the large departure biases, in the vertical range of 5-30 km, peaking at around 20km (Figure 1). The percentage of profiles ~~effected~~ affected was about 13~15%. This bias problem is not seen with other RO missions, and it was found to be related to GNOS GPS L2 signal tracking problems, and the subsequent extrapolation of the L2 signal. ~~Although this ROPP extrapolation approach may~~could ~~be reasonable for other missions where L2 penetrates deeper, it does not appear to be valid for GNOS.~~

It was found that most of the bad GNOS cases are rising occultations~~, which is easy to understand.~~ .To improve the tracking in the lower troposphere and the quality of rising occultations, open loop tracking is implemented for GNOS GPS L1 signal, but not for L2 (Ao et al., 2009). In general, ~~the~~ SNR falls under the complicated

带格式的：正文

atmospheric conditions in troposphere because of atmospheric defocusing. The GPS L2 signal is modulated by a pseudo-random precision ranging code (P code) for the purpose of anti-spoofing. Although GPS L2 can be demodulated using the semi-codeless method, it will be at the expense of SNR and precision (Kursinski et al., 1997). Therefore, the performance of L2 signal tracking is not as good as that of L1, especially for the rising occultations. Figure 2 shows the lowest Straight Line Tangent Altitude (SLTA) percentages of L1 and L2 signals, for both the rising and the setting occultations. It shows that the lowest tracking height of L1 C/A of both the rising or setting measurements are reasonable (Sokolovskiy —,2001), with more than 98.5% profiles with a below zero SLTA. However, for the L2P, only 70% of the rising measurements reach below 20km. There are 24.8% of rising profiles stopping in the range of 20 ~70km, and 5.2% stopping above 70km, meaning effectively they contain no valid measurements. In contrast, 89.9% of setting occultations can get below 20km, which is better than the rising, but about 10% stop above that height. Those profiles that have bad L2 signal observations significantly affect the retrievals when using ROPP software to process the GNOS data.

–Figure 3 shows an example of GNOS performance in terms of excess phase, SNR, and bending angle for two bad cases where the L2 stops early. In these two cases, there are no valid L2 excess phase observations below 25km or 30km SLTA, respectively. However, there are L2 bending angles, extending to the near surface because of extrapolation within ROPP. ~~(ROM SAF, 2016).~~ Figure 4 is the same as Figure 3 but for two good cases where the L2 measurements get to 20km SLTA. Compared with the bad cases, ~~the good cases show deeper penetration for L2. Thus,~~ the retrieved bending angles of L1, L2 and LC ~~are~~ span a similar vertical interval ~~overlapping~~, and show good ~~consistency~~ agreement even at the lower part of the profiles.

ROPP includes a pre-processing step designed to correct degraded L2 data. The approach is based on Gorbunov et al (2005, 2006), and it is used successfully ~~routinely~~ for other GPS-RO missions. Briefly, smoothed L1 and L2 bending angle and

带格式的：缩进：首行缩进： 0 字符

impact parameters are computed. An impact height, "PC", above which the L2 data is considered reliable, is estimated using an empirical "badness score". The empirical badness score at time t, is defined as,

$$Q(t) = \left(\frac{abs(\overline{p_1(t)} - \overline{p_2(t)})}{\Delta p_a} + \frac{\delta p_2(t)}{\Delta p_b}\right)^2 \quad (2.1)$$

where δp_2 is a measure of the width of the L2 spectrum, $\overline{p_1(t)}$ and $\overline{p_2(t)}$ are the L1 and L2 impact parameters, respectively, computed from smoothed timeseries, Δp_a=200 m and Δp_b=150 m (See also, Eq. 11 Gorbunov et al, 2006 for a slightly modified form). The largest $Q(t)$ value in the impact height interval between 15 km to 50 km is stored as the badness score for the occultation, potentially for quality control purposes.

The mean L1 and L2 bending angle and impact parameters are then computed in a 2 km impact parameter interval directly above PC. Simulated L2 bending angles and impact parameters are computed by adding the mean (L2-L1) differences to both the L1 bending angle and impact parameter values, using the data in the 2 km interval. Simulated L2 and L1 phase values are then computed from these bending angles. Corrected L2 excess phase values are computed by merging the observed L2 phase above PC, with the simulated values below PC, using a smooth transition over 2 km, centered on PC. The corrected L2 phase values are subsequently used in the wave optics processing of the L2 signals.

A specific difficulty with the GNOS processing is related to determining the impact height PC, used for both the computation of the mean L1 and L2 differences, and defining the transition between observed and modelled L2 phase values. Although the "badness score" is used to determine PC, PC also has a maximum value (20 km). This is defined as the wave optics processing height (25 km) minus a 5 km "safety border". Therefore, the mean bending angles and impact parameters used in the L2-L1

带格式的: 字体: Times New Roman, 非倾斜

correction can only be computed in a 2 km interval up to a maximum impact height of 22 km. Unfortunately, this is not high enough for GNOS L2 signals, with the result that the mean L2-L1 bending angle and impact parameters computed in the 2 km interval above PC are corrupted, prior to the extrapolation.

带格式的：缩进：首行缩进： 0 字符

3 New L2 extrapolation –

带格式的：缩进：首行缩进： 0 字符

As mentioned in the Section 2, some formsort of extrapolation of the observed L2 signal is required before it can be combined with the L1 signal, in order to remove the ionospheric contribution to the bending. However, the current L2 extrapolation implemented in ROPP leads to ~~obvious errors~~large bending angle and refractivity departures when processing GNOS RO data. Therefore, an alternative L2 extrapolation method has been implemented in the ROPP to solve the GNOS problem. The new approach is based on (unpublished) work by Culverwell and Healy (2015), who modelled the bending angles produced by a Chapman layer model ionosphere ~~and other profiles~~, and established some basic theory for the relationship between fitting L1 and L2. A key underlying assumption in the L2 extrapolation approach is that the total bending angle can be written as~~is~~ a linear combination of the neutral bending plus a frequency dependent ionospheric bending term.~~.~~ Therefore, we assume that –subtracting the L1 bending angle from the L2 value at a common impact parameter, removes the neutral bending contribution. This is a common assumption, and it is also made in the standard ionospheric methods used in GPS-RO (Vorob'ev and Krasil'nikova, 1994).

The extrapolation method adopted here is based on a "thin" ionospheric shell model, where the ionosphere approaches a Delta function, at a specified height (See section 3.1, Culverwell and Healy, 2015). This~~e~~ ionospheric model is crude, and it clearly would not be appropriate ~~valid~~ if we were attempting to retrieve ionospheric information. However, in the context of GNOS processing, we are mainly~~only~~

interested in modelling the impact of the ionosphere on bending angles with a tangent height well below the ionosphere, typically in the 25-60 km vertical interval. The neutral free L2-L1 bending angle differences in this interval vary slowly with height (impact parameter) (e.g., see Figures 2 and 3, Zeng et al, 2016). For example, adding a sporadic E layer near 100 km would not change the shape of the L2-L12 difference curve below 60 km significantly. Conversely, we cannot retrieve an E-Layer information from the L2-L1 differences below 60 km.

~~Alternative approaches are described by Zeng. et al., (2016).~~

Thus, ~~F~~for a vertically localized region of refractivity, sited well above tangent points of interest, the ionospheric contribution to the bending angle, α, at frequency f can be simply expressed by (Eq. 2.6, Culverwell and Healy, 2015):

$$\alpha(a) = 2a\frac{k_4}{f^2}\int_a^\infty \frac{xn_e(x)}{(x^2-a^2)^{\frac{3}{2}}}dx \qquad (3.1)$$

where $x = nr$, is product of the refractive index, n, and radius value r, a is the impact parameter, $k_4 = \frac{e^2}{8\pi^2 m_e \varepsilon_0} = 40.3m^3s^{-2}$, and n_e is the electron number density. Commonly, the electron number density can be expressed in terms of the vertically integrated total electron content, TEC, which is defined as $TEC = \int n_e dr$. The equation above can be simplified by assuming a very narrow ionospheric shell and written as (Eq. 3.2, Culverwell and Healy, 2015):

$$\alpha(a) = 2a\frac{k_4}{f^2}TEC\frac{r_0}{(r_0{}^2-a^2)^{\frac{3}{2}}} \qquad (for\ a < r_0) \qquad (3.2)$$

r_0 is height of the peak electron density, which is assumed to be 300 km above the surface in this work.

The GPS L1 and L2 frequency bending angle difference is expressed as:

$$\alpha_2(a) - \alpha_1(a) = 2ak_4TEC(\frac{1}{f_2^2} - \frac{1}{f_1^2})\frac{r_0}{(r_0{}^2-a^2)^{\frac{3}{2}}} \qquad (3.3)$$

If we define $x_{so} = 2ak_4TEC(\frac{1}{f_2^2} - \frac{1}{f_1^2})$, then,

$$\alpha_2(a) = \alpha_1(a) + x_{so}\frac{r_0}{(r_0{}^2-a^2)^{\frac{3}{2}}} \qquad (3.4)$$

带格式的：缩进：首行缩进： 0 字符

In this work we estimate x_{so} from a least-square fit based on observed L1 and L2 bending angle differences produced with geometrical optics, over a 20 km vertical above the lowest valid L2 bending angle value. The maximum height of the vertical interval is limited to be 70 km. In theory, for a spherically symmetric ionosphere, x_{so} should be proportional to the ionospheric TEC, because the L2-L1 differences should be proportional to the TEC. However, we are not trying to retrieve the TEC here, and the quality of the TEC estimates has not been assessed. We simply estimate the parameter x_{so} in order to extrapolate the L2-L1 differences below 25 km using a reasonable, physically plausible curve.

We currently assume –the Delta function –ionospheric model peaks at –300km above the surface.~~.~~ Experiments ~~for~~ testing the sensitivity of the extrapolated bending angles to changes in the peak height from 250km to 350km, in 10 km increments have been performed. The largest differences between the 250 km and 350 km experiments about 1.0 microradians near the surface (Figure not shown)–. To put this in some context, the corrected bending angle value at an impact height of 20 km is typically 1600 micro-radians, and ~~t~~the neutral bending grows exponentially towards the surface, with the density scale-height (~7 km). Therefore, the sensitivity to the assumed peak height is low.

Two bad profiles, where the L2 signal stops above 20 km SLTA, have been chosen for demonstrating the extrapolation method. Their detailed information is listed in Table 2. Because the ionospheric effect becomes smaller in relative terms with the decreasing height, the magnitude of the relative L2-L1 bending angle differences gets smaller with height. Seen from the direct comparisons between the new and the old extrapolation results of case 1 (Figure 5 and 6), L2 bending angles are very different from the L1 bending angles before correction.~~is very different to L1 before correction.~~ After applying the new extrapolation approach, the L2 bending angles below 20 km are consistent with both L1 and LC bending angles. It is concluded that a more reliable LC bending angle can be obtained by using the new L2 extrapolation

带格式的：缩进：首行缩进： 0 字符

approach than the original L2 extrapolation method implemented in ROPP.

Clearly, using the new simple ionospheric model for the L2 extrapolation performs very well for the bad profiles with large biases. It is also useful to demonstrate the new extrapolation method for normal cases. Here the normal profiles are defined as the lowest SLTA reaching below 20 km, and the mean standard deviation to the reanalysis data is within 2% from surface to 35 km. Therefore, two good profiles (Table 3) are selected to test the new extrapolation.

Generally, the new extrapolation method does not degrade the good profiles. In fact, the new method smooths some occultation points, and improves the consistency of L1 and L2, as shown in Figure 7 and 8, for example.

An alternative way to demonstrate the accuracy of the different extrapolation methods is to compare their refractivity retrievals with the forecast model data. One day of data is used to test the new L2 extrapolation method. Figure 9 shows that the new method can effectively eliminate ~90 % of the problematic "branches" with the large percentage refractivity errors often are exceeding 100 %. In this plot, eight profiles still have a large bias after the new extrapolation, because the L2 SLTA stops above 70 km, which is out of the processing range used in the extrapolation (below 70 km). These cases can be removed by using~~including~~ ~~some~~ a simple ~~additional~~ QC ~~steps~~.

4 Quality control methods

~~Although the new L2 extrapolation method removes more than 90% poor quality profiles, there are still some profiles with obvious errors. Therefore, additional QC methods need to be implemented.~~ Based on the GPS RO error sources and characteristics, many internal QC methods have proposed in the literature. For example, the COSMIC Data Analysis and Archive Center (CDAAC) define an altitude, *Z*, below which a low quality of L2 signal has been detected. The maximum difference of Ll and L2 bending angle above Z, and the ionospheric scintillation index analyzed from the amplitude of L1 signal at high altitudes are used in the QC (Kuo et al., 2004). Gorbunov (2002) proposed a QC procedure in terms of the analysis of the

带格式的：缩进：首行缩进： 0 字符

amplitude of the RO data transformed by the Canonical Transform (CT) or the Full Spectrum Inversion (FSI) method (Gorbunov and Lauritsen, 2004), which is useful to catch the corrupted data because of phase lock loop failures. Beyerle et al. (2004) also suggested a QC approach to reject the RO observations degraded by ionospheric disturbances based on the phase delay of L1 and L2 signals. Zou et al (2006) use the bi-weight check, removing large departure data from the statisticals point of view. More recently, Liu et al (2018) introduced a local spectral width based quality control, which improves the application in lower troposphere. The quality indicator "badness score" in ROPP is successfully applied for CHAMP, COSMIC, METOP and other observations. However, just like the failure of processing GNOS data, the badness score is not adequate for identifying the GNOS data. The reason might be related to the empirical parameters (see formula 2.1). These parameters are formed based on the performances of CHAMP, COSMIC and METOP missions, whose L2 signals are not degraded too much as GNOS. Considering the new L2 extrapolation method and the characteristics of GNOS data, we introduce a new indicator to detect the poor quality profiles based on the noise estimate of the L1 and L2 fit.

~~In light of the characteristics of GNOS RO data, we developed and tested some new internal QC methods to detect the poor quality profiles based on the noise estimate of the L1 and L2 fit.~~

4.1 Noise estimate of the L1 and L2 fit

As noted earlier, as a result to L2 signal tracking problems, around 15% profiles are degraded with the old processing. After applying the new L2 extrapolation method, most of them can be effectively corrected. As seen from the Eq. 3.4, the key to the correction is how well the retrieved parameter, x_{so}, fits the difference of L1 and L2 bending angles in the 20km fitting interval. Currently, 25 km or the minimum L2 SLTA is the lower limit of the fitting interval.

We have introduced a new parameter, *noise_estimate*, to test the quality of the least-square fit in the 20 km interval. It can be expressed as:

$$noise\_estimate = \frac{\sqrt{\sum(x_{so} * \frac{r_0}{(r_0{}^2 - a^2)^{\frac{3}{2}}} - \Delta\alpha(a))^2}}{n} * 10^6 \quad (4.1)$$

w~~W~~here $\Delta\alpha$ is the difference of L1 and L2 bending angles, and the sum is over the n (L2-L1) values in the 20 km fitting interval. The parameter ~~physical meaning of~~ *noise_estimate* ~~is easy to understand. It~~ is the root-mean-square ~~the standard deviation~~ of the difference between the fitting model and (L2-L1) values~~observations~~. Clearly, it provides information about how well we are able to fit the L2-L1 bending angle differences with the model, in a~~the~~ fitting interval where we trust the data. We assume that i~~I~~f the fitting model can reproduce the L2-L1 bending angle differences accurately in the fitting interval, we can then use the retrieved parameter x_{so} to extrapolate the L2-L1 differences below 25 km, to produce reasonable ionospheric corrected bending angles used for NWP applications.

~~–~~

带格式的：缩进：首行缩进： 0 字符

A histogram of the *noise_estimate* values has been obtained by accumulating statistics over a seven day period (Figure 10), and we use this to determine a QC threshold value as 20 microradian. Clearly, t~~T~~he 20 microradian threshold is empirical, but it can be related to the assumed bending angle error statistics used in the assimilation of GNSS-RO data. At ECMWF, the assumed bending angle uncertainty is 1.25 % from around 10 km to ~32 km, and the 3 micro-radians above this height.This translates into around 7.5 microradians at 26 km, increasing to around 20 micro-radians at 20 km. The 20 microradian threshold is designed to screen out cases where the L2-L1 extrapolation could introduce significant additional errors. In summary, in the operational GNOS processing, if the value of the *noise_estimate* is greater than 20 micro-radians, the profiles will be rejected.

带格式的：缩进：首行缩进： 0 字符

~~We have used one day of data to test the performance of the θ_α*noise_estimate* as a QC parameter, for detecting the large bias cases. The θ_α*noise_estimate* of the good profiles are highly focused on the values are below 20; while the θ_α*noise_estimate* of the bad profiles, with large biases, have the largest θ_α*noise_estimate* values. It demonstrates that setting the θ_α*noise_estimate* parameter threshold at 20~~

~~microradians can distinguish between many of the good and the bad GNOS cases. This parameter can be used as one factor, .but other parameters are still needed to complete the QC.~~

4.2 Mean phase delays of L1 and L2

The *noise_estimate* QC parameter does not detect all the poor quality profiles, and we need ~~extra~~ additional quality control methods to identify them. We find that it is also necessary to monitor the performance of GNOS mean L1 and L2 phase delays in the height interval of 60 to 80 km, because this can also indicate the observational quality of GPS RO data. However, the L1 and L2 SNR values, ~~that~~ which are commonly used as a QC indicator, are not found to be useful for identifying the large bias cases of GNOS data. For the rising profiles, the absolute accumulated phase delay should increase with height. Despite reasonable SNR above the height of 60 km , in some cases the mean phase delays have small values, leading to problems in the inversions.

Figure 11 and Figure 12 show the histograms of the L1 and L2 mean delay phase in rising occultations. They show that there is a clear separation of the mean phase delays. ~~relationship between the poor profiles and the mean phase delay of L1 and L2.~~ To clarify the quality of the two groups of samples, we identify them as “GOOD” or “BAD” profiles. The criterion for good or bad is that the mean bias relative to the background data is smaller than or greater than 5% at the height interval of 10 to 40km, respectively. Figure 13 and 14 demonstrate the distribution of L1 and L2 mean phase delay. Different colour represents different overlap density, the dark blue is the lowest density and the dark red is the highest one. The colours between them represent increasing density. The “GOOD” samples gather around -8000 meters, while the “BAD” samples accumulate around -100 meters. Therefore, we can identify most of the bad rising occultations, when both L1 and L2 absolute mean phase values are ~~greater~~ smaller than - 150 m. This threshold value is empirical considering the

amount of the samples. ~~–~~Unavoidably, a ~~few of the~~small number of good profiles could be wrongly detected as well and few bad ones could be missed. ~~However~~Generally, the statistical performance is reasonable, as will be demonstrated in Section 4.3.

4.3 The statistical performance of the applied QC methods

After checking a number of QC parameters, we use the following three QC tests:

(1) If the occultation is rising, and the absolute~~both~~ mean phase delays of L1 and L2 are both ~~greater~~ smaller than ~~-~~150m, the profile will be identified as "bad";

(2) If the value of *noise_estimate* is greater than 20 microradians, the profile will be identified as "bad";

(3) If the lowest SLTA of L2 is greater than 50 km, the profile will be identified as "bad".

These have been tested with three months of data, as to whether they can identify the "good" or "bad" large bias cases. The criterion for good or bad is similar to those mentioned above that the mean bias relative to the background data is smaller than or greater than 2% at the height interval of 10 to 40km, respectively .

41,928 samples are collected from April 1 to June 30, 2018. There are 38,752 good profiles and 3,176 bad profiles evaluated by background data (e.g. The ECMWF reanalysis). The QC scheme applied in this paper identifies 37,627 good profiles and 4,301 bad ones. According to statistics, the number of profiles that can be accurately identified is 36,957, the accuracy rate is 95.4%, the number of missed is 1,795, the missed rate is 4.6%, 670 are misjudged, and the false positive rate is 1.8%. See Table 4 for clarification. Unavoidably, a small number of good profiles could be wrongly detected as well and few bad ones could be missed. In general, the performance of this kind of QC method can effectively identify most of the bad profiles.

~~For example, t~~These have been tested with one day of data, as to whether they can identify the "bad" large bias cases. The percentage of the true bad profiles for one day is 9.7% of the data. After applying the QC method, the ratio of the profiles

~~identified as "bad" is 11.1%. Unavoidably, a small number of good profiles could be wrongly detected as well and few bad ones could be missed. It can be correctly identified 8.0% of the bad profiles can be correctly identified, which means 3.1% profiles are mistakenly identified and 1.7% of the profiles are still missing (Table 4). In general, the performance of this kind of QC method can effectively identify most of the bad profiles.~~

5 Comparison with ECMWF forecast data

This section demonstrates the performances of the comparison between the observational GNOS bending angles and the simulated ones using ECMWF short-range forecast data. GNOS bending angle profiles are those which are carried out using the new L2 extrapolation and quality controls mentioned in section 3 and section 4, respectively. The period is from 6th July to 2nd Aug. 2018. The ECMWF data used as the background is the state-of-the-art short-range forecast data with 137 vertical levels extending from surface to 0.01 hPa. Using the 2D bending angle forward operator, ECMWF forecast data can be projected into the bending angle space at the GNOS locations.

GNOS observations are provided BUFR format for NWP applications, with the bending angles given on 247 vertical levels from the surface to 60 km. To provide a context for the comparisons, Metop-A GRAS profiles from the same period are also selected as a benchmark. Figure ~~13~~ 15 displays the mean bias for the GNOS and GRAS bending angle profiles both separated into rising and setting occultations, showing that GNOS and GRAS are very consistent with each other above 10 km. Figure ~~14~~ 16 shows the standard deviation of the bending angle departures for the GNOS and GRAS. Their standard deviations are about 1% between 10 – 35 km, increasing to about 12% at 50 km and more than 15% below 5 km impact height. It is clear that the GNOS standard deviations are comparable to GRAS in the 10 - 40km interval. The difference in the 20 to 25 km interval is related to the transition from wave optics to geometric optics for the GNOS. ~~The GRAS standard deviations are~~

~~worse in the troposphere but this is probably due to sampling; essentially GRAS is able to measure more difficult cases.~~ Generally, the two datasets have similar error characteristics in terms of both the mean bias and standard deviation over most of the height interval, but especially in the GPS-RO core range between 10-35 km. The standard deviations of the GNOS departures below 10 km are smaller than the GRAS statistics. However, we do not believe that this indicates that GNOS data is superior to GRAS below 10 km. In general, GRAS measurements tend to penetrate more deeply in the troposphere, and this will affect the statistical comparison with GNOS. Furthermore, the difference between the setting and rising GRAS statistics is known but not fully understood, and it is an area of current investigation. Nevertheless, we believe that Figures 15-16 provide evidence that the GNOS and GRAS measurements have similar performance in the "core region" as a result the processing and QC methods introduced here.

Note that further GNOS occultation departure statistics, including comparisons with other GPS-RO measurements in bending angle space, are now routinely available from the ROM SAF web pages.
See,http://www.romsaf.org/monitoring/matched.php

~~The comparison between GRAS and GNOS is not the most important part of the manuscript, thus a general remark is made. GNOS occultations are routinely available from the ROM SAF web pages. For more details of different kinds of statistics can be found on ROM SAF web pages. See,http://www.romsaf.org/monitoring/matched.php~~

6 Conclusions

This study has focused on three main areas. Firstly, we have developed and tested a new L2 extrapolation for GNOS GPS-RO profiles. Secondly, we have investigated QC method~~s~~ for GNOS after applying the new L2 extrapolation. Thirdly, we have estimated the bending angle departure ~~–~~statistics by comparing GNOS and ECMWF short-range forecast data. The main results are summarized below.

We have identified and investigated the GNOS GPS-RO cases that fail quality control with large bending angle departures, after the processing with the ROPP software.

带格式的：缩进：首行缩进： 0 字符

These large departures can be attributed to the GPS L2 signal tracking problems for signals that stop above 20 km in terms of SLTA, and the related L2 extrapolation. The percentage of the profiles with large departure is about 13~15%. Therefore, we focused on a better L2 extrapolation for GNOS when the L2 signal stops early. A new L2 extrapolation approach has been implemented in ROPP to mitigate the problem. (These modifications will be available in ROPP 9.1; see http://www.romsaf.org/ropp/) The main procedure is in bending angle space, and it is based on the (unpublished) study of Culverwell and Healy (2015). The new method can effectively remove about 90% of the large departures. The remaining poor cases are mostly due to the L2 being completely missing.

We have studied and established the quality control method~~s~~ suitable for GNOS GPS-RO profiles after correcting the large departures. The new L2 extrapolation θ_α ~~*noise_estimate*~~ value can be taken as a QC parameter to evaluate the performance of the extrapolation. It is the ~~standard deviation~~ root-mean-square of the difference between the fit and observations above the extrapolated height. The 20 microradian threshold is used to judge the good or bad profile after implementing the new L2 extrapolation method. The mean phase delays of L1 and L2 in the tangent height interval of 60 to 80 km are analysed and applied in the QC as well. The lowest SLTA of L2 is also set as a threshold to identify the bad profiles. Using the parameters mentioned above, the QC method can correctly identify ~~82.5~~95.4% of the ~~bad~~ profiles ~~with a mean bias is greater than 5%~~.

~~–~~Finally, we have assessed the quality of the GNOS bending angles after implementing the new processing and QC by comparing with the background bending angles computed from the operational ECMWF ~~short range~~ forecasts. GRAS profiles from the same period are selected as a benchmark. The departure statistics for the GNOS and GRAS bending angle profiles in terms of the mean bias and standard deviations are similar at most of the heights, especially in the GPS-RO core region between 10-35 km.

As a result of this work, the GNOS data ~~is~~are now assimilated in operational NWP systems at, for example, the European Centre for Medium-Range Weather Forecasts

(ECMWF), Deutscher Wetterdienst (DWD) and the Met Office.

~~The GNOS measurements processed with methods outlined in this study have been assimilated into operational NWP systems since March 6, 2018.~~

Acknowledgments

This work was undertaken as part of a visiting scientist study funded by the Radio Occultation Meteorology Satellite Application Facility (ROM SAF), which is a decentralised processing centre under the European Organisation for the Exploitation of Meteorological Satellites (EUMETSAT).

We have to express ~~my~~ our appreciation to Christian Marquardt for his valuable suggestions with respect to the RO processing and QC methods. In addition, we want to thank Ian Culverwell and Chris Burrow for their discussions. Finally, we would like to thank the fund support of National Key R&D Program of China (No.*2018YFB0504900*) and Special Fund for Meteorology Research in the Public Interest (No.*201506074)*.

References

Anthes, R. A., Ector, D., Hunt, D. C., Kuo, Y.-H., Rocken, C., Schreiner, W. S., Sokolovskiy, S. V., Syndergaard, S., Wee, T.- K., Zeng, Z., Bernhardt, P. A., Dymond, K. F., Chen, Y., Liu, H., Manning, K., Randel, W. J., Trenberth, K. E., Cucurull, L., Healy, S. B., Ho, S.-P., McCormick, C., Meehan, T. K., Thompson, D. C., and Yen, N. L.: The cosmic/formosat-3 mission: Early results, B. Am. Meteorol. Soc., 89, 313–333, 2008.

Ao, C. O., Hajj, G. A., Meehan, T. K., Dong, D., Iijima, B. A., Mannucci, J. A., and Kursinski, E. R.: Rising and setting GPS occultations by use of open-loop tracking, J. Geophys. Res., 114, D04101, doi:10.1029/2008JD010483, 2009.

Bai, W. H., Sun, Y. Q., Du, Q. F., Yang, G. L., Yang, Z. D., Zhang, P., Bi, Y. M., Wang, X. Y., Cheng, C., and Han, Y.: An introduction to the FY3 GNOS instrument and mountain-top tests, Atmos. Meas. Tech., 7, 1817–1823,

doi:10.5194/amt-7-1817-2014, 2014.

Beutler, G.: Methods of Celestial Mechanics, Springer-Verlag, Berlin, Heidelberg, New York, Germany, USA, ISBN 3-211- 82364-6, 2005.

Beyerle, G., 1. Wickert., T Schmidt, and C. Reigber., Atmospheric sounding by GNSS radio occultation: An analysis of the negative refractivity bias using CHAMP observations, J Geophys.Res., 109, D01106, doi:10.102912003JD003922,2004.

Culverwell, I. D. and S. B. Healy: Simulation of L1 and L2 bending angles with a model ionosphere, ROM SAF Report 17, 2015. Available at http://www.romsaf.org/general-documents/rsr/rsr_17.pdf, 2015.

Culverwell, I. D., Lewis, H. W., Offiler, D., Marquardt, C., and Burrows, C. P.: The Radio Occultation Processing Package, ROPP, Atmos. Meas. Tech., 8, 1887-1899, https://doi.org/10.5194/amt-8-1887-2015, 2015.

Dach, R., Hugentobler, U., Fridez, P., and Meindl, M.: Bernese GPS Software Version 5.0. Astronomical Institute, University of Bern, Switzerland, 2007.

Gorbunov, M. E.: Ionospheric correction and statistical optimization of radio occultation data, Radio Sci., 37, 17-1–17-9, doi:10.1029/2000RS002370, 2002.

Gorbunov, M. E. and Lauritsen, K. B.: Analysis of wave fields by Fourier Integral Operators and their application for radio occultations, Radio Sci., 39, RS4010, doi:10.1029/2003RS002971, 2004.

Gorbunov, M. E., ~~K. B.~~ Lauritsen, K. B., ~~A.~~ Rhodin, A.,, ~~M.~~ Tomassinin M., , and ~~L.~~ Kornblueh, L., Radio holographic filtering, error estimation, and quality control of radio occultation data, J. Geophys. Res., 111, D10105, doi:10.1029/2005JD006427, 2006.

~~Liu, H.; Kuo, Y. H.; Sokolovskiy, S.; Zou, X.; Zeng, Z.; Hsiao, L. F. & Ruston, B. C. (2018), 'A quality control procedure based on bending angle measurement uncertainty for radio occultation data assimilation in the tropical lower troposphere', J. Atmos. Oceanic Technol. 35(10), 2117–2131.~~

~~M. E.~~ Gorbunov, M. E, ~~K. B.~~ Lauritsen, K.B.,~~A.~~ Rodin A., ~~M.~~ Tomassini, M., and ~~L.~~ Kornblueh, L. (2005), Analysis of the CHAMP Experimental Data on

Radio-Occultation Sounding of the Earth's Atmosphere, Izvestiya, Atmospheric and Oceanic Physics, 41, No. 6, 726–740.

Kuo, Y.-H., Wee, T.-K., Sokolovskiy, S., Rocken, C., Schreiner, W., Hunt, D., and Anthes, R. A.: Inversion and error estimation of GPS radio occultation data, J. Meteor. Soc. Japan, 82, 507–531,2004.

Kursinski, E. R., Hajj, G. A., Hardy, K. R., Schofield, J. T., and Lin- field, R.: Observing Earth's atmosphere with radio occultation measurements, J. Geophys. Res., 102, 23429–23465, 1997.

Larsen, G.B., Syndergaard, S. Høeg,P., and Sørensen, M.B.: Single frequency processing of Ørsted GPS radio occultation measurements, GPS Solut,9,144-155,doi 10.1007/s10291-005-0142-x,2005.

Liu, H.; Kuo, Y.-H.; Sokolovskiy, S.; Zou, X.; Zeng, Z.; Hsiao, L.-F. & Ruston, B. C. (2018), 'A quality control procedure based on bending angle measurement uncertainty for radio occultation data assimilation in the tropical lower troposphere', J. Atmos. Oceanic Technol. 35(10), 2117--2131.

Montenbruck O.: Kinematic GPS positioning of LEO satellites using ionosphere-free single frequency measurements, Aerospace Science and Technology 7:396–405, 2003.

ROM SAF http://www.romsaf.org/product_documents/romsaf_atbd_ba.pdf, 2016.

Shi C, Zhao Q, Lou Y. Recent development of PANDA software in GNSS data processing[J]. Proc. SPIE, 7285:231-249, 2008.

Sokolovskiy, S. V., Tracking tropospheric radio occultation signals from low Earth orbit, Radio Sci., 36(3), 483– 498, 2001.

Von Engeln, A., Healy, S., Marquardt, C., Andres, Y., and Sancho, F.: Validation of operational GRAS radio occultation data, Geo- phys. Res. Lett., 36, L17809, doi:10.1029/2009GL039968, 2009.

Vorob'ev, V. V. and Krasil'nikova, G. K.: Estimation of the accuracy of the atmospheric refractive index recovery from doppler shift measurements at

带格式的：字体：8 磅

带格式的：字体：（默认）Times New Roman，（中文）+中文正文（宋体），小四，字体颜色：黑色

frequencies used in the NAVSTAR system,USSR Phys. Atmos. Ocean, Engl. Transl., 29, 602–609, 1994.

Ware, R., Rocken, C., Solheim, F., Exner, M., Schreiner, W., An- thes, R., Feng, D., Herman, B., Gorbunov, M., Sokolovskiy, S., Hardy, K., Kuo, Y., Zou, X., Trenberth, K., Meehan, T., Melbourne, W., and Businger, S.: GPS sounding of the atmosphere from lower Earth orbit: preliminary results, B. Am. Meteorol. Soc., 77, 19–40, 1996.

Yang, J., Zhang, P., Lu, N.-M., Yang, Z.-D., Shi, J.-M., and Dong, C.-H.: Improvements on global meteorological observations from the current Fengyun 3 satellites and beyond, Int. J. Digital Earth, 5, 251–265, 2012.

Zeng.Z-, Sokolovskiy,S., Schreiner,W., Hunt,D., Lin,J., and Kuo,Y.-H.: Ionospheric correction of GPS radio occultation data in the troposphere, Atmos. Meas. Tech., 9, 335–346, 2016.

Zou, X., Zeng, Z., 'A quality control procedure for GPS radio occultation data', J. Geophys. Res. 111, D02112,2006.

Table 1 Main instrumental parameters for FY-3C/GNOS

Parameters	FY-3C/GNOS
Orbit Height	~836 km
Orbit Type	sun synchronous
Inclination	98.75 °
Spacecraft mass	~750kg
Instrument mass	7.5kg
Constellation	GPS L1 C/A, L2 P
	BDS B1I,B2I
Channels	GPS：14 BDS：8
Sampling	POD 1Hz
	ATM.occ. (closed loop)50Hz
	ATM.occ.(open loop) 100 Hz
	ION occ. 1Hz
Open loop	GPS L1 C/A
Clock stability	1×10－12（1secAllan）
Pseudo-range precision	≤30cm
Carrier phase precision	≤2mm
Beam width of atmosphere occultation antenna	≥±30°(azimuth)

Table 2. Details of the selected bad occultations

No.	Occ. time (yymmdd.hhmm)	Longitude (deg.)	Latitude (deg.)	Occ. direction	SLTA_L2 (km)
1	170128.0332	-99.154	25.070	rising	21.917
2	170128.0740	24.705	-4.222	rising	25.793

Table 3. Details of the good profiles

No.	Occ. time (yymmdd.hhmm)	Longitude (degree)	Latitude (degree)	Occ. direction	SLTA_L2 (km)
1	20170128.0103	149.508	-38.445	rising	4.011
2	20170128.0251	70.857	-51.463	rising	12.928

~~Table 4. The 2×2 table values~~

		~~Bad case (True)~~	
		~~YES~~	~~NO~~
~~Bad case (Identified by QC parameters)~~	~~YES~~	~~8.0% (hits)~~	~~3.1%(false identified)~~
	~~NO~~	~~1.7%(misses)~~	~~87.2%(correct negatives)~~

Table 4. The 2×2 table values

		Evaluated by background data	
		GOOD (38752 profiles)	BAD (3176 profiles)
Identified by QC parameters	GOOD (37627 profiles)	36957 (hits)	670(misses)
	BAD (4301 profiles)	1795(false identified)	2506(correct negatives)

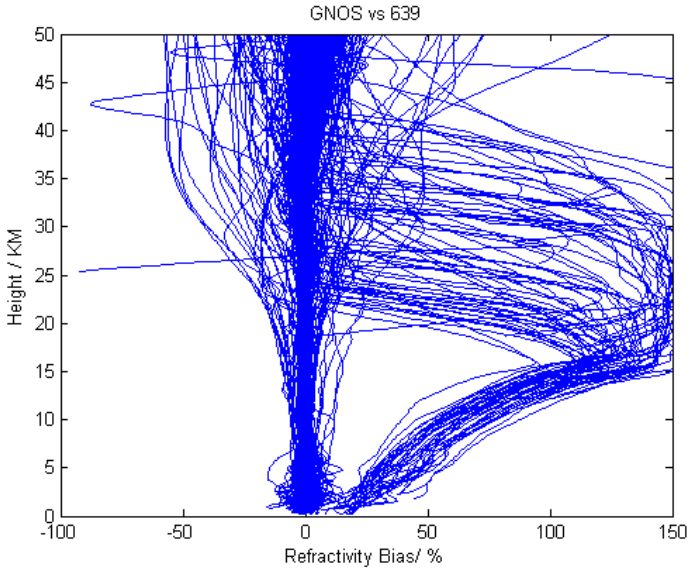

Figure 1. FY-3C/ GNOS GPS refractivity bias compared to T639 (the Chinese forecast model data), on 28th Jan.2017 with 489 samples.

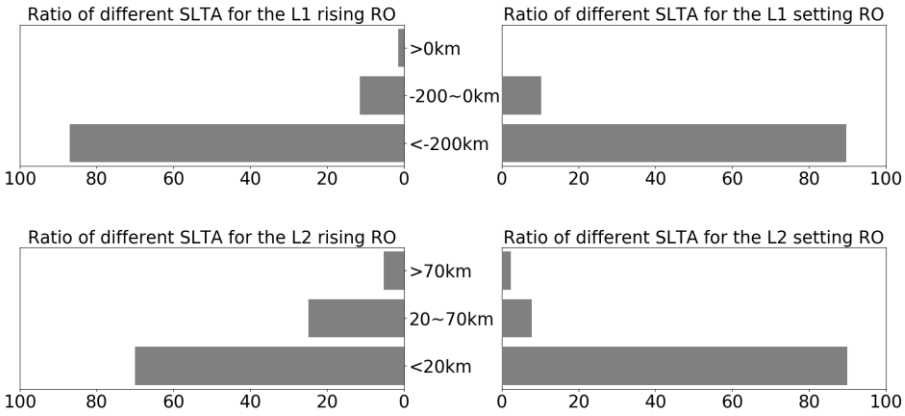

Figure 2. Ratio of different SLTA of the L1 C/A and L2 P for the rising and setting occultations, statistics result is from 28th Jan to 2nd Feb. 2017.

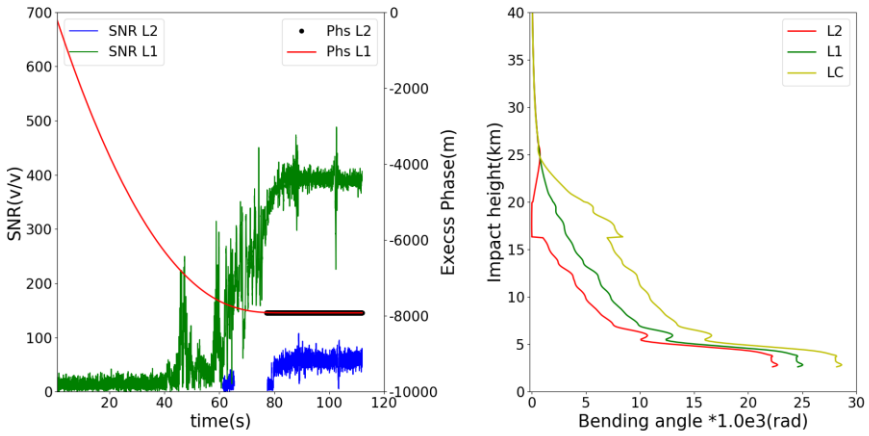

(a)

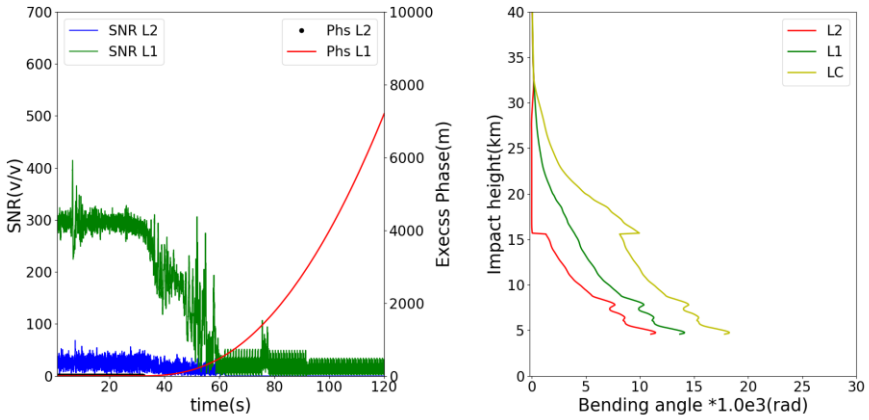

(b)

Figure 3. Two bad cases (a) A rising profile (FY3C_GNOSX_GBAL_L1_20170128_0332_AEG15_MS.NC), (b) a setting profile (FY3C_GNOSX_GBAL_L1_20170128_0850_AEG18_MS.NC). Example L1 (red) and L2 (black) SNR and excess phase measured data. The resulting L1 bending angle (green), L2 bending angle (red), and LC bending angle (yellow) profiles as a function of impact parameter computed using ropp_pp routines.

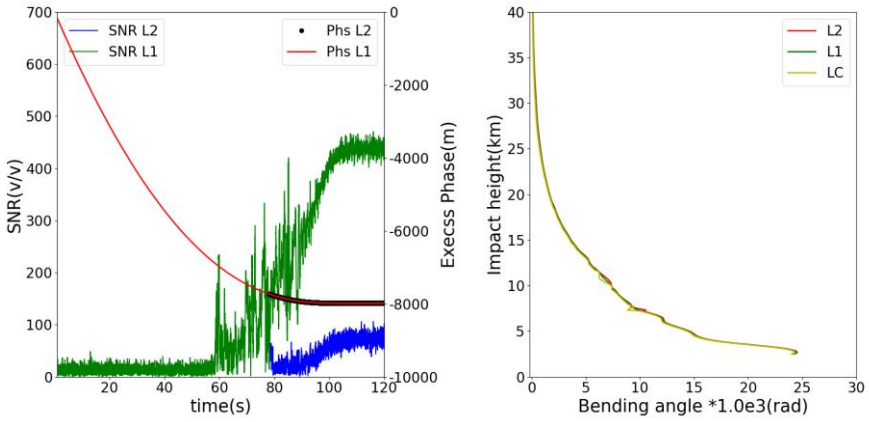

(a)

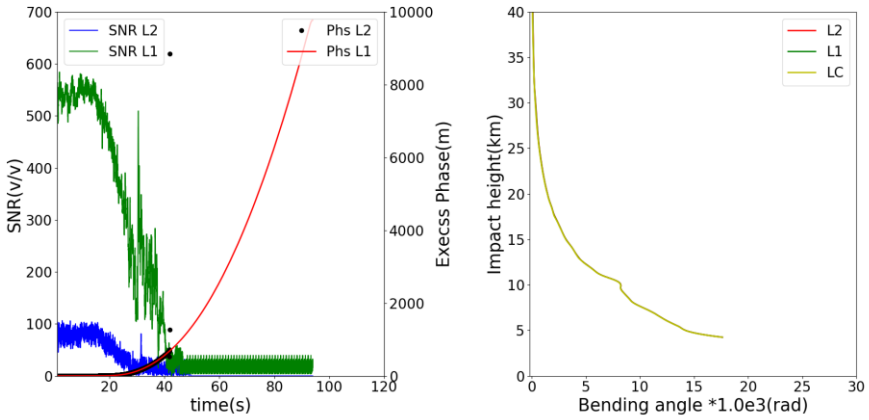

(b)

Figure 4. Two good cases (a) A rising profile (FY3C_GNOSX_GBAL_L1_20170128_1138_AEG27_MS.NC), (b) a setting profile (FY3C_GNOSX_GBAL_L1_20170128_1648_AEG31_MS.NC). Example L1 (red) and L2 (black) SNR and excess phase measured data. The resulting L1 bending angle (green), L2 bending angle (red), and LC bending angle (yellow) profiles as a function of impact parameter computed using ROPP routines.

带格式的：居中

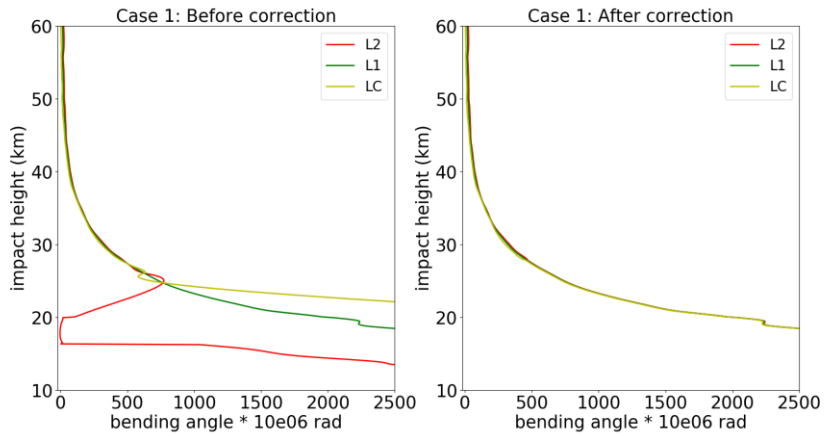

Figure 5. Case1: the bending angle of L2 (red), L1 (green) and LC (yellow) before (right) and after (left) correction.
(FY3C_GNOSX_GBAL_L1_20170128_0332_AEG15_MS.NC)

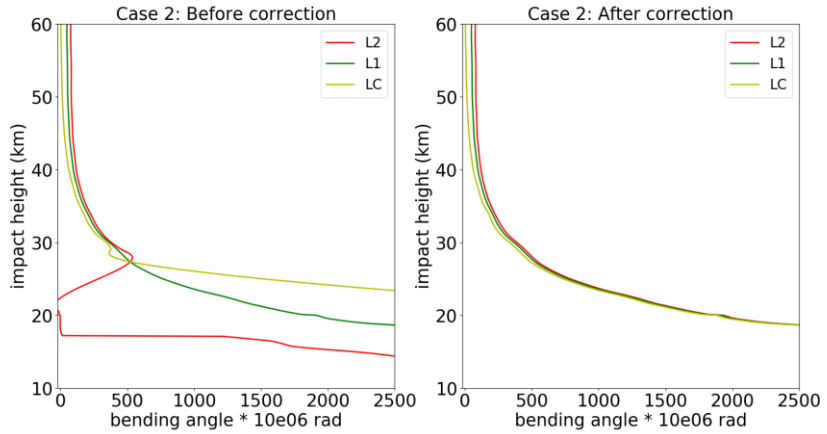

Figure 6. The same as Figure 5 but for Case 2.
(FY3C_GNOSX_GBAL_L1_20170128_0850_AEG18_MS.NC)

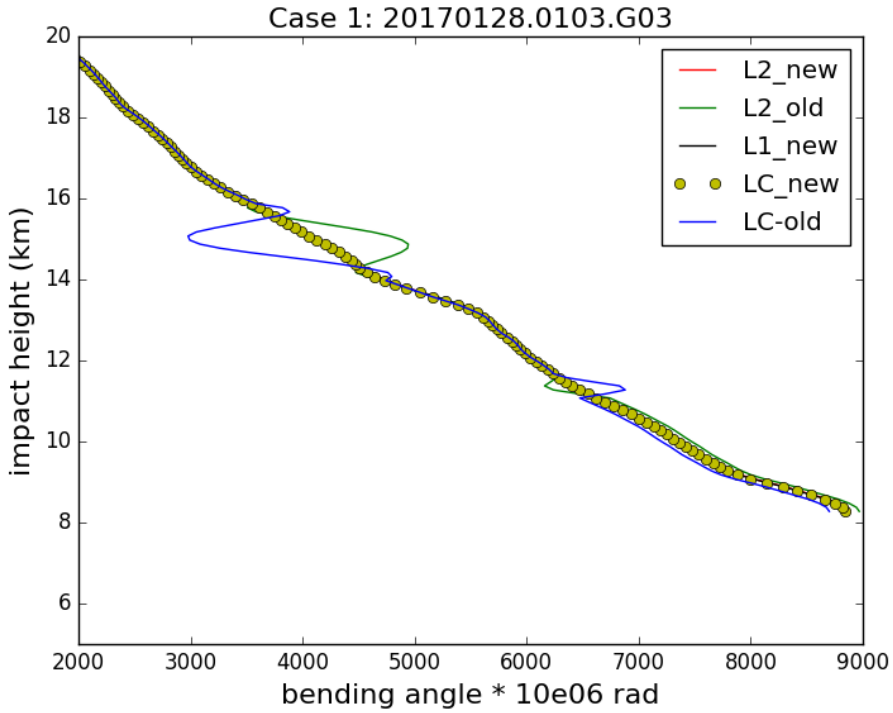

Figure 7. Good Case 1: the bending angle of L2, L1 and LC before and after correction.

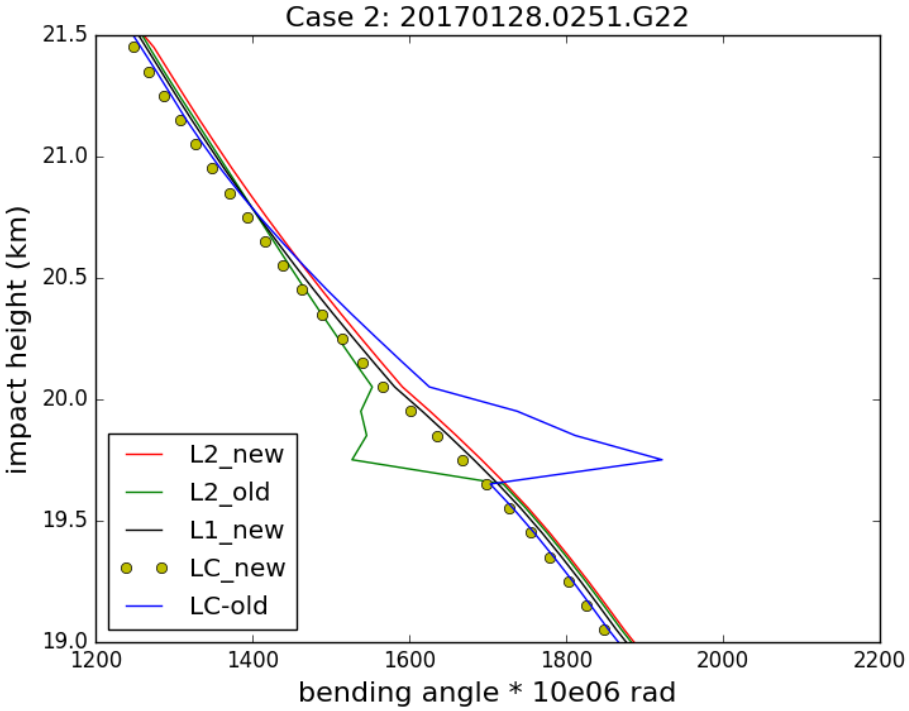

Figure 8. Good Case2: the bending angle of L2, L1 and LC before and after correction.

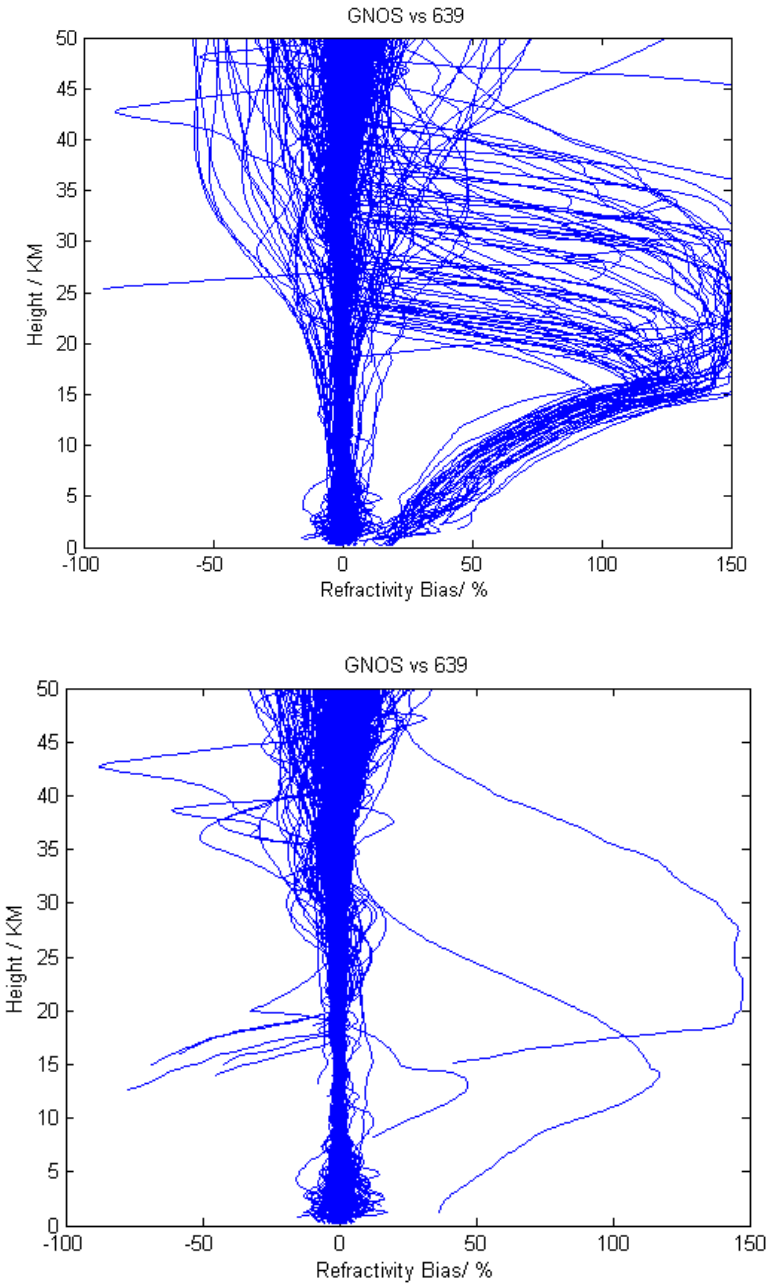

Figure 9. FY-3C/ GNOS GPS refractivity bias compared to T639 (the Chinese forecast model data), on 28th Jan.2017 with 489 samples. The upper plot reproduces Figure 1 and is the result of the original GNOS GPS data, and the lower plot isafter implementing the new L2 extrapolation approach.

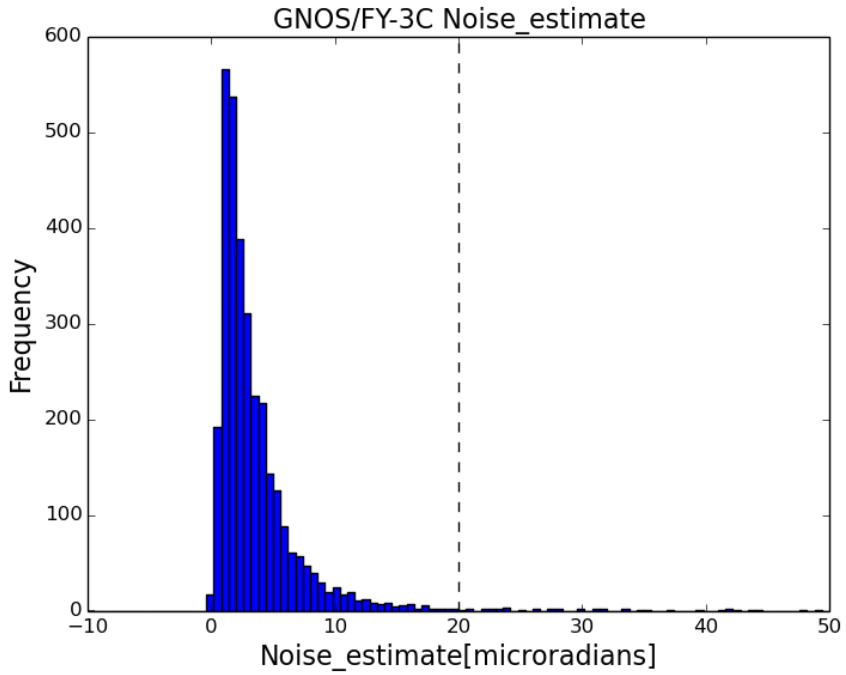

Figure 10. The histogram of the *noise_estimate* parameter using seven days of data from 16th Feb. to 22nd Feb 2017

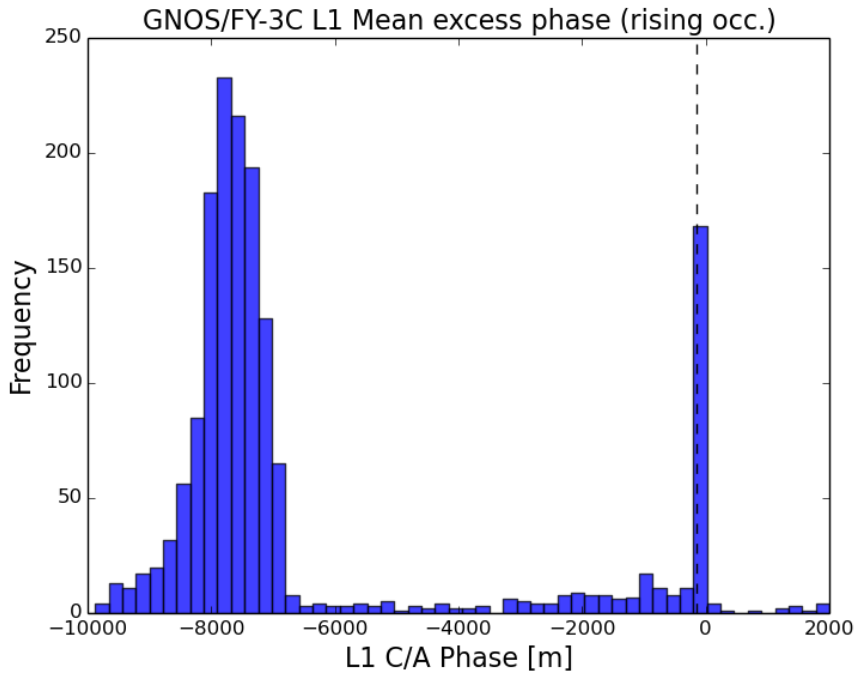

Figure 11. The histograms of L1 mean excess phase for the rising occultation at the height of 60 – 80 km SLTA using seven days of data from 16th Feb. to 22nd Feb.2017.

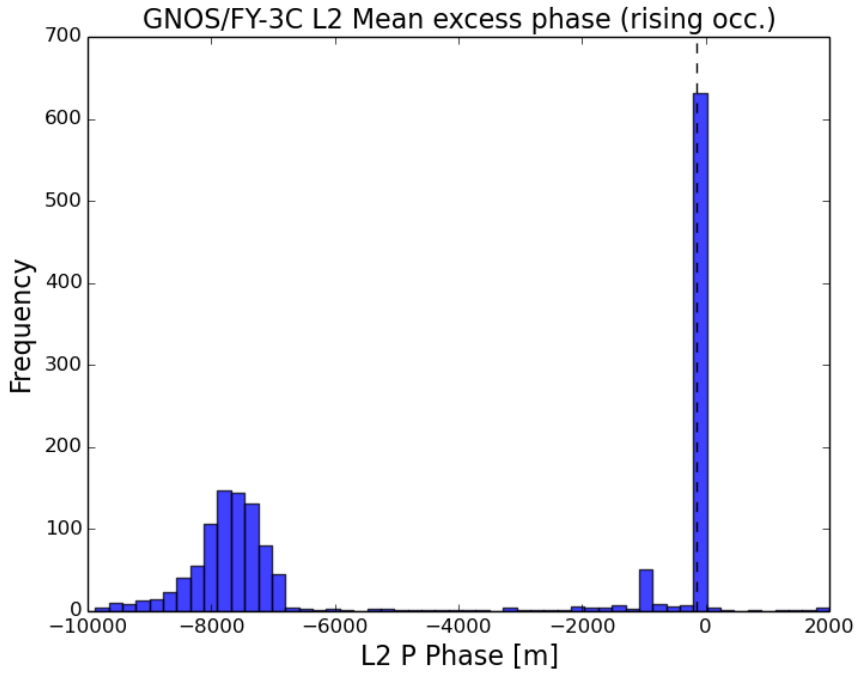

Figure 12. The histograms of L2 mean excess phase for the rising occultation at the height of 60 – 80 km SLTA using seven days of data from 16th Feb. to 22nd Feb.2017.

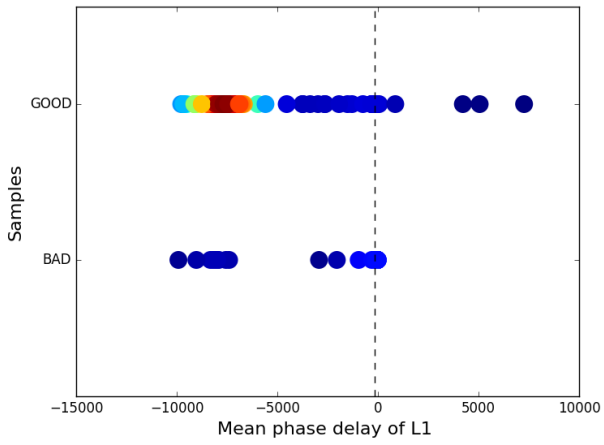

Figure 13. The L1 mean phase delay (meters) versus the good and bad samples. Different colour represents different overlap density, the dark blue is the lowest and the dark red is the highest, the colours between them show gradually higher density.

带格式的: 字体: Times New Roman, 小四, 英语(英国)

带格式的: 字体: Times New Roman, 小四, 英语(英国)

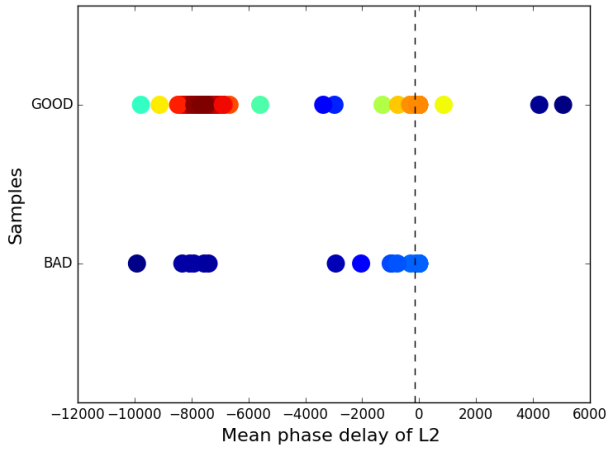

Figure 14. The L2 mean phase delay (meters) versus the good and bad samples. Different colour represents different overlap density, the dark blue is the lowest and the dark red is the highest, the colours between them show gradually higher density.

带格式的: 字体: Times New Roman, 小四, 英语(英国)

带格式的: 字体: Times New Roman, 小四, 英语(英国)

带格式的: 字体: Times New Roman, 小四, 英语(英国)

带格式的: 字体: Times New Roman, 小四

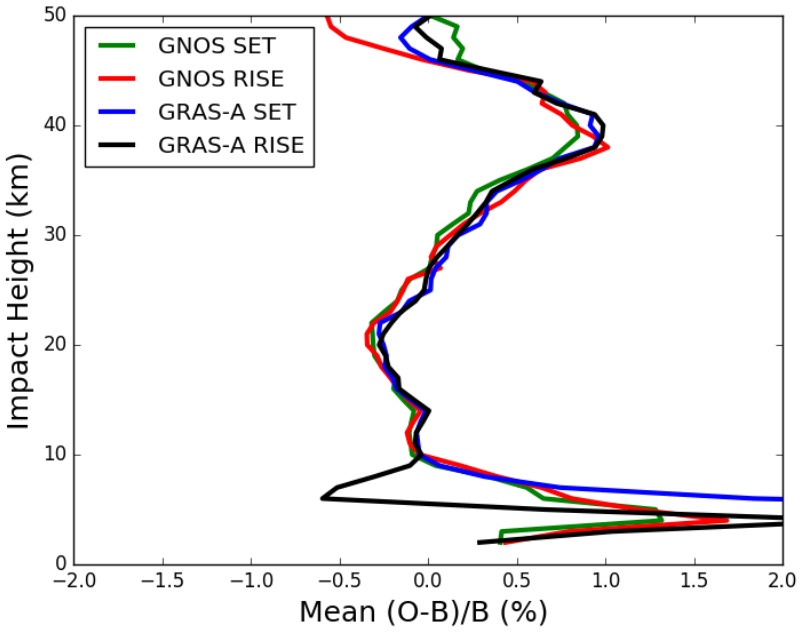

Figure ~~13~~1~~4~~5. Global bending angle departure results, as a function of impact height, for the mean bias. The green, red, blue and black lines are representative of setting

occultation for GNOS, rising occultation for GNOS, setting occultation for GRAS and rising occultation for GRAS.

带格式的：左

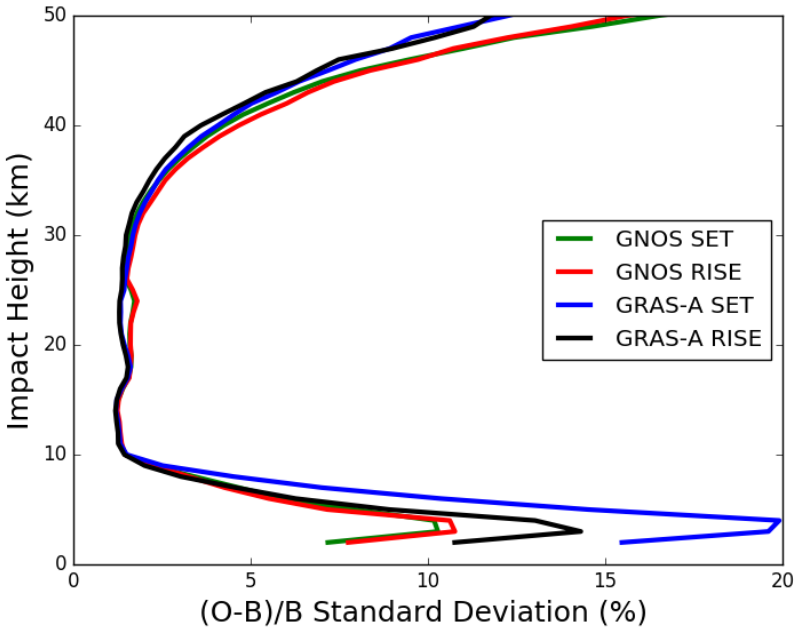

Figure ~~14~~12~~6~~. Global bending angle departure results, as a function of impact height, for the standard deviation. The green, red, blue and black lines are representative of setting occultation for GNOS, rising occultation for GNOS, setting occultation for GRAS and rising occultation for GRAS.